The Application of Empirical Phase Diagrams to the Biophysical Characterization and Stabilization of Viral Vaccine Candidates

BY

Julian Kissmann

Submitted to the graduate degree program in Pharmaceutical Chemistry and the Graduate Faculty of the University of Kansas in partial fulfillment of the requirements for the degree of Doctor of Philosophy.

_____

Dr. C. Russell Middaugh, Chairperson

Committee members

_____

Dr. Teruna J. Siahaan

_____

Dr. Sunil A. David

_____

Dr. Jennifer S. Laurence

_____

Dr. M. Laird Forrest

Date defended: August 31st, 2009

The Dissertation Committee for Julian Kissmann certifies that this is the approved version of the following dissertation:

The Application of Empirical Phase Diagrams to the Biophysical Characterization and Stabilization of Viral Vaccine Candidates

_____

Dr. C. Russell Middaugh, Chairperson

_____

Date approved

Dedicated to my friend and mentor, Russ Middaugh

Table of Contents

Chapter 1

Introduction

The positive impact of viral vaccines on global health is difficult to overstate. Since Edward Jenner's pioneering work in the late 18th century, viral vaccines have proven their ability to control smallpox, poliomyelitis, yellow fever, rabies, measles, mumps, and rubella.[1, 2] In developed countries, these diseases are now extremely rare if not completely eradicated. The continuing efforts of vaccinologists and virologists have lead to the conception, clinical evaluation, and licensure of several other virally-based vaccines, including those that protect against influenza, tick-borne encephalitis, varicella, hepatitis A and B, rotavirus, Japanese encephalitis, and human papilloma virus (HPV). Others are highly anticipated; among these are vaccines for human immunodeficiency virus (HIV), respiratory syncytial virus (RSV), and several other forms of hepatitis. While a variety of antigenic particles, including recombinant and purified viral protein monomers, are utilized in the formulation of current and next-generation vaccines, this work focuses on the application of a unique characterization technique to the stabilization of fully assembled vaccine candidate viruses and virus-like particles. A brief introduction to this technique shall be given, but first a short review of the use of whole viruses and other particles that contain certain virus-like properties as vaccines is warranted.

A variety of supramolecular assemblies have been utilized in the laboratory development of new vaccines. These include (but are not limited to) virus-like particles (VLPs) and several types of lipid-based particulates such as liposomes, virosomes,

micelles, solid lipid nanoparticles (SLNs), and immune stimulating complexes (ISCOMs). In fact, at least three virosome formulations have been licensed for vaccine use in Europe and other non-US countries. Inflexal® V and Epaxal® are marketed by the Swiss company Crucell for protection against influenza and hepatitis A, respectively, while Solvay Healthcare (Belgium) offers Inviviac®, also for influenza.[3-7] Although several other promising vaccine candidates have been produced in the lipid-based systems mentioned above (as well as others), the following paragraphs will focus only on the use of whole viruses and VLPs as vaccine antigens. The lipid-based systems have been well-reviewed[8-13] and are less germane to the case studies that will be presented in subsequent chapters.

In most cases, the intended result of vaccination is the prophylaxis of infection. Virally-based vaccines are formulations of either whole viruses or of virus-derived materials whose purpose is to elicit a protective immune response from the patient without conferring the pathology associated with actual infection by wild-type virus. While certain vaccines are composed of purified viral proteins as the primary antigen (*e.g.,* subunit influenza vaccines[14-17]), the majority rely upon the enhanced immunogenicity of either attenuated or chemically inactivated whole viruses (or particles that resemble them). Vaccines that are composed of monomeric viral proteins are characterized by reduced immunogenicity and typically make use of adjuvants (chemical compounds which stimulate the immune system without themselves having any significant antigenic effect).[18, 19] Whole viruses and particles that mimic natural viruses in terms of their size and the repetitive presentation of antigen on the particle surface, however, have been proposed to more effectively activate antigen-presenting cells

(APCs). These specialized cells of the innate immune system stimulate the induction of cell-based immunity through presentation of viral peptides bound to their surface major histocompatibility complex (MHC) proteins.[20-28] Such antigen presentation is capable of stimulating not only CD8+ cytotoxic T lymphocytes (CTLs, via the MHC Class I pathway), but also CD4+ helper T cells (via the MHC Class II pathway) whose function is to stimulate the activation of B cells and CTLs. It is now generally accepted that both B and T cell responses to vaccination are required for the induction of long-lasting immunity, emphasizing the role of professional APCs such as dendritic cells (DCs) and macrophages in mounting a protective immune response.[29-32]

Most human viral vaccines are composed of either killed or live, attenuated whole viruses. Besides their intrinsic instability, a concern regarding the use of live, attenuated viruses is the potential for reversion to virulence.[33-36] Averse side effects to components of both killed and live virus formulations have also been reported; typically, these are allergic responses to animal derived proteins (*e.g.,* gelatin in the measles-mumps-rubella vaccine or egg proteins in influenza vaccines).[37, 38] An advantage in the case of live virus formulations, which are intended to infect and replicate non-pathogenically within the host, is the persistence of intact viral genomic materials (*i.e.,* double- and single-stranded RNA or DNA), which have been shown to interact with Toll-like receptors expressed by APCs and trigger the release of pro-inflammatory cytokines that stimulate a more focused adaptive response.[39-48] For this reason (and perhaps others), live virus formulations are generally more immunogenic in comparison to inactivated vaccines.[31]

Other particulate systems that resemble viruses in size and presentation of antigen are being evaluated (and in a few cases, licensed) for use as vaccines. Perhaps foremost

among these are VLPs: self-assembled particles that form spontaneously upon recombinant expression of one or more structural viral proteins.[49-55] While these particles contain none of the native viral genetic information (and thus are replication incompetent), they are otherwise structurally similar to native viruses - so much so that they can be administered as vaccines to induce a protective immune response. VLP-based vaccines have been licensed for both HPV[56-61] and hepatitis B.[62, 63] VLP vaccine candidates for Norwalk virus are now in clinical trials,[64-66] with several others in preclinical development (including influenza VLPs,[67, 68] and additional others that are reviewed in reference 69). Not only have these particles been produced for both enveloped and non-enveloped viral strains,[50, 69] but also chimeric VLPs have been generated from the expression of proteins from multiple strains. The purpose of producing a chimeric VLP is to either confer altered tropism through the expression of non-native cell-targeting proteins, or simply to introduce new immunogens into a familiar vector whose manufacturing and purification requirements are already well-understood.[35, 70-78] In some cases even non-viral antigens have been incorporated; a phase I trial of hepatitis B VLPs containing epitopes from the malaria parasite *Plasmodium falciparum* was recently conducted. Unfortunately, although the vaccine was well-tolerated, it did not induce a strong immune response.[79] VLPs as vaccines offer at least two significant advantages over whole viruses. First, as recombinant particles they are easily produced in insect, yeast, or mammalian cells. The scalability of such production systems offers obvious advantages over the egg-based production method used in several vaccine manufacturing processes (*e.g.,* rabies, influenza).[80] Second, the particles produced do not contain viral genomic material, so the costly (and in some cases dangerous) process of

viral inactivation is simplified if not abrogated. In a similar fashion, the problem of mammalian viral contaminants is abolished if a non-mammalian expression system is utilized.[50, 52, 81]

A number of studies have been devoted to determining the mechanisms by which VLPs are able to induce a protective immune response, showing in some cases that VLPs do not require adjuvants in order to achieve potent immune stimulation. VLPs have been shown to induce cellular maturation and subsequent secretion of cytokines from DCs.[82] One study involving hepatitis B surface antigen showed that both macrophages and DCs are capable of processing and presenting fragments of the 22-nm particles via the MHC Class I pathway.[83] This is true of VLPs derived from non-enveloped viruses such as HPV, [84, 85] as well as those derived from Ebola and Marburg viruses with intact viral envelopes.[86] VLPs can activate both CD4+ and CD8+ lymphocytes, and also instigate humoral immunity.[34, 87-96] One review[69] points out that VLPs may actually have a therapeutic advantage over whole viruses in this context; certain viruses that infect DCs interfere with cellular activation and maturation through the expression of certain viral proteins,[97-99] and even inactivated Marburg and Ebola viruses suppress the activation of DCs, apparently by the presence of one or more native proteins that are absent from VLPs.[86]

The complex molecular architecture of viral assemblies and intricate system of immunological recognition events necessary to induce protective immunity can make the formulation of viral vaccines a difficult task. Mitigating the strong dependence of vaccine potency on storage temperature is perhaps foremost among the concerns of a formulation scientist; a large number of viral vaccines are characterized by thermal instability.[100-102]

Many vaccines that have high immunogenicity (*e.g.,* unadjuvanted formulations of live, attenuated viruses) are formulated as lyophilized solids for this very reason. Adjuvant-containing vaccines typically cannot be frozen, however; aluminum salt adjuvants (the only USFDA-approved adjuvants for human administration) are known to agglomerate upon freezing.[103, 104] Recent work by Chen *et al* indicates a strong correlation between particle agglomeration and reduced potency of an aluminum salt-containing hepatitis B vaccine.[105] On the other hand, Clausi *et al* have demonstrated that the aggregation of Alhydrogel™ (a commercial aluminum hydroxide adjuvant) can be minimized or eliminated if faster drying rates are used, or if sufficient amounts of glass-forming excipients (such as trehalose) are added.[106] The requirement (and industrial preference) that many vaccines be formulated as liquids means that they are susceptible to a multiplicity of chemical and physical degradation processes that must be characterized to support the development of stable formulations. Chemical degradation processes applicable to vaccines include the covalent modification of macromolecular components – often these are induced by light or the presence of chemical contaminants (*e.g.,* oxidants), though processes such as the deamidation of asparagine residues will occur as a function of proton concentration (and protein structure).[107] Physical degradation processes represent another important set of inactivation pathways applicable to all vaccine materials. Physical stability in this context refers to the propensity of vaccine macromolecular components to alter in some way their non-covalent physical properties (such as size, shape, morphology, etc.). Specific examples include changes in protein conformation, and particle aggregation or disintegration. Disruption of protein secondary, tertiary, or quaternary structure can result in the formation of partially unfolded,

aggregation-competent conformations.[108] Another potential result of the structural disruption of vaccine proteins is loss of three-dimensional epitopes or other functional structures required for recognition by the immune system. A similar problem applies to whole viruses and virus-like particles; physical degradation in the form of particle aggregation, disintegration of viral capsids, or disruption of viral membranes can interfere with recognition by the immune system and/or infection of target cells. While chemical modifications to vaccine components are easily detected by well-established chromatographic and mass spectrometry-based techniques, a number of calorimetric, spectroscopic, and light scattering methods are available that enable characterization of the physical stability of macromolecular systems, including virally-based vaccine candidates. A brief and general description of a relevant subset of these techniques will be given here, while notes on their specific application will appear in the case studies outlined in following chapters.

Differential scanning calorimetry (DSC) is a relatively simple technique that can yield quantitative comparisons of the thermostabilty of vaccine formulations.[109-113] Since it is a general method that measures the change in heat capacity as a function of temperature,[114, 115] it typically does not provide molecular level detail when used in the characterization of complex macromolecular assemblies. Rigorous thermodynamic analysis can be performed using DSC data when the measured transitions are reversible, but this is rarely observed in the case of complicated, multicomponent particles such as viruses and VLPs. One drawback to DSC is that, in comparison to light scattering and spectroscopic techniques, it typically requires samples of higher concentration to accurately measure reproducible thermal transitions

Both static and dynamic light scattering measurements are useful in the analysis of the physical stability of macromolecular systems, including viral particulates.[116-120] Static light scattering (SLS) can be used to determine the molecular weight and radius of gyration of particles in solution. As the intensity of scattered light depends on the refractive index increment as well as the size and shape of scattering particles,[114] SLS is also sensitive to physical alterations that lead to changes in particle refractive index (*e.g.,* changes in particle density due to swelling). Dynamic light scattering (DLS) methods make direct measurements of particle hydrodynamic radii through mathematical analysis of fluctuations in the intensity of scattered light caused by the particles' Brownian motion within a small solution volume,[121] and are thus well-suited to detecting changes in particle size due to aggregation, swelling, or disintegration.[122-124]

A variety of spectroscopic techniques are applicable to the physical characterization of vaccine materials. Circular dichroism (CD) and fluorescence spectroscopies are among the most versatile and widely-implemented, though high-resolution second derivative ultraviolet (UV) absorption spectroscopy has also been used in many cases for the characterization of vaccines and other protein-containing materials.[125-128] CD, which detects differences between sample absorption of right- and left-handed circularly polarized light, is used to monitor the secondary structure of proteins when the incident light is from the far-UV region.[114, 129] Due to electronic transitions that are controlled by the interaction between amide group electric and magnetic dipole transition moments,[130] secondary structural elements (*i.e.,* α-helix, β-sheet, random coil, etc.) have characteristic spectral signatures that result from the repeating conformation of the amide polypeptide backbone.[114, 131] The intrinsic

fluorescence of proteins is due to the aromatic side chains of phenylalanine, tryptophan, and tyrosine, although the fluorescence of tryptophan is of much greater magnitude (and utility) due to its significantly higher quantum yield. Due to their apolar character, the side chains of aromatic amino acids are often located in solvent-restricted domains of ordered proteins. As the fluorescence properties of these residues are sensitive to the polarity of their local environment, intrinsic fluorescence measurements are commonly used to detect the presence of non-native protein tertiary structural conformations that result from changes to the solvent accessibility of amino acid fluorophores.[132-136] Extrinsic fluorescence methods that make use of small molecular probes to detect physical changes to macromolecular systems are also available.[137] The use of these compounds also generally relies on the response of their fluorescence properties to the polarity of their local environment. The structural variety and small size of these molecules allows the selection of probes that display affinity for specific viral structures, such as non-polar protein regions[138-140] or the lipid bilayer[141, 142] that surrounds enveloped viruses.

The use of biophysical characterization methods as formulation tools for virus-derived vaccines relies on the widely accepted relationship between macromolecular structure and function. In the context of viral systems, the techniques described above cannot be used to derive high-resolution (atomic level) descriptions of physical stability. On the other hand, viruses and VLPs are composed of macromolecular structural elements that have well-defined physical structures essential for their normal functions *in vivo*. Such virus-derived particles are therefore normally characterized by well-defined size and shape parameters, and also typically yield reproducible spectroscopic signatures

that can be detected by an assortment of complementary techniques. As the signals from these techniques derive from the well-defined structural elements of viral particulates, changes in their values can reasonably be assigned to alterations in critical structural features responsible for immunogenicity. One challenge in the use of these measurements as formulation tools is the integration of signals from the oft-required large number of techniques required to obtain a comprehensive representation of the physical stability of complex particles. One way to overcome this difficulty is the use of a relatively recent vector-based visualization technique that is capable of synthesizing a large number of biophysical measurements from a variety of techniques into an empirical phase diagram (EPD) that represents changes in physical state as a function of relevant stress factors.[127, 143-145] While other, high-resolution structural techniques such as nuclear magnetic resonance (NMR) and X-ray crystallography literally strive to obtain atomic-level pictures of macromolecular systems, the EPD approach is somewhat opposite. The basis of this approach is the construction of an abstract, highly dimensional vector-based description of the system under scrutiny. This completely mathematical representation of the system is then subjected to a series of linear algebraic operations, allowing distillation of a large number of vector components (directly obtained from the original biophysical dataset) into a three-color block diagram that discriminates the most important physical alterations by analysis of their relative magnitudes. These physical alterations are represented by boundaries between colored blocks (phases) that appear as a function of stress factors applied in the original experiments. The following chapters present a series of case-studies in which this approach has been applied to the stabilization of several

viral vaccine candidates, including VLPs for Norwalk and influenza viruses, as well as a live, attenuated measles virus.

References

1. Andre, F. E., Vaccinology: past achievements, present roadblocks and future promises. *Vaccine* **2003,** 21, (7-8), 593-5.
2. Hansson, M.; Nygren, P. A.; Stahl, S., Design and production of recombinant subunit vaccines. *Biotechnol Appl Biochem* **2000,** 32 (Pt 2), 95-107.
3. Herzog, C.; Hartmann, K.; Kunzi, V.; Kursteiner, O.; Mischler, R.; Lazar, H.; Gluck, R., Eleven years of Inflexal V-a virosomal adjuvanted influenza vaccine. *Vaccine* **2009,** 27, (33), 4381-7.
4. Schijns, V. E. J. C.; O'Hagan, D. T., *Immunopotentiators in modern vaccines*. Elsevier Academic Press: Amsterdam ; Boston, 2006.
5. Huckriede, A.; Bungener, L.; Stegmann, T.; Daemen, T.; Medema, J.; Palache, A. M.; Wilschut, J., The virosome concept for influenza vaccines. *Vaccine* **2005,** 23 Suppl 1, S26-38.
6. de Bruijn, I. A.; Nauta, J.; Cramer, W. C.; Gerez, L.; Palache, A. M., Clinical experience with inactivated, virosomal influenza vaccine. *Vaccine* **2005,** 23 Suppl 1, S39-49.
7. Mischler, R.; Metcalfe, I. C., Inflexal V a trivalent virosome subunit influenza vaccine: production. *Vaccine* **2002,** 20 Suppl 5, B17-23.
8. Morein, B.; Simons, K., Subunit vaccines against enveloped viruses: virosomes, micelles and other protein complexes. *Vaccine* **1985,** 3, (2), 83-93.
9. Vajdy, M.; Srivastava, I.; Polo, J.; Donnelly, J.; O'Hagan, D.; Singh, M., Mucosal adjuvants and delivery systems for protein-, DNA- and RNA-based vaccines. *Immunol Cell Biol* **2004,** 82, (6), 617-27.

10. Copland, M. J.; Rades, T.; Davies, N. M.; Baird, M. A., Lipid based particulate formulations for the delivery of antigen. *Immunol Cell Biol* **2005,** 83, (2), 97-105.

11. Cusi, M. G., Applications of influenza virosomes as a delivery system. *Hum Vaccin* **2006,** 2, (1), 1-7.

12. Scheerlinck, J. P.; Greenwood, D. L., Virus-sized vaccine delivery systems. *Drug Discov Today* **2008,** 13, (19-20), 882-7.

13. Sharma, S.; Mukkur, T. K.; Benson, H. A.; Chen, Y., Pharmaceutical aspects of intranasal delivery of vaccines using particulate systems. *J Pharm Sci* **2009,** 98, (3), 812-43.

14. Wilschut, J.; McElhaney, J. E., *Rapid reference to influenza*. Mosby Elsevier Limited: London ;, 2005; 216 p.

15. Wood, J.; Williams, M., History of Inactivated Vaccines. In *Textbook of influenza*, Nicholson, K. G.; Webster, R. G.; Hay, A. J., Eds. Blackwell Science: Oxford ; Malden, Mass, 1998; pp 317-323.

16. Furminger, I., Vaccine Production. In *Textbook of influenza*, Nicholson, K. G.; Webster, R. G.; Hay, A. J., Eds. Blackwell Science: Oxford ; Malden, Mass, 1998; pp 324-332.

17. Wood, J., Standardization of inactivated influenza vaccines. In *Textbook of influenza*, Nicholson, K. G.; Webster, R. G.; Hay, A. J., Eds. Blackwell Science: Oxford ; Malden, Mass, 1998; pp 333-345.

18. Singh, M.; O'Hagan, D., Advances in vaccine adjuvants. *Nat Biotechnol* **1999,** 17, (11), 1075-81.

19. Singh, M.; O'Hagan, D. T., Recent advances in vaccine adjuvants. *Pharm Res* **2002,** 19, (6), 715-28.

20. Bungener, L.; Huckriede, A.; de Mare, A.; de Vries-Idema, J.; Wilschut, J.; Daemen, T., Virosome-mediated delivery of protein antigens in vivo: efficient induction of class I MHC-restricted cytotoxic T lymphocyte activity. *Vaccine* **2005,** 23, (10), 1232-41.

21. Bungener, L.; Serre, K.; Bijl, L.; Leserman, L.; Wilschut, J.; Daemen, T.; Machy, P., Virosome-mediated delivery of protein antigens to dendritic cells. *Vaccine* **2002,** 20, (17-18), 2287-95.

22. Durrer, P.; Gluck, U.; Spyr, C.; Lang, A. B.; Zurbriggen, R.; Herzog, C.; Gluck, R., Mucosal antibody response induced with a nasal virosome-based influenza vaccine. *Vaccine* **2003,** 21, (27-30), 4328-34.

23. Fifis, T.; Gamvrellis, A.; Crimeen-Irwin, B.; Pietersz, G. A.; Li, J.; Mottram, P. L.; McKenzie, I. F.; Plebanski, M., Size-dependent immunogenicity: therapeutic and protective properties of nano-vaccines against tumors. *J Immunol* **2004,** 173, (5), 3148-54.

24. Gamvrellis, A.; Leong, D.; Hanley, J. C.; Xiang, S. D.; Mottram, P.; Plebanski, M., Vaccines that facilitate antigen entry into dendritic cells. *Immunol Cell Biol* **2004,** 82, (5), 506-16.

25. Lambkin, R.; Oxford, J. S.; Bossuyt, S.; Mann, A.; Metcalfe, I. C.; Herzog, C.; Viret, J. F.; Gluck, R., Strong local and systemic protective immunity induced in the ferret model by an intranasal virosome-formulated influenza subunit vaccine. *Vaccine* **2004,** 22, (31-32), 4390-6.

26. Yewdell, J. W.; Bennink, J. R., Cell biology of antigen processing and presentation to major histocompatibility complex class I molecule-restricted T lymphocytes. *Adv Immunol* **1992,** 52, 1-123.

27. Germain, R. N.; Margulies, D. H., The biochemistry and cell biology of antigen processing and presentation. *Annu Rev Immunol* **1993,** 11, 403-50.

28. Serre, K.; Machy, P.; Grivel, J. C.; Jolly, G.; Brun, N.; Barbet, J.; Leserman, L., Efficient presentation of multivalent antigens targeted to various cell surface molecules of dendritic cells and surface Ig of antigen-specific B cells. *J Immunol* **1998,** 161, (11), 6059-67.

29. Banchereau, J.; Briere, F.; Caux, C.; Davoust, J.; Lebecque, S.; Liu, Y. J.; Pulendran, B.; Palucka, K., Immunobiology of dendritic cells. *Annu Rev Immunol* **2000,** 18, 767-811.

30. Banchereau, J.; Steinman, R. M., Dendritic cells and the control of immunity. *Nature* **1998,** 392, (6673), 245-52.

31. Fields, B. N.; Knipe, D. M.; Howley, P. M., *Fields' virology*. 5th ed.; Wolters Kluwer Health/Lippincott Williams & Wilkins: Philadelphia, 2007; 3091 p.

32. Zinkernagel, R. M.; Hengartner, H., Regulation of the immune response by antigen. *Science* **2001,** 293, (5528), 251-3.

33. Peek, L. J.; Middaugh, C. R.; Berkland, C., Nanotechnology in vaccine delivery. *Adv Drug Deliv Rev* **2008,** 60, (8), 915-28.

34. Young, K. R.; McBurney, S. P.; Karkhanis, L. U.; Ross, T. M., Virus-like particles: designing an effective AIDS vaccine. *Methods* **2006,** 40, (1), 98-117.

35. Doan, L. X.; Li, M.; Chen, C.; Yao, Q., Virus-like particles as HIV-1 vaccines. *Rev Med Virol* **2005,** 15, (2), 75-88.

36. Kew, O. M.; Wright, P. F.; Agol, V. I.; Delpeyroux, F.; Shimizu, H.; Nathanson, N.; Pallansch, M. A., Circulating vaccine-derived polioviruses: current state of knowledge. *Bull World Health Organ* **2004,** 82, (1), 16-23.

37. Kelso, J. M.; Yunginger, J. W., Immunization of egg-allergic individuals with egg- or chicken-derived vaccines. *Immunol Allergy Clin North Am* **2003,** 23, (4), 635-48.

38. Patja, A.; Makinen-Kiljunen, S.; Davidkin, I.; Paunio, M.; Peltola, H., Allergic reactions to measles-mumps-rubella vaccination. *Pediatrics* **2001,** 107, (2), E27.

39. Fearon, D. T., Seeking wisdom in innate immunity. *Nature* **1997,** 388, (6640), 323-4.

40. Fearon, D. T.; Locksley, R. M., The instructive role of innate immunity in the acquired immune response. *Science* **1996,** 272, (5258), 50-3.

41. Kawai, T.; Akira, S., Innate immune recognition of viral infection. *Nat Immunol* **2006,** 7, (2), 131-7.

42. Schulz, O.; Diebold, S. S.; Chen, M.; Naslund, T. I.; Nolte, M. A.; Alexopoulou, L.; Azuma, Y. T.; Flavell, R. A.; Liljestrom, P.; Reis e Sousa, C., Toll-like receptor 3 promotes cross-priming to virus-infected cells. *Nature* **2005,** 433, (7028), 887-92.

43. Wang, T.; Town, T.; Alexopoulou, L.; Anderson, J. F.; Fikrig, E.; Flavell, R. A., Toll-like receptor 3 mediates West Nile virus entry into the brain causing lethal encephalitis. *Nat Med* **2004,** 10, (12), 1366-73.

44. Heil, F.; Hemmi, H.; Hochrein, H.; Ampenberger, F.; Kirschning, C.; Akira, S.; Lipford, G.; Wagner, H.; Bauer, S., Species-specific recognition of single-stranded RNA via toll-like receptor 7 and 8. *Science* **2004,** 303, (5663), 1526-9.

45. Diebold, S. S.; Kaisho, T.; Hemmi, H.; Akira, S.; Reis e Sousa, C., Innate antiviral responses by means of TLR7-mediated recognition of single-stranded RNA. *Science* **2004,** 303, (5663), 1529-31.

46. Lund, J. M.; Alexopoulou, L.; Sato, A.; Karow, M.; Adams, N. C.; Gale, N. W.; Iwasaki, A.; Flavell, R. A., Recognition of single-stranded RNA viruses by Toll-like receptor 7. *Proc Natl Acad Sci U S A* **2004,** 101, (15), 5598-603.

47. Colonna, M.; Trinchieri, G.; Liu, Y. J., Plasmacytoid dendritic cells in immunity. *Nat Immunol* **2004,** 5, (12), 1219-26.

48. Liu, Y. J., IPC: professional type 1 interferon-producing cells and plasmacytoid dendritic cell precursors. *Annu Rev Immunol* **2005,** 23, 275-306.

49. French, T. J.; Marshall, J. J.; Roy, P., Assembly of double-shelled, viruslike particles of bluetongue virus by the simultaneous expression of four structural proteins. *J Virol* **1990,** 64, (12), 5695-700.

50. Noad, R.; Roy, P., Virus-like particles as immunogens. *Trends Microbiol* **2003,** 11, (9), 438-44.

51. Pattenden, L. K.; Middelberg, A. P.; Niebert, M.; Lipin, D. I., Towards the preparative and large-scale precision manufacture of virus-like particles. *Trends Biotechnol* **2005,** 23, (10), 523-9.

52. Roy, P.; Noad, R., Virus-like particles as a vaccine delivery system: myths and facts. *Hum Vaccin* **2008,** 4, (1), 5-12.

53. Miyanohara, A.; Imamura, T.; Araki, M.; Sugawara, K.; Ohtomo, N.; Matsubara, K., Expression of hepatitis B virus core antigen gene in Saccharomyces cerevisiae: synthesis of two polypeptides translated from different initiation codons. *J Virol* **1986,** 59, (1), 176-80.

54. Delchambre, M.; Gheysen, D.; Thines, D.; Thiriart, C.; Jacobs, E.; Verdin, E.; Horth, M.; Burny, A.; Bex, F., The GAG precursor of simian immunodeficiency virus assembles into virus-like particles. *Embo J* **1989,** 8, (9), 2653-60.

55. Gheysen, D.; Jacobs, E.; de Foresta, F.; Thiriart, C.; Francotte, M.; Thines, D.; De Wilde, M., Assembly and release of HIV-1 precursor Pr55gag virus-like particles from recombinant baculovirus-infected insect cells. *Cell* **1989,** 59, (1), 103-12.

56. Zhou, J.; Sun, X. Y.; Stenzel, D. J.; Frazer, I. H., Expression of vaccinia recombinant HPV 16 L1 and L2 ORF proteins in epithelial cells is sufficient for assembly of HPV virion-like particles. *Virology* **1991,** 185, (1), 251-7.

57. Kirnbauer, R.; Booy, F.; Cheng, N.; Lowy, D. R.; Schiller, J. T., Papillomavirus L1 major capsid protein self-assembles into virus-like particles that are highly immunogenic. *Proc Natl Acad Sci U S A* **1992,** 89, (24), 12180-4.

58. Franco, E. L.; Harper, D. M., Vaccination against human papillomavirus infection: a new paradigm in cervical cancer control. *Vaccine* **2005,** 23, (17-18), 2388-94.

59. Harper, D. M.; Franco, E. L.; Wheeler, C. M.; Moscicki, A. B.; Romanowski, B.; Roteli-Martins, C. M.; Jenkins, D.; Schuind, A.; Costa Clemens, S. A.; Dubin, G., Sustained efficacy up to 4.5 years of a bivalent L1 virus-like particle vaccine

against human papillomavirus types 16 and 18: follow-up from a randomised control trial. *Lancet* **2006,** 367, (9518), 1247-55.

60. Evans, T. G.; Bonnez, W.; Rose, R. C.; Koenig, S.; Demeter, L.; Suzich, J. A.; O'Brien, D.; Campbell, M.; White, W. I.; Balsley, J.; Reichman, R. C., A Phase 1 study of a recombinant viruslike particle vaccine against human papillomavirus type 11 in healthy adult volunteers. *J Infect Dis* **2001,** 183, (10), 1485-93.

61. Kirnbauer, R.; Taub, J.; Greenstone, H.; Roden, R.; Durst, M.; Gissmann, L.; Lowy, D. R.; Schiller, J. T., Efficient self-assembly of human papillomavirus type 16 L1 and L1-L2 into virus-like particles. *J Virol* **1993,** 67, (12), 6929-36.

62. McAleer, W. J.; Buynak, E. B.; Maigetter, R. Z.; Wampler, D. E.; Miller, W. J.; Hilleman, M. R., Human hepatitis B vaccine from recombinant yeast. *Nature* **1984,** 307, (5947), 178-80.

63. Venters, C.; Graham, W.; Cassidy, W., Recombivax-HB: perspectives past, present and future. *Expert Rev Vaccines* **2004,** 3, (2), 119-29.

64. Ball, J. M.; Graham, D. Y.; Opekun, A. R.; Gilger, M. A.; Guerrero, R. A.; Estes, M. K., Recombinant Norwalk virus-like particles given orally to volunteers: phase I study. *Gastroenterology* **1999,** 117, (1), 40-8.

65. Tacket, C. O.; Sztein, M. B.; Losonsky, G. A.; Wasserman, S. S.; Estes, M. K., Humoral, mucosal, and cellular immune responses to oral Norwalk virus-like particles in volunteers. *Clin Immunol* **2003,** 108, (3), 241-7.

66. Mason, H. S.; Ball, J. M.; Shi, J. J.; Jiang, X.; Estes, M. K.; Arntzen, C. J., Expression of Norwalk virus capsid protein in transgenic tobacco and potato and

its oral immunogenicity in mice. *Proc Natl Acad Sci U S A* **1996,** 93, (11), 5335-40.

67. Bright, R. A.; Carter, D. M.; Crevar, C. J.; Toapanta, F. R.; Steckbeck, J. D.; Cole, K. S.; Kumar, N. M.; Pushko, P.; Smith, G.; Tumpey, T. M.; Ross, T. M., Cross-clade protective immune responses to influenza viruses with H5N1 HA and NA elicited by an influenza virus-like particle. *PLoS One* **2008,** 3, (1), e1501.

68. Haynes, J. R., Influenza virus-like particle vaccines. *Expert Rev Vaccines* **2009,** 8, (4), 435-45.

69. Grgacic, E. V.; Anderson, D. A., Virus-like particles: passport to immune recognition. *Methods* **2006,** 40, (1), 60-5.

70. Niikura, M.; Takamura, S.; Kim, G.; Kawai, S.; Saijo, M.; Morikawa, S.; Kurane, I.; Li, T. C.; Takeda, N.; Yasutomi, Y., Chimeric recombinant hepatitis E virus-like particles as an oral vaccine vehicle presenting foreign epitopes. *Virology* **2002,** 293, (2), 273-80.

71. Netter, H. J.; Macnaughton, T. B.; Woo, W. P.; Tindle, R.; Gowans, E. J., Antigenicity and immunogenicity of novel chimeric hepatitis B surface antigen particles with exposed hepatitis C virus epitopes. *J Virol* **2001,** 75, (5), 2130-41.

72. Pumpens, P.; Grens, E., HBV core particles as a carrier for B cell/T cell epitopes. *Intervirology* **2001,** 44, (2-3), 98-114.

73. Sojikul, P.; Buehner, N.; Mason, H. S., A plant signal peptide-hepatitis B surface antigen fusion protein with enhanced stability and immunogenicity expressed in plant cells. *Proc Natl Acad Sci U S A* **2003,** 100, (5), 2209-14.

74. Bisht, H.; Chugh, D. A.; Swaminathan, S.; Khanna, N., Expression and purification of Dengue virus type 2 envelope protein as a fusion with hepatitis B surface antigen in Pichia pastoris. *Protein Expr Purif* **2001,** 23, (1), 84-96.

75. Bisht, H.; Chugh, D. A.; Raje, M.; Swaminathan, S. S.; Khanna, N., Recombinant dengue virus type 2 envelope/hepatitis B surface antigen hybrid protein expressed in Pichia pastoris can function as a bivalent immunogen. *J Biotechnol* **2002,** 99, (2), 97-110.

76. Deml, L.; Speth, C.; Dierich, M. P.; Wolf, H.; Wagner, R., Recombinant HIV-1 Pr55gag virus-like particles: potent stimulators of innate and acquired immune responses. *Mol Immunol* **2005,** 42, (2), 259-77.

77. Liu, W. J.; Liu, X. S.; Zhao, K. N.; Leggatt, G. R.; Frazer, I. H., Papillomavirus virus-like particles for the delivery of multiple cytotoxic T cell epitopes. *Virology* **2000,** 273, (2), 374-82.

78. Dale, C. J.; Liu, X. S.; De Rose, R.; Purcell, D. F.; Anderson, J.; Xu, Y.; Leggatt, G. R.; Frazer, I. H.; Kent, S. J., Chimeric human papilloma virus-simian/human immunodeficiency virus virus-like-particle vaccines: immunogenicity and protective efficacy in macaques. *Virology* **2002,** 301, (1), 176-87.

79. Gregson, A. L.; Oliveira, G.; Othoro, C.; Calvo-Calle, J. M.; Thorton, G. B.; Nardin, E.; Edelman, R., Phase I trial of an alhydrogel adjuvanted hepatitis B core virus-like particle containing epitopes of Plasmodium falciparum circumsporozoite protein. *PLoS One* **2008,** 3, (2), e1556.

80. Maranga, L.; Rueda, P.; Antonis, A. F.; Vela, C.; Langeveld, J. P.; Casal, J. I.; Carrondo, M. J., Large scale production and downstream processing of a

recombinant porcine parvovirus vaccine. *Appl Microbiol Biotechnol* **2002,** 59, (1), 45-50.

81. Rueda, P.; Fominaya, J.; Langeveld, J. P.; Bruschke, C.; Vela, C.; Casal, J. I., Effect of different baculovirus inactivation procedures on the integrity and immunogenicity of porcine parvovirus-like particles. *Vaccine* **2000,** 19, (7-8), 726-34.

82. Stahl, S. J.; Murray, K., Immunogenicity of peptide fusions to hepatitis B virus core antigen. *Proc Natl Acad Sci U S A* **1989,** 86, (16), 6283-7.

83. Eckhart, L.; Raffelsberger, W.; Ferko, B.; Klima, A.; Purtscher, M.; Katinger, H.; Ruker, F., Immunogenic presentation of a conserved gp41 epitope of human immunodeficiency virus type 1 on recombinant surface antigen of hepatitis B virus. *J Gen Virol* **1996,** 77 (Pt 9), 2001-8.

84. Lenz, P.; Day, P. M.; Pang, Y. Y.; Frye, S. A.; Jensen, P. N.; Lowy, D. R.; Schiller, J. T., Papillomavirus-like particles induce acute activation of dendritic cells. *J Immunol* **2001,** 166, (9), 5346-55.

85. Yang, R.; Wheeler, C. M.; Chen, X.; Uematsu, S.; Takeda, K.; Akira, S.; Pastrana, D. V.; Viscidi, R. P.; Roden, R. B., Papillomavirus capsid mutation to escape dendritic cell-dependent innate immunity in cervical cancer. *J Virol* **2005,** 79, (11), 6741-50.

86. Bosio, C. M.; Moore, B. D.; Warfield, K. L.; Ruthel, G.; Mohamadzadeh, M.; Aman, M. J.; Bavari, S., Ebola and Marburg virus-like particles activate human myeloid dendritic cells. *Virology* **2004,** 326, (2), 280-7.

87. Kang, S. M.; Yoo, D. G.; Lipatov, A. S.; Song, J. M.; Davis, C. T.; Quan, F. S.; Chen, L. M.; Donis, R. O.; Compans, R. W., Induction of long-term protective immune responses by influenza H5N1 virus-like particles. *PLoS One* **2009,** 4, (3), e4667.

88. Lo-Man, R.; Rueda, P.; Sedlik, C.; Deriaud, E.; Casal, I.; Leclerc, C., A recombinant virus-like particle system derived from parvovirus as an efficient antigen carrier to elicit a polarized Th1 immune response without adjuvant. *Eur J Immunol* **1998,** 28, (4), 1401-7.

89. Paliard, X.; Liu, Y.; Wagner, R.; Wolf, H.; Baenziger, J.; Walker, C. M., Priming of strong, broad, and long-lived HIV type 1 p55gag-specific CD8+ cytotoxic T cells after administration of a virus-like particle vaccine in rhesus macaques. *AIDS Res Hum Retroviruses* **2000,** 16, (3), 273-82.

90. Sedlik, C.; Saron, M.; Sarraseca, J.; Casal, I.; Leclerc, C., Recombinant parvovirus-like particles as an antigen carrier: a novel nonreplicative exogenous antigen to elicit protective antiviral cytotoxic T cells. *Proc Natl Acad Sci U S A* **1997,** 94, (14), 7503-8.

91. Moron, G.; Rueda, P.; Casal, I.; Leclerc, C., CD8alpha- CD11b+ dendritic cells present exogenous virus-like particles to CD8+ T cells and subsequently express CD8alpha and CD205 molecules. *J Exp Med* **2002,** 195, (10), 1233-45.

92. Roth, J. F., The yeast Ty virus-like particles. *Yeast* **2000,** 16, (9), 785-95.

93. Pumpens, P.; Borisova, G. P.; Crowther, R. A.; Grens, E., Hepatitis B virus core particles as epitope carriers. *Intervirology* **1995,** 38, (1-2), 63-74.

94. Schiller, J. T.; Lowy, D. R., Papillomavirus-like particles and HPV vaccine development. *Semin Cancer Biol* **1996,** 7, (6), 373-82.

95. Warfield, K. L.; Bosio, C. M.; Welcher, B. C.; Deal, E. M.; Mohamadzadeh, M.; Schmaljohn, A.; Aman, M. J.; Bavari, S., Ebola virus-like particles protect from lethal Ebola virus infection. *Proc Natl Acad Sci U S A* **2003,** 100, (26), 15889-94.

96. Chackerian, B.; Lowy, D. R.; Schiller, J. T., Conjugation of a self-antigen to papillomavirus-like particles allows for efficient induction of protective autoantibodies. *J Clin Invest* **2001,** 108, (3), 415-23.

97. Hertel, L.; Lacaille, V. G.; Strobl, H.; Mellins, E. D.; Mocarski, E. S., Susceptibility of immature and mature Langerhans cell-type dendritic cells to infection and immunomodulation by human cytomegalovirus. *J Virol* **2003,** 77, (13), 7563-74.

98. Ostrowski, M.; Vermeulen, M.; Zabal, O.; Geffner, J. R.; Sadir, A. M.; Lopez, O. J., Impairment of thymus-dependent responses by murine dendritic cells infected with foot-and-mouth disease virus. *J Immunol* **2005,** 175, (6), 3971-9.

99. Teleshova, N.; Frank, I.; Pope, M., Immunodeficiency virus exploitation of dendritic cells in the early steps of infection. *J Leukoc Biol* **2003,** 74, (5), 683-90.

100. Newman, J. F.; Tirrell, S.; Ullman, C.; Piatti, P. G.; Brown, F., Stabilising oral poliovaccine at high ambient temperatures. *Dev Biol Stand* **1996,** 87, 103-11.

101. Burke, C. J.; Hsu, T. A.; Volkin, D. B., Formulation, stability, and delivery of live attenuated vaccines for human use. *Crit Rev Ther Drug Carrier Syst* **1999,** 16, (1), 1-83.

102. Peetermans, J., Factors affecting the stability of viral vaccines. *Dev Biol Stand* **1996,** 87, 97-101.

103. Maa, Y. F.; Zhao, L.; Payne, L. G.; Chen, D., Stabilization of alum-adjuvanted vaccine dry powder formulations: mechanism and application. *J Pharm Sci* **2003,** 92, (2), 319-32.

104. Clausi, A.; Cummiskey, J.; Merkley, S.; Carpenter, J. F.; Braun, L. J.; Randolph, T. W., Influence of particle size and antigen binding on effectiveness of aluminum salt adjuvants in a model lysozyme vaccine. *J Pharm Sci* **2008,** 97, (12), 5252-62.

105. Chen, D.; Tyagi, A.; Carpenter, J.; Perkins, S.; Sylvester, D.; Guy, M.; Kristensen, D. D.; Braun, L. J., Characterization of the freeze sensitivity of a hepatitis B vaccine. *Hum Vaccin* **2009,** 5, (1), 26-32.

106. Clausi, A. L.; Merkley, S. A.; Carpenter, J. F.; Randolph, T. W., Inhibition of aggregation of aluminum hydroxide adjuvant during freezing and drying. *J Pharm Sci* **2008,** 97, (6), 2049-61.

107. Wakankar, A. A.; Borchardt, R. T., Formulation considerations for proteins susceptible to asparagine deamidation and aspartate isomerization. *J Pharm Sci* **2006,** 95, (11), 2321-36.

108. Chi, E. Y.; Krishnan, S.; Randolph, T. W.; Carpenter, J. F., Physical stability of proteins in aqueous solution: mechanism and driving forces in nonnative protein aggregation. *Pharm Res* **2003,** 20, (9), 1325-36.

109. Abdul-Fattah, A. M.; Truong-Le, V.; Yee, L.; Pan, E.; Ao, Y.; Kalonia, D. S.; Pikal, M. J., Drying-induced variations in physico-chemical properties of

amorphous pharmaceuticals and their impact on Stability II: stability of a vaccine. *Pharm Res* **2007,** 24, (4), 715-27.

110. Le Tallec, D.; Doucet, D.; Elouahabi, A.; Harvengt, P.; Deschuyteneer, M.; Deschamps, M., Cervarix, the GSK HPV-16/HPV-18 AS04-adjuvanted cervical cancer vaccine, demonstrates stability upon long-term storage and under simulated cold chain break conditions. *Hum Vaccin* **2009,** 5, (7), 467-74.

111. Ausar, S. F.; Foubert, T. R.; Hudson, M. H.; Vedvick, T. S.; Middaugh, C. R., Conformational stability and disassembly of Norwalk virus-like particles. Effect of pH and temperature. *J Biol Chem* **2006,** 281, (28), 19478-88.

112. Chen, C. H.; Wu, R.; Roth, L. G.; Guillot, S.; Crainic, R., Elucidating mechanisms of thermostabilization of poliovirus by D2O and MgCl2. *Arch Biochem Biophys* **1997,** 342, (1), 108-16.

113. Krell, T.; Manin, C.; Nicolai, M. C.; Pierre-Justin, C.; Berard, Y.; Brass, O.; Gerentes, L.; Leung-Tack, P.; Chevalier, M., Characterization of different strains of poliovirus and influenza virus by differential scanning calorimetry. *Biotechnol Appl Biochem* **2005,** 41, (Pt 3), 241-6.

114. Van Holde, K. E.; Johnson, W. C.; Ho, P. S., *Principles of physical biochemistry*. 2nd ed.; Pearson/Prentice Hall: Upper Saddle River, N.J., 2006; 710 p.

115. Krishinan, K. S.; Brandts, J. F., Scanning calorimetry. *Methods Enzymol* **1978,** 49, 3-14.

116. Cai, S.; He, F.; Samra, H. S.; de la Maza, L. M.; Bottazzi, M. E.; Joshi, S. B.; Middaugh, C. R., Biophysical and Stabilization Studies of the Chlamydia

trachomatis Mouse Pneumonitis Major Outer Membrane Protein. *Mol Pharm* **2009**.

117. He, F.; Joshi, S. B.; Bosman, F.; Verhaeghe, M.; Middaugh, C. R., Structural stability of hepatitis C virus envelope glycoprotein E1: effect of pH and dissociative detergents. *J Pharm Sci* **2009,** 98, (9), 3340-57.

118. Minton, A. P., Static light scattering from concentrated protein solutions, I: General theory for protein mixtures and application to self-associating proteins. *Biophys J* **2007,** 93, (4), 1321-8.

119. Ehrlich, L. S.; Liu, T.; Scarlata, S.; Chu, B.; Carter, C. A., HIV-1 capsid protein forms spherical (immature-like) and tubular (mature-like) particles in vitro: structure switching by pH-induced conformational changes. *Biophys J* **2001,** 81, (1), 586-94.

120. Zanier, K.; Nomine, Y.; Charbonnier, S.; Ruhlmann, C.; Schultz, P.; Schweizer, J.; Trave, G., Formation of well-defined soluble aggregates upon fusion to MBP is a generic property of E6 proteins from various human papillomavirus species. *Protein Expr Purif* **2007,** 51, (1), 59-70.

121. Lomakin, A.; Teplow, D. B.; Benedek, G. B., Quasielastic light scattering for protein assembly studies. *Methods Mol Biol* **2005,** 299, 153-74.

122. Tran, T. L.; Castagne, N.; Dubosclard, V.; Noinville, S.; Koch, E.; Moudjou, M.; Henry, C.; Bernard, J.; Yeo, R. P.; Eleouet, J. F., The respiratory syncytial virus M2-1 protein forms tetramers and interacts with RNA and P in a competitive manner. *J Virol* **2009,** 83, (13), 6363-74.

123. Mellado, M. C.; Mena, J. A.; Lopes, A.; Ramirez, O. T.; Carrondo, M. J.; Palomares, L. A.; Alves, P. M., Impact of physicochemical parameters on in vitro assembly and disassembly kinetics of recombinant triple-layered rotavirus-like particles. *Biotechnol Bioeng* **2009**.

124. Hagenaars, N.; Mastrobattista, E.; Verheul, R. J.; Mooren, I.; Glansbeek, H. L.; Heldens, J. G.; van den Bosch, H.; Jiskoot, W., Physicochemical and immunological characterization of N,N,N-trimethyl chitosan-coated whole inactivated influenza virus vaccine for intranasal administration. *Pharm Res* **2009,** 26, (6), 1353-64.

125. Mach, H.; Thomson, J. A.; Middaugh, C. R., Quantitative analysis of protein mixtures by second derivative absorption spectroscopy. *Anal Biochem* **1989,** 181, (1), 79-85.

126. Mach, H.; Volkin, D. B.; Burke, C. J.; Middaugh, C. R., Ultraviolet absorption spectroscopy. *Methods Mol Biol* **1995,** 40, 91-114.

127. Fan, H.; Ralston, J.; Dibiase, M.; Faulkner, E.; Middaugh, C. R., Solution behavior of IFN-beta-1a: an empirical phase diagram based approach. *J Pharm Sci* **2005,** 94, (9), 1893-911.

128. Mach, H.; Middaugh, C. R., Simultaneous monitoring of the environment of tryptophan, tyrosine, and phenylalanine residues in proteins by near-ultraviolet second-derivative spectroscopy. *Anal Biochem* **1994,** 222, (2), 323-31.

129. Sreerama, N.; Woody, R. W., Circular dichroism of peptides and proteins. In *Circular dichroism : principles and applications*, 2nd ed.; Berova, N.; Nakanishi, K. o.; Woody, R., Eds. Wiley-VCH: New York, 2000; pp 601-620.

130. Woody, R. W., Theory of circular dichroism of proteins. In *Circular dichroism and the conformational analysis of biomolecules*, Fasman, G. D., Ed. Plenum Press: New York, 1996; pp 25-67.

131. Rosenheck, K.; Doty, P., The far ultraviolet absorption spectra of polypeptide and protein solutions and their dependence on conformation. *Proc Natl Acad Sci U S A* **1961,** 47, 1775-85.

132. Santos, J. L.; Aparicio, R.; Joekes, I.; Silva, J. L.; Bispo, J. A.; Bonafe, C. F., Different urea stoichiometries between the dissociation and denaturation of tobacco mosaic virus as probed by hydrostatic pressure. *Biophys Chem* **2008,** 134, (3), 214-24.

133. Pakkanen, K.; Karttunen, J.; Virtanen, S.; Vuento, M., Sphingomyelin induces structural alteration in canine parvovirus capsid. *Virus Res* **2008,** 132, (1-2), 187-91.

134. Lorent, E.; Bierau, H.; Engelborghs, Y.; Verheyden, G.; Bosman, F., Structural characterisation of the hepatitis C envelope glycoprotein E1 ectodomain derived from a mammalian and a yeast expression system. *Vaccine* **2008,** 26, (3), 399-410.

135. Homer, R. B.; Goodman, R. M., Circular dichroism and fluorescence studies on potato virus X and its structural components. *Biochim Biophys Acta* **1975,** 378, (2), 296-304.

136. Volkin, D. B.; Burke, C. J.; Sanyal, G.; Middaugh, C. R., Analysis of vaccine stability. *Dev Biol Stand* **1996,** 87, 135-42.

137. Lakowicz, J. R., *Principles of fluorescence spectroscopy*. 3rd ed.; Springer: New York, 2006; 954 p.

138. Nelson, C. D.; Minkkinen, E.; Bergkvist, M.; Hoelzer, K.; Fisher, M.; Bothner, B.; Parrish, C. R., Detecting small changes and additional peptides in the canine parvovirus capsid structure. *J Virol* **2008,** 82, (21), 10397-407.

139. Thompson, A. A.; Albertini, R. A.; Peersen, O. B., Stabilization of poliovirus polymerase by NTP binding and fingers-thumb interactions. *J Mol Biol* **2007,** 366, (5), 1459-74.

140. Lidon-Moya, M. C.; Barrera, F. N.; Bueno, M.; Perez-Jimenez, R.; Sancho, J.; Mateu, M. G.; Neira, J. L., An extensive thermodynamic characterization of the dimerization domain of the HIV-1 capsid protein. *Protein Sci* **2005,** 14, (9), 2387-404.

141. Pozzi, D.; Lisi, A.; Lanzilli, G.; Grimaldi, S., Role of membrane fluidity in Epstein Barr virus (EBV) infectivity on Akata cell line. *Biochim Biophys Acta* **1996,** 1280, (1), 161-8.

142. Lisi, A.; Pozzi, D.; Grimaldi, S., Use of the fluorescent probe Laurdan to investigate structural organization of the vesicular stomatitis virus (VSV) membrane. *Membr Biochem* **1993,** 10, (4), 203-12.

143. Kueltzo, L. A.; Ersoy, B.; Ralston, J. P.; Middaugh, C. R., Derivative absorbance spectroscopy and protein phase diagrams as tools for comprehensive protein characterization: a bGCSF case study. *J Pharm Sci* **2003,** 92, (9), 1805-20.

144. Rexroad, J.; Evans, R. K.; Middaugh, C. R., Effect of pH and ionic strength on the physical stability of adenovirus type 5. *J Pharm Sci* **2006,** 95, (2), 237-47.

145. Fan, H.; Kashi, R. S.; Middaugh, C. R., Conformational lability of two molecular chaperones Hsc70 and gp96: effects of pH and temperature. *Arch Biochem Biophys* **2006,** 447, (1), 34-45.

Chapter 2

Physical Stabilization of Norwalk Virus-Like Particles

Overview

Norwalk Virus (NV) and Norwalk-like viruses, collectively known as Noroviruses, are recognized as the most common cause of viral gastroenteritis among adults in the United States.[1] It is estimated that more than 40% of foodborne outbreaks of gastroenteritis are attributable to Noroviruses.[2] These highly contagious viruses can be transmitted by contaminated food, water, or direct person-to-person contact.[3] Norovirus outbreaks have been documented on cruise ships, at daycare centers and schools, and among members of the military.[4] Severe illness is rare, but unusual complications can occur in the elderly, in children, and in immunocompromised individuals.

Since its discovery more than thirty years ago, NV has become one of the most extensively studied and best-understood viruses of the genus *Norovirus*. NV is a nonenveloped virus with a unique capsid composed almost entirely of 180 copies of a 58 kDa protein (VP1).[5] A few copies of a small basic protein, the minor capsid protein (VP2), are also present in the virions, and are believed to be important for stabilization of the icosahedral structure.[6]

Several expression systems have been developed for the production of VP1, including baculovirus-infected insect cells,[7] bacteria,[8] yeast,[9] and transgenic plants.[10] Recombinantly-expressed VP1 monomers spontaneously assemble into non-replicating, non-pathogenic virus-like particles (NV-VLPs). NV-VLPs are morphologically identical

to native capsids, with a T=3 icosahedral symmetry and a diameter of approximately 38 nm.[7] NV-VLPs have been shown to be immunogenic in mice and humans[11,12], inducing systemic and mucosal responses. Since NV infects the gastrointestinal tract, immunization strategies that elicit enhanced mucosal responses may play an important role in development of an efficacious vaccine.[12]

Interest in using VLPs as vaccine antigens has been fueled by the recent licensure of a VLP-based vaccine that protects against different types of human papillomavirus (HPV).[13] VLPs are also being considered as antigens for vaccination against other virally-mediated pathologies, including human immunodeficiency virus (HIV)[14] and influenza virus.[15] Although VLPs are generally considered more stable than attenuated viral vaccines,[16-18] formulation activities for pharmaceutical application should consider stabilization of their native particulate structure.

We recently characterized the stability of NV-VLPs over a broad range of pH and temperature.[19] The resulting empirical phase diagram[20,21] indicated significant NV-VLP conformational stability at neutral and acidic pH up to 55 °C. However, over the same pH range, temperatures at or greater than ~ 60 °C caused extensive NV-VLP aggregation.[19] In the current work, this latter observation served to define the conditions used to screen an excipient library for substances that would inhibit the rate of particle aggregation. Those excipients shown to inhibit aggregation were subjected to more rigorous analyses in attempts to elucidate their mode of action. Several excipients were found to enhance the conformational stability of NV-VLPs, as well as inhibit their aggregation under stress conditions.

Materials

Purified Norwalk virus-like particles (NV-VLPs) were obtained from LigoCyte Pharmaceuticals, Inc. Reagents and materials used for purification of NV-VLPs are as follows. Sodium phosphate, ammonium sulfate, and Sepharose® CL6-B resin were purchased from Sigma Aldrich (St. Louis, Missouri). Hydroxyapatite resin, CHT Type II, and methyl-hydrophobic interaction (Me-HIC) resins were obtained from Bio-Rad (Hercules, CA). PBS pH 6.5 solution and 0.2 μm cellulose acetate syringe filters were supplied by Fisher Chemical (Fair Lawn, NJ). Ten kDa nominal mol. wt. cutoff (NMWCO) Amicon ultrafiltration concentrators were obtained from Millipore (Billerica, MA), and 10 kDa NMWCO Slide-A-Lyzer dialysis cassettes were purchased from Pierce (Rockford, IL).

D-sucrose was obtained from Fluka/Sigma-Aldritch Chemie GmbH (St. Louis, Missouri). D-lactose monohydrate, glycerol, D-sorbital, and dextrose were obtained from Sigma-Aldrich (St. Louis, Missouri). D-mannitol was obtained from Fisher Chemical (Fairlawn, New Jersey), and α,α-trehalose dihydrate was purchased from Ferro Pfanstiehl Laboratories, Inc. (Waukegan, Illinois). Concentrated stock solutions of the aforementioned compounds were prepared by dissolution in 20 mM citrate/phosphate (CP) buffer, pH 5 or 7 (reported final concentrations are weight-by-volume (w/v) percent, except for glycerol, for which the concentration is reported as volume (v/v) percent). Following dissolution, the pH was adjusted to 7 with NaOH or HCl. Chitosan glutamate (Protasan™ UP G 213) was obtained from NovaMatrix, FMC BioPolymer AS (Drammen Norway). A 1% weight-by-volume chitosan solution was prepared by dissolution in 20

mM acetate buffer, pH 5. Following dissolution, the pH was adjusted to 5 with NaOH or HCl. Other library compounds were obtained as described elsewhere.[22]

ANS (8-anilino-1-naphthalene sulfonate) was from Molecular Probes (Eugene, Oregon); a 10 mM stock solution was prepared by dissolution of ANS in dimethylsulfoxide (DMSO, Fisher Chemical).

Methods

Purification of NV-VLPs

Norwalk VP1 monomers were expressed in a baculovirus-transformed *Spodoptera frugiperda* (Sf9) ovarian cell line as described by Jiang, *et al*.[7] Intact NV-VLPs were purified as follows: 5-6 days post infection, cellular milieu was cleared by centrifugation at 1000 x g for 10 min at 4 °C. All other steps were conducted at room temperature. One L of clarified supernatant fraction was loaded at 10 mL/min onto a 100 mL CHT column previously equilibrated with 10 column volumes (CV) of buffer A (5 mM sodium phosphate buffer, pH 6.5), followed by continued washing with buffer A at 10 mL/min until baseline was reached (~ 2 CV). Using 5 CV of buffer B (150 mM sodium phosphate, pH 6.8), NV-VLPs were eluted at a flow rate of 10 mL/min from the CHT column and collected in 100 mL volumes. Aliquots from collected fractions were analyzed by SDS-PAGE and Coomassie staining. Fractions that contained NV-VLP protein were pooled, and solid ammonium sulfate was added to a final concentration of 0.6 mM and stirred until the ammonium sulfate was dissolved. Pooled fractions were loaded at 10 mL/min onto a 100 mL Me-HIC column previously equilibrated with 5 CV of buffer C (100 mM sodium phosphate, pH 6.8 supplemented with 2.4 M ammonium

sulfate). The Me-HIC column was then washed with buffer C until the UV trace returned to baseline (~ 3 CV), followed by a second wash with 10 CV of buffer D (100 mM sodium phosphate, pH 6.8 supplemented with 1.68 M ammonium sulfate), both at 10 mL/min flow rate. NV-VLPs eluted from the Me-HIC column using 100% buffer B at 10 mL/min were collected into 10 mL fractions, and aliquots were removed for analysis by SDS-PAGE and Coomassie staining. Fractions that contained NV-VLPs were pooled, and further purified using a 400 mL gravity flow size exclusion column with Sepharose® CL6-B resin previously equilibrated with 3 CV of PBS, pH 6.5 at 10 mL/min flow rate. The exclusion volume fractions with UV absorbance were collected, concentrated using a 10 kDa nominal mol. wt. cutoff (NMWCO) concentrator, and dialyzed extensively against deionized water using a 10 kDa dialysis cassette. The retentate was sterile filtered with a syringe filter and stored in water at 4 °C.

Screening of stabilizers

An aggregation kinetic assay was used to screen a library of primarily GRAS excipients for their ability to prevent aggregation of NV-VLPs at 60 °C at pH 5. These conditions were based on studies reported previously.[19] A complete description of the library is given elsewhere.[22] Optical density (OD) measurements at 360 nm of NV-VLP samples in the presence of various excipients were taken every 2.5 minutes over the course of 1 h with a Hewlett-Packard 8453 UV-Visible diode-array spectrophotometer (Agilent, Palo Alto, California) equipped with a Peltier temperature controller. A NV-VLP concentration of 50 μg/mL was employed for all experiments; samples were

prepared in duplicate. Compounds that inhibited aggregation of NV-VLPs relative to a control sample (prepared without excipients) were selected for further study.

Circular dichroism spectroscopy

Circular dichroism (CD) spectra were acquired with a Jasco J-810 spectropolarimeter (Tokyo, Japan) equipped with a Peltier temperature control device and a six position sample holder. The effect of temperature on the secondary structure of NV-VLPs (in the presence or absence of excipients) was investigated by monitoring the CD signal at 222 nm as the temperature was ramped at a rate of 15 °C/hour. Measurements were taken every 0.5 °C over the temperature range of 10-90 ºC. Duplicate samples of NV-VLPs were prepared at a concentration of 100 μg/mL for all experiments. Baseline measurements were taken of buffer prepared with the appropriate concentration of excipient(s) and subtracted from the measurements made of NV-VLP-containing samples prior to data analysis. For ease of data comparison, CD measurement values were normalized between 0 and -1.

Fluorescence spectroscopy

Fluorescence of the molecular probe ANS was used to characterize stabilization of the tertiary structure of NV-VLPs by various excipients. A 10 mM solution of ANS in DMSO was added to NV-VLP samples prepared with and without excipients to give a final ANS concentration of 80 μM. Using an excitation wavelength of 385 nm, the fluorescence intensity of ANS at 485 nm was recorded every 2.5 °C over the temperature range of 10-85 °C; a temperature ramp rate of 15 °C/min was employed for these

experiments. Fluorescence measurements were made with a Photon Technologies International, Inc. (Birmingham, New Jersey) Quanta Master fluorometer equipped with a temperature-controlled four-position cell holder. Duplicate NV-VLP samples were prepared at a protein concentration of 100 μg/mL. Baseline spectra of samples composed of buffer, ANS, and excipient (where applicable) were subtracted from each sample spectrum prior to analysis. Fluorescence intensity measurements were normalized between 0 and 1 to facilitate comparisons between data sets.

Differential scanning calorimetry

Calorimetric measurements of NV-VLP samples prepared with and without excipients were performed with a VPCap-DSC autosampling differential scanning microcalorimeter (MicroCal, LLC, Northampton, Massachusetts). A scan rate of 60 °C/hour was used over the temperature range 10-115 °C. Duplicate samples prepared at a NV-VLP concentration of 500 μg/mL were loaded into 96-well plates and maintained at 4 °C in the instrument autosampler. Scans of NV-VLPs in the presence of excipient were compared to reference thermograms of samples containing excipient alone in buffer (no NV-VLPs). Data analysis was performed using the MicroCal LLC DSC plug-in for the Origin 7.0 software package.

Results

Screening for inhibitors of NV-VLP aggregation

The rate of aggregation of NV-VLPs at 60 °C and pH 5.0, measured as the increase in optical density at 360 nm over time, was used to screen for potential

stabilizers. These conditions were selected based on preliminary studies and the apparent phase boundaries identified in the previously reported empirical phase diagram (EPD).[19] A library of 30 (primarily GRAS) compounds, including carbohydrates, detergents, amino acids, and polyions[22] were screened for their ability to inhibit NV-VLP aggregation. Although aggregation was measured, the observed changes may also reflect alterations in structure (conformational changes) that are responsible for the subsequent particle association.

Based on the kinetic aggregation assay, several of the excipients displayed the ability to inhibit aggregation of NV-VLPs (Figure 2.1). These include chitosan glutamate (a polysaccharide), the disaccharides lactose, trehalose, and sucrose (not shown), and the monosaccharide dextrose. In addition, glycerol, sorbitol, and mannitol (not shown) were also effective in preventing aggregation of NV-VLPs. Each of the excipients listed were selected for more detailed study to examine their specific influence on the structural stability of the NV-VLPs.

Circular dichroism studies

The effect of various stabilizers on the stability of NV-VLP secondary structural elements was studied by monitoring the ellipticity at 222 nm over the course of a temperature ramp from 10-90 °C. Using this method, an increase in the midpoint temperature at which structural transitions occur (T_m) is interpreted as increased stability. Figure 2.2 shows representative CD melting curves for NV-VLPs formulated with selected excipients. The results, summarized in Table 2.1, indicate that both sugars and polyols stabilized the NV-VLP secondary structure as evidenced by shifts to higher T_m

values relative to control samples (*i.e.,* NV-VLPs without stabilizers). NV-VLPs alone at pH 7 have a T_m of 61.0 °C, while NV-VLPs formulated with various excipients manifested increased T_m values in the range of 64.1 – 69.6 °C (ΔT_m ~ 3-9 °C). Chitosan glutamate, which is poorly soluble at pH 7, was tested at pH 5, and yielded a T_m of 70 °C at a concentration of 0.75 % (w/v). Unfortunately, at pH 5 a clean scan of a control sample of NV-VLPs was not obtained due to extensive aggregation. The consequent low signal-to-noise ratio precluded accurate calculation of the T_m in this case.

The ability of certain excipients to stabilize NV-VLP secondary structure was also shown to be concentration-dependent. As illustrated in Figure 2.3, most of the selected stabilizers exhibited a concentration-dependent increase in stabilization as reflected by an elevated T_m.

Fluorescence studies

The ability of various stabilizers to protect NV-VLP tertiary structure against thermal perturbation was assessed using the fluorescent molecular probe ANS. ANS preferentially binds apolar protein regions resulting in an increase in fluorescence at 485 nm. In an aqueous system, the majority of the non-polar side chains of a protein in the native state are typically buried and not solvent-accessible. Thermally-induced structural perturbations tend to increase exposure of apolar protein regions, which in turn results in increased binding of ANS and a corresponding increase in fluorescence. Figure 2.4 shows an example of the effect of temperature on the fluorescence intensity of ANS in the presence of NV-VLPs and selected excipients. All of the excipients listed in section 3.1 displayed the ability to inhibit NV-VLPs tertiary structural transitions (see Table 2.1). At

pH 7, the control sample exhibited a T_m of 58.7 °C, while NV-VLPs formulated with the various sugars and polyols produced T_m values in the range of 60.8 – 64.4 °C. At pH 5, the control sample had a T_m of 63.4 °C, while NV-VLPs in the presence of chitosan glutamate or a combination of chitosan glutamate and sucrose had slightly elevated T_m values of 65.4 and 65.3 °C, respectively.

The effect of selected excipients on NV-VLP tertiary structure was also concentration dependent. Figure 2.5 illustrates the relationship between T_m and concentration of the excipients sucrose, trehalose, and sorbitol. For the disaccharides, incremental increases in excipient concentration yielded a quasi-linear increase in T_m over the concentration range examined. Sorbitol, on the other hand, conferred increasing stability up to a concentration of 20%, but decreased the T_m at 25%.

Differential scanning calorimetry

Consistent with previous work,[19] DSC thermograms of NV-VLP suspensions showed two endothermic transitions when fit to a non-two-state model (representative examples of baseline subtracted raw thermograms are shown in Figure 2.6). The T_m values measured for NV-VLPs in the presence of various excipients are summarized in Table 2.2. While the spectroscopic results reported above indicate improved overall stability of NV-VLPs when formulated with excipients, the DSC experimental results were somewhat less predictable. Improved stability, implied by increased T_m values, was inconsistent – in fact, many of the excipients actually reduced the T_m values, especially for T_{m2} (*i.e.,* the transition occurring at higher temperature). Figure 2.7 compares the DSC thermograms of NV-VLPs in the presence of selected excipients, showing that

while there may not have been a dramatic effect on the T_m values compared to the control sample, each of the excipients did seem to exert a unique influence on the thermal energies required for each of the two transitions. As an example, the T_{m1} peak area of the control sample was almost six times larger than that of T_{m2}, indicating that greater thermal energy was required to produce the initial transition. In contrast, in the NV-VLP sample formulated with 20% dextrose, both transition peaks had nearly identical areas, implying that the associated energies were similar in magnitude.

Once again, the effect of incrementally increasing the concentration of selected stabilizers was examined, this time by DSC. Figure 2.8 shows the effect of increasing concentration of either sucrose (pH 7) or chitosan glutamate (pH 5) in NV-VLP suspensions. In terms of T_m values, increasing concentrations of chitosan glutamate yielded higher T_m values for both of the transitions. Sucrose, on the other hand, had little effect on T_{m1} and actually reduced the value of T_{m2}. With respect to the relative transition peak areas, T_{m1} was clearly dominant in the control sample. However, as the concentration of sucrose was increased, the T_{m2} peak area increased relative to T_{m1} and eventually became dominant at a sucrose concentration of 40%. In contrast, increasing concentrations of chitosan glutamate had little effect on T_{m2} peak areas. T_{m1} peak areas, on the other hand, increased substantially at 0.5% chitosan glutamate but diminished to near control sample levels at 0.75%.

Discussion

The analysis of physical changes in the active ingredient(s) of a vaccine under pharmaceutically-relevant stress conditions (*e.g.,* changes in temperature, pH, etc.)

provides information that can be used for rational design of formulations with superior stability characteristics. In the preceding sections, a simple, rapid process for identifying physical stabilizers of NV-VLPs in aqueous suspension is described. This approach was used previously to guide the formulation of other vaccine candidates, including respiratory syncytial virus (RSV), malaria, and anthrax.[22-24] In the current study, a variety of sugars and polyols were shown to inhibit the rate of aggregation of NV-VLPs in solution. Based on previous studies with these particles,[19] thermally-induced aggregation appears to be the result of interactions between NV-VLP capsid proteins that have adopted non-native conformations: most probably, exposure of apolar amino acid side-chains to the aqueous solvent promotes intermolecular interactions that result in capsid aggregation. Based on this assumption, stabilizers that prevent aggregation may exert their effect by stabilizing the native state of the capsid proteins, allowing apolar functional groups to remain buried in protein interiors or at subunit interfaces. On the other hand, the stabilizers could have simply interfered with the protein-protein interactions that are responsible for the aggregation process. Therefore, structural integrity of the antigen cannot be inferred based on lack of aggregation alone.

If the antigenicity of NV-VLPs relies on epitopes that exist in the native state,[25] additional analytical methods must be employed to examine how stabilizers impart their effects. To this end, the effect of each excipient on NV-VLP protein secondary and tertiary structure was examined by spectroscopic techniques. From within the group of excipients chosen for detailed analyses, all were shown to stabilize both the secondary and tertiary structure of NV-VLPs. This result is not unexpected, given that sugars and polyols have been shown to be effective stabilizers in other vaccine formulations[22-24,26]

and are well-known general stabilizers of protein structure.[27,28] Compounds such as those studied here are proposed to stabilize the protein native-state through a "preferential hydration" mechanism, in which the presence of osmolyte-like molecules in solution lowers the free energy of the native state relative to structurally disrupted forms.[29] On the other hand, T_m values measured in the presence of sorbitol above a concentration of 20% indicate either no improvement (Figure 2.3) or a decrease (Figure 2.5) in conformational stability. It is possible that, at concentrations in the range of 20 to 25%, sorbitol is able to bind directly to the surface of NV-VLPs and thereby reduce their conformational stability. The number of replicates performed in these experiments does not permit statistical discrimination between the mean values reported, however, so the possibility of experimental error should be taken into account when analyzing these data. It should also be noted that, in general, the transition temperatures detected by ANS fluorescence are always lower than those observed by CD (2-5 °C on average). This may suggest the existence of a molten globule-like conformational intermediate, but further experiments are necessary to fully demonstrate the presence of such an intermediate in the unfolding of NV-VLPs.

X-ray crystallographic studies[5] of the NV-VLP revealed an icosahedral structure formed from repeating, non-covalently bound pentameric structures composed of dimers of VP1. The two principal domains of VP1 are denoted P (protruding) and S (shell). The P domain is proposed to coordinate interactions to form VP1 dimers, while the S domain is responsible for dimer-dimer interactions. Calorimetric studies conducted on non-stabilized NV-VLPs by Ausar *et al*[19] have shown that each of the two domains exhibits a

distinct thermal transition. The intensities of the two transitions differ, with the more intense of the two assigned to the P domain.

In the present work, thermograms of control NV-VLPs at pH 5 (Figure 2.8) showed two distinct transitions at temperatures consistent with those observed by Ausar *et al*. Chitosan glutamate at 0.5% concentration caused an increase in both transition temperatures and a considerable increase in T_{m1} peak area, suggesting that the increased stability was primarily attributable to stabilization of the P domain. At 0.75% chitosan glutamate concentration, transition temperatures were increased slightly above those observed at 0.5% chitosan glutamate, but the peak area of T_{m1} was diminished to near that of the control (Figure 2.8). This complex, concentration-dependent behavior suggests that the apparent increased thermal stability was due to multiple mechanisms.

When NV-VLPS were formulated at pH 7 with the various polyols, mono-, or disaccharides, the observed effects on thermal stability were not straightforward. The T_m of the transition corresponding to the P domain, (*i.e.*, the transition of greatest intensity) changed relative to the T_m of the S domain transition. This effect was dependent on the excipient and its concentration (Figures 2.7 and 2.8). In most cases, the relative intensities of the two transitions also change, confounding the assignment of either peak to a particular domain of VP1. Only sucrose, at a concentration of 20%, increased the midpoint temperature of both transitions. No other excipient was able to increase the thermal stability of the higher temperature transition at pH 7, and only a few were able to increase the T_m of the lower temperature transition. The differential effect that many of the potential stabilizers produced on NV-VLP thermal stability (*i.e.,* increasing T_{m1} while reducing T_{m2}) could be due to the fact that the monomeric protein has two strongly

delineated subdomains that serve separate functions and presumably are subject to different molecular environments while contributing to the overall NV-VLP structure. Clearly, additional study is required to elucidate this complex behavior. In addition, care must be taken when using T_m values to predict stability of macromolecular systems at temperatures much lower than the T_m (*e.g.,* storage conditions). Given the temperature dependant nature of destabilizing processes such as protein unfolding, it is possible that observations of increased stability in the presence of excipients based on T_m values may not necessarily be predictive of increased conformational stability at lower temperatures. On the other hand, the successful use of T_m values in the empirical rank-ordering of potential formulations has been demonstrated in numerous cases.[30-32] Finally, we emphasize that the stability of NV-VLPs in the presence of excipients has only been measured from a purely physical standpoint. Future work should address evaluating these potential stabilizers for their ability to preserve the antigenicity and/or inhibit the rate of chemical degradation of NV-VLPs.

References

1. Glass, R. I.; Noel, J.; Ando, T.; Fankhauser, R.; Belliot, G.; Mounts, A.; Parashar, U. D.; Bresee, J. S.; Monroe, S. S., The epidemiology of enteric caliciviruses from humans: a reassessment using new diagnostics. *J Infect Dis* **2000,** 181 Suppl 2, S254-61.

2. Mead, P. S.; Slutsker, L.; Dietz, V.; McCaig, L. F.; Bresee, J. S.; Shapiro, C.; Griffin, P. M.; Tauxe, R. V., Food-related illness and death in the United States. *Emerg Infect Dis* **1999,** 5, (5), 607-25.

3. Goodgame, R., Norovirus gastroenteritis. *Curr Gastroenterol Rep* **2006,** 8, (5), 401-8.

4. Hutson, A. M.; Atmar, R. L.; Estes, M. K., Norovirus disease: changing epidemiology and host susceptibility factors. *Trends Microbiol* **2004,** 12, (6), 279-87.

5. Prasad, B. V.; Hardy, M. E.; Dokland, T.; Bella, J.; Rossmann, M. G.; Estes, M. K., X-ray crystallographic structure of the Norwalk virus capsid. *Science* **1999,** 286, (5438), 287-90.

6. Bertolotti-Ciarlet, A.; Crawford, S. E.; Hutson, A. M.; Estes, M. K., The 3' end of Norwalk virus mRNA contains determinants that regulate the expression and stability of the viral capsid protein VP1: a novel function for the VP2 protein. *J Virol* **2003,** 77, (21), 11603-15.

7. Jiang, X.; Wang, M.; Graham, D. Y.; Estes, M. K., Expression, self-assembly, and antigenicity of the Norwalk virus capsid protein. *J Virol* **1992,** 66, (11), 6527-32.

8. Yoda, T.; Terano, Y.; Shimada, A.; Suzuki, Y.; Yamazaki, K.; Sakon, N.; Oishi, I.; Utagawa, E. T.; Okuno, Y.; Shibata, T., Expression of recombinant Norwalk-like virus

capsid proteins using a bacterial system and the development of its immunologic detection. *J Med Virol* **2000,** 60, (4), 475-81.

9. Xia, M.; Farkas, T.; Jiang, X., Norovirus capsid protein expressed in yeast forms virus-like particles and stimulates systemic and mucosal immunity in mice following an oral administration of raw yeast extracts. *J Med Virol* **2007,** 79, (1), 74-83.

10. Mason, H. S.; Ball, J. M.; Shi, J. J.; Jiang, X.; Estes, M. K.; Arntzen, C. J., Expression of Norwalk virus capsid protein in transgenic tobacco and potato and its oral immunogenicity in mice. *Proc Natl Acad Sci U S A* **1996,** 93, (11), 5335-40.

11. Guerrero, R. A.; Ball, J. M.; Krater, S. S.; Pacheco, S. E.; Clements, J. D.; Estes, M. K., Recombinant Norwalk virus-like particles administered intranasally to mice induce systemic and mucosal (fecal and vaginal) immune responses. *J Virol* **2001,** 75, (20), 9713-22.

12. Tacket, C. O.; Sztein, M. B.; Losonsky, G. A.; Wasserman, S. S.; Estes, M. K., Humoral, mucosal, and cellular immune responses to oral Norwalk virus-like particles in volunteers. *Clin Immunol* **2003,** 108, (3), 241-7.

13. Ault, K. A., Vaccines for the prevention of human papillomavirus and associated gynecologic diseases: a review. *Obstet Gynecol Surv* **2006,** 61, (6 Suppl 1), S26-31.

14. Young, K. R.; McBurney, S. P.; Karkhanis, L. U.; Ross, T. M., Virus-like particles: designing an effective AIDS vaccine. *Methods* **2006,** 40, (1), 98-117.

15. Quan, F. S.; Huang, C.; Compans, R. W.; Kang, S. M., Virus-like particle vaccine induces protective immunity against homologous and heterologous strains of influenza virus. *J Virol* **2007**.

16. Gomez-Gutierrez, J.; Rodriguez-Crespo, I.; Gonzalez-Ros, J. M.; Ferragut, J. A.; Paul, D. A.; Peterson, D. L.; Gavilanes, F., Thermal stability of hepatitis B surface antigen S proteins. *Biochim Biophys Acta* **1992,** 1119, (3), 225-31.

17. Shank-Retzlaff, M. L.; Zhao, Q.; Anderson, C.; Hamm, M.; High, K.; Nguyen, M.; Wang, F.; Wang, N.; Wang, B.; Wang, Y.; Washabaugh, M.; Sitrin, R.; Shi, L., Evaluation of the thermal stability of Gardasil. *Hum Vaccin* **2006,** 2, (4), 147-54.

18. Volkin, D. B.; Burke, C. J.; Sanyal, G.; Middaugh, C. R., Analysis of vaccine stability. *Dev Biol Stand* **1996,** 87, 135-42.

19. Ausar, S. F.; Foubert, T. R.; Hudson, M. H.; Vedvick, T. S.; Middaugh, C. R., Conformational stability and disassembly of Norwalk virus-like particles. Effect of pH and temperature. *J Biol Chem* **2006,** 281, (28), 19478-88.

20. Fan, H.; Kashi, R. S.; Middaugh, C. R., Conformational lability of two molecular chaperones Hsc70 and gp96: effects of pH and temperature. *Arch Biochem Biophys* **2006,** 447, (1), 34-45.

21. Kueltzo, L. A.; Ersoy, B.; Ralston, J. P.; Middaugh, C. R., Derivative absorbance spectroscopy and protein phase diagrams as tools for comprehensive protein characterization: a bGCSF case study. *J Pharm Sci* **2003,** 92, (9), 1805-20.

22. Ausar, S. F.; Espina, M.; Brock, J.; Thyagarayapuran, N.; Repetto, R.; Khandke, L.; Middaugh, C. R., High-throughput screening of stabilizers for respiratory syncytial virus: identification of stabilizers and their effects on the conformational thermostability of viral particles. *Hum Vaccin* **2007,** 3, (3), 94-103.

23. Jiang, G.; Joshi, S. B.; Peek, L. J.; Brandau, D. T.; Huang, J.; Ferriter, M. S.; Woodley, W. D.; Ford, B. M.; Mar, K. D.; Mikszta, J. A.; Hwang, C. R.; Ulrich, R.;

Harvey, N. G.; Middaugh, C. R.; Sullivan, V. J., Anthrax vaccine powder formulations for nasal mucosal delivery. *J Pharm Sci* **2006,** 95, (1), 80-96.

24. Peek, L. J.; Brandau, D. T.; Jones, L. S.; Joshi, S. B.; Middaugh, C. R., A systematic approach to stabilizing EBA-175 RII-NG for use as a malaria vaccine. *Vaccine* **2006,** 24, (31-32), 5839-51.

25. Chakravarty, S.; Hutson, A. M.; Estes, M. K.; Prasad, B. V., Evolutionary trace residues in noroviruses: importance in receptor binding, antigenicity, virion assembly, and strain diversity. *J Virol* **2005,** 79, (1), 554-68.

26. Evans, R. K.; Nawrocki, D. K.; Isopi, L. A.; Williams, D. M.; Casimiro, D. R.; Chin, S.; Chen, M.; Zhu, D. M.; Shiver, J. W.; Volkin, D. B., Development of stable liquid formulations for adenovirus-based vaccines. *J Pharm Sci* **2004,** 93, (10), 2458-75.

27. Lee, J. C.; Timasheff, S. N., The stabilization of proteins by sucrose. *J Biol Chem* **1981,** 256, (14), 7193-201.

28. Shimizu, S.; Smith, D. J., Preferential hydration and the exclusion of cosolvents from protein surfaces. *J Chem Phys* **2004,** 121, (2), 1148-54.

29. Kendrick, B. S.; Chang, B. S.; Arakawa, T.; Peterson, B.; Randolph, T. W.; Manning, M. C.; Carpenter, J. F., Preferential exclusion of sucrose from recombinant interleukin-1 receptor antagonist: role in restricted conformational mobility and compaction of native state. *Proc Natl Acad Sci U S A* **1997,** 94, (22), 11917-22.

30. Remmele, R. L., Jr.; Nightlinger, N. S.; Srinivasan, S.; Gombotz, W. R., Interleukin-1 receptor (IL-1R) liquid formulation development using differential scanning calorimetry. *Pharm Res* **1998,** 15, (2), 200-8.

31. Chen, B. L.; Arakawa, T., Stabilization of recombinant human keratinocyte growth factor by osmolytes and salts. *J Pharm Sci* **1996,** 85, (4), 419-26.

32. Remmele Jr., R. L.; Gombotz, W. R., Differential Scanning Calorimetry A Practical Tool for Elucidating Stability of Liquid Biopharmaceuticals. *BioPharm* **2000,** 13, (6), 36-46.

Table 2.1. Summary of results from circular dichroism and ANS fluorescence studies of NV-VLPs in the presence of selected compounds. All samples were prepared at pH 7, with the exception of those that contained chitosan, which were prepared at pH 5. T_m values are in units of °C.

Excipient	Excipient Concentration	CD			ANS		
		T_m	SD	ΔT_m	T_m	SD	ΔT_m
none (control, pH 7)	-	61.0	0.0	-	58.7	0.1	
Sucrose	20%	64.8	0.1	3.8	61.8	0.0	3.1
	30%	65.6	0.0	4.6	63.6	0.6	4.9
	40%	69.6	0.5	8.6	64.4	0.1	5.7
Trehalose	20%	65.5	0.1	4.5	62.3	0.3	3.6
	30%	66.3	0.6	5.3	63.1	0.3	4.4
	40%	68.4	0.6	7.4	64.4	0.1	5.7
Sorbitol	15%	64.8	0.5	3.8	62.0	0.7	3.3
	20%	67.2	0.2	6.2	62.8	0.1	4.1
	25%	67.2	0.1	6.2	62.0	0.4	3.3
Mannitol	15%	66.7	0.4	5.7	61.5	0.2	2.8
Lactose	15%	67.8	0.1	6.8	61.3	0.2	2.6
Glycerol	20%	64.1	0.7	3.1	60.8	0.2	2.1
Dextrose	20%	69.2	0.2	8.2	62.7	0.3	4.0
none (control, pH 5)	-	-	-	-	63.4	0.3	-
Chitosan	0.50%	69.5	0.1	-	-	-	-
	0.75%	70.0	0.4	-	65.4	0.0	2.0
Combination: Sucrose / Chitosan	2% / 0.20%	69.9	0.1	-	65.3	0.3	1.9

Table 2.2. Summary of results from differential scanning calorimetry studies of NV-VLP stability in the presence of selected excipients at various concentrations. All samples were prepared at pH 7, with the exception of those that contained chitosan, which were prepared at pH 5.

Excipient	Excipient Concentration	T_{m1} (°C)			T_{m2} (°C)		
		Mean	SD	ΔT_{m1}	Mean	SD	ΔT_{m2}
none (control, pH 7)	-	62.3	0.2	-	68.9	0.0	-
Sucrose	20%	63.9	0.1	1.6	70.5	0.2	1.6
	30%	62.3	0.0	-0.1	64.9	0.1	-4.0
	40%	62.5	0.3	0.2	65.2	0.3	-3.7
Trehalose	20%	61.7	0.2	-0.6	64.5	0.1	-4.4
	30%	64.1	0.3	1.8	65.3	0.3	-3.5
	40%	63.8	0.9	1.5	65.5	0.1	-3.4
Sorbitol	15%	61.6	0.0	-0.8	64.5	0.1	-4.3
	20%	62.8	0.7	0.5	65.1	0.2	-3.7
	25%	62.0	0.2	-0.4	65.0	0.1	-3.8
Mannitol	15%	62.1	0.2	-0.2	64.9	0.0	-4.0
Lactose	15%	62.2	0.1	-0.2	64.7	0.2	-4.1
Glycerol	20%	62.1	0.1	-0.3	64.1	0.0	-4.8
Dextrose	20%	64.6	0.3	2.3	66.8	0.2	-2.1
none (control, pH 5)	-	67.3	0.1	-	83.5	0.1	-
Chitosan	0.50%	70.1	0.4	2.9	90.7	0.8	7.2
	0.75%	70.7	0.1	3.4	92.3	0.2	8.7

Figure 2.1. Kinetics of aggregation of NV-VLPs in the presence of excipients. Optical density measurements at 360 nm were taken every 2.5 min. Samples were prepared in duplicate at pH 5 and analyzed at 60 °C. Data points shown are mean values (error bars omitted for simplicity).

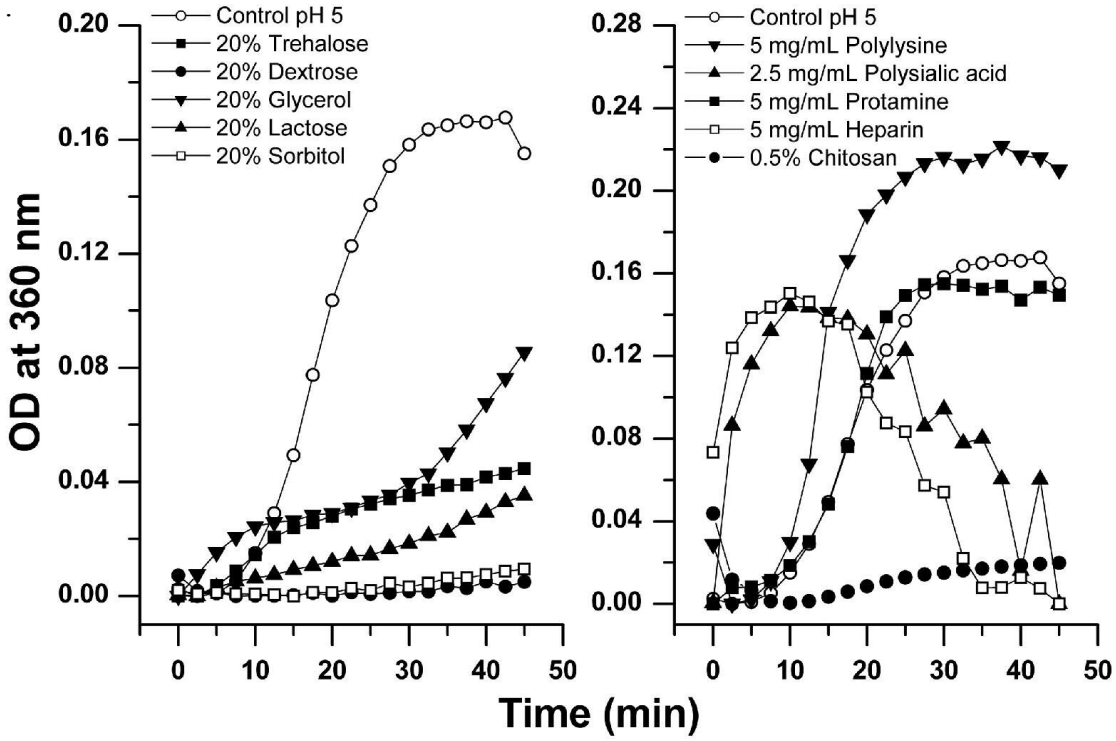

Figure 2.2. The effect of various excipients on the stability of the secondary structure of NV-VLPs, as evaluated by CD spectroscopy. The ellipticity at 222 nm of NV-VLPs in the presence of lactose, glycerol, dextrose, or mannitol was determined as a function of temperature at pH 7. Data shown are mean values (n=3), ± the standard deviation (error bars).

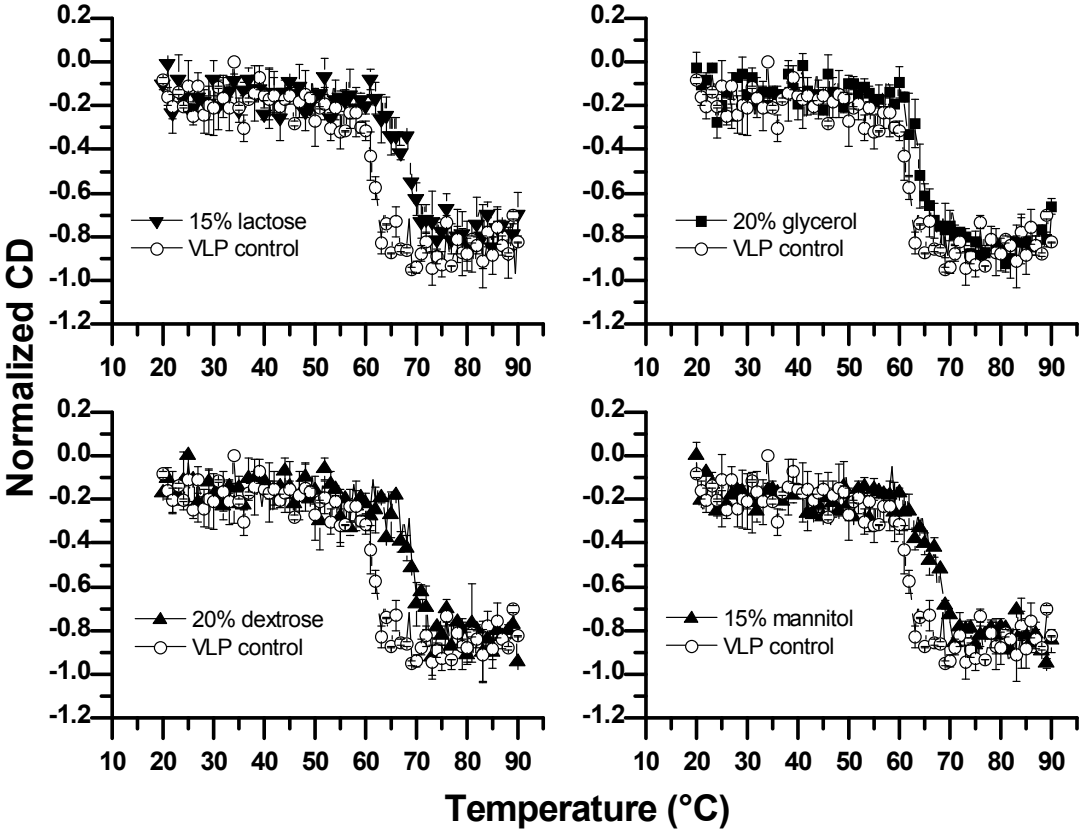

Figure 2.3. **The effect of excipient concentration on the secondary structure stability of NV-VLPs, evaluated by CD spectroscopy. (A) As an example, the ellipticity at 222 nm of NV-VLPs in the presence of sucrose at various concentrations is shown as a function of temperature at pH 7. (B) The concentration dependence of NV-VLP stabilization for the excipients sucrose, trehalose, and sorbitol is illustrated. Data shown are mean values (n=3), ± the standard deviation (error bars).**

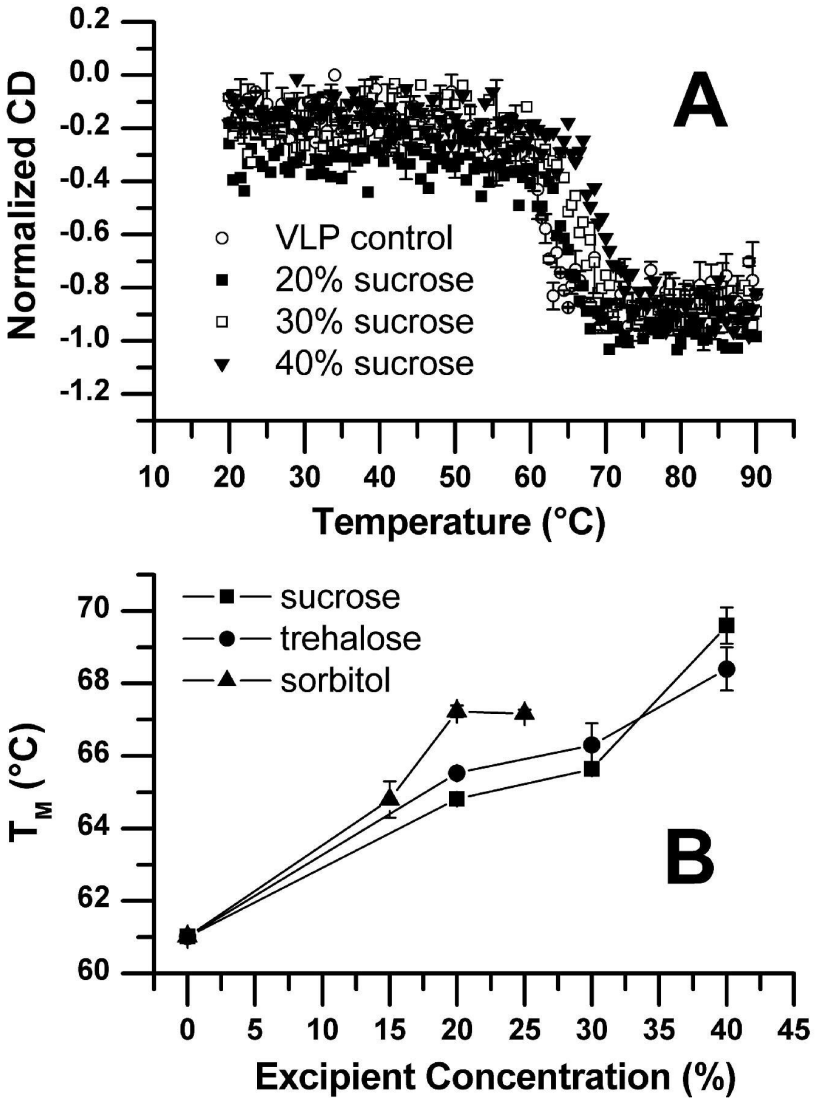

Figure 2.4. **The effect of various excipients on the stability of the tertiary structure of NV-VLPs as evaluated by ANS fluorescence spectroscopy. The fluorescence intensity at 485 nm of ANS in the presence of NV-VLPs formulated with lactose, dextrose, chitosan, or chitosan/sucrose was monitored as a function of temperature at the indicated pH values. Data shown are mean values (n=3), ± the standard deviation (error bars).**

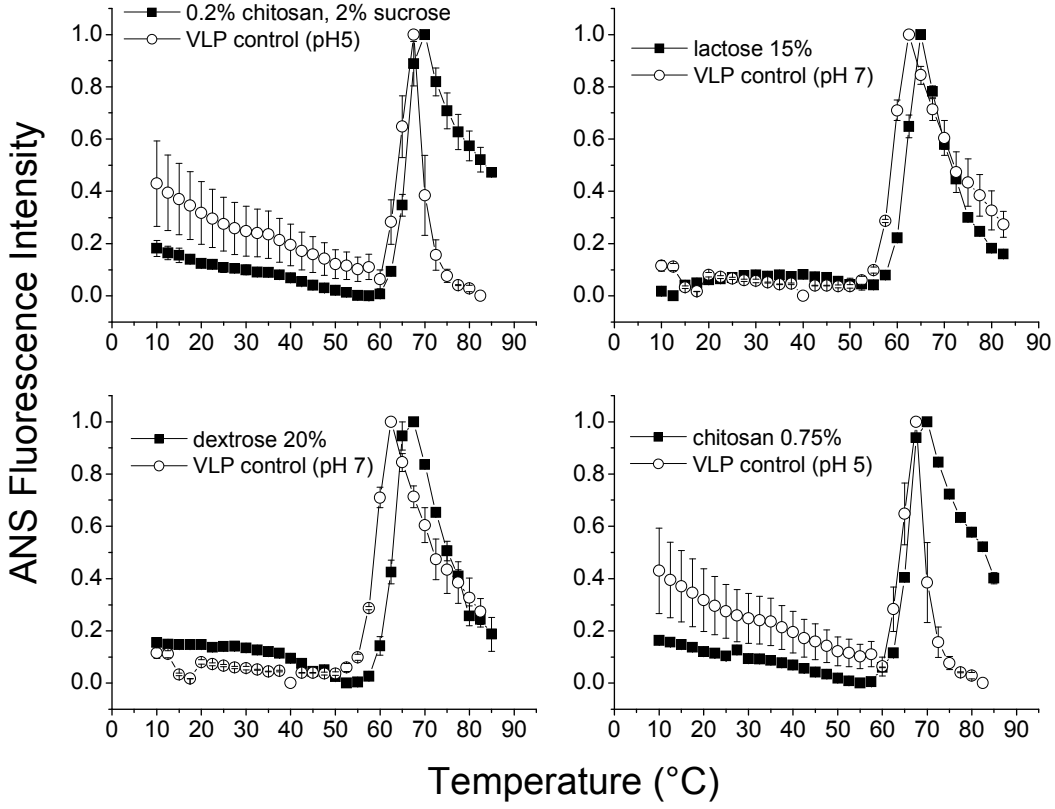

Figure 2.5. The effect of excipient concentration on the tertiary structure stability of NV-VLPs evaluated by ANS fluorescence spectroscopy. (A) As an example, the fluorescence intensity at 485 nm of ANS in the presence NV-VLPs formulated with sorbitol at various concentrations is shown as a function of temperature at pH 7. (B) The concentration dependence of NV-VLP stabilization for the excipients sucrose, trehalose, and sorbitol is illustrated. Data shown are mean values (n=3), ± the standard deviation (error bars).

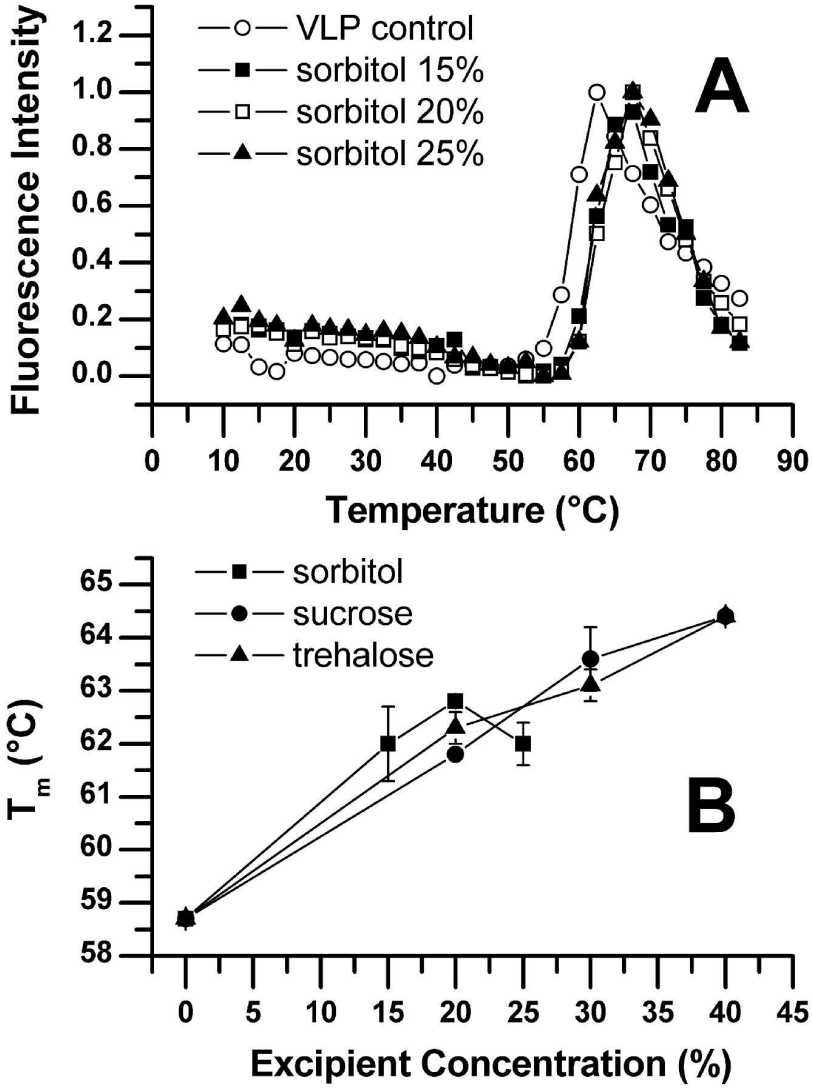

Figure 2.6. The thermostability of NV-VLPs was determined by differential scanning calorimetry. Raw baseline subtracted thermograms of unstabilized NV-VLPs at pH 5 and 7 are shown as representative examples.

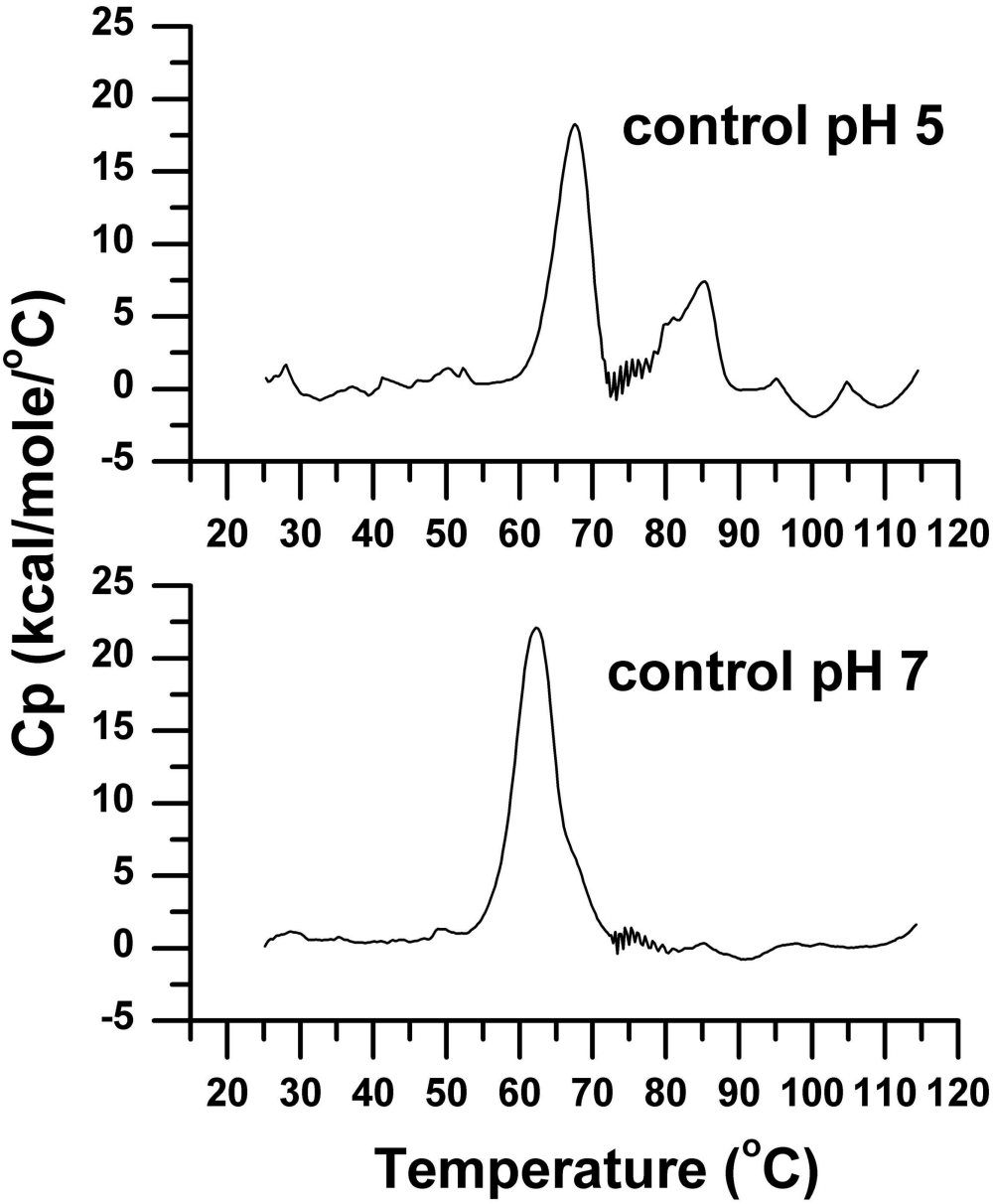

Figure 2.7. DSC analysis of NV-VLPs in the presence of selected excipients at pH 7.

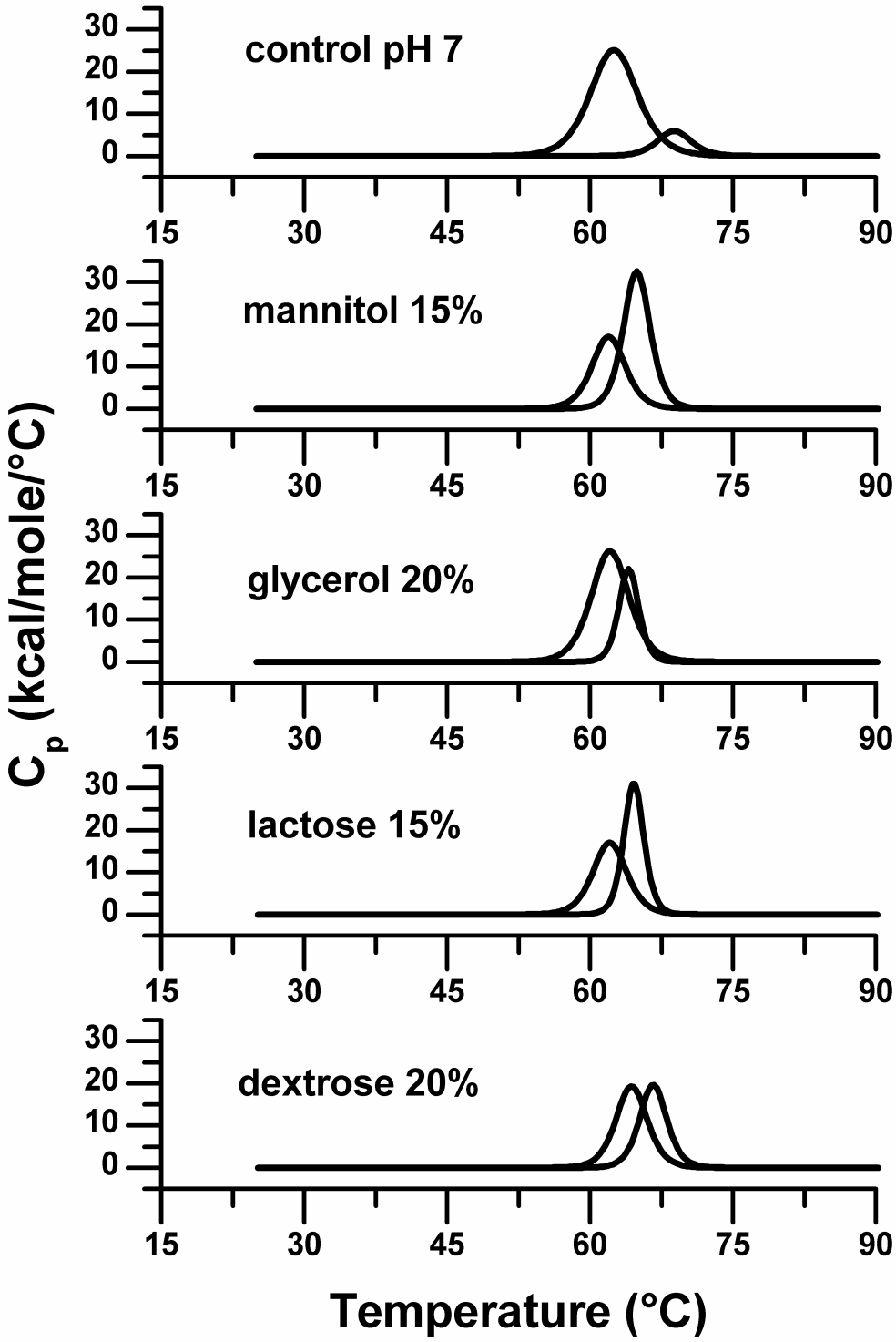

Figure 2.8. The effect of excipient concentration on NV-VLP thermal stability, as measured by DSC. NV-VLPs were formulated in solution with increasing amounts of sucrose at pH 7 (left), or chitosan at pH 5 (right).

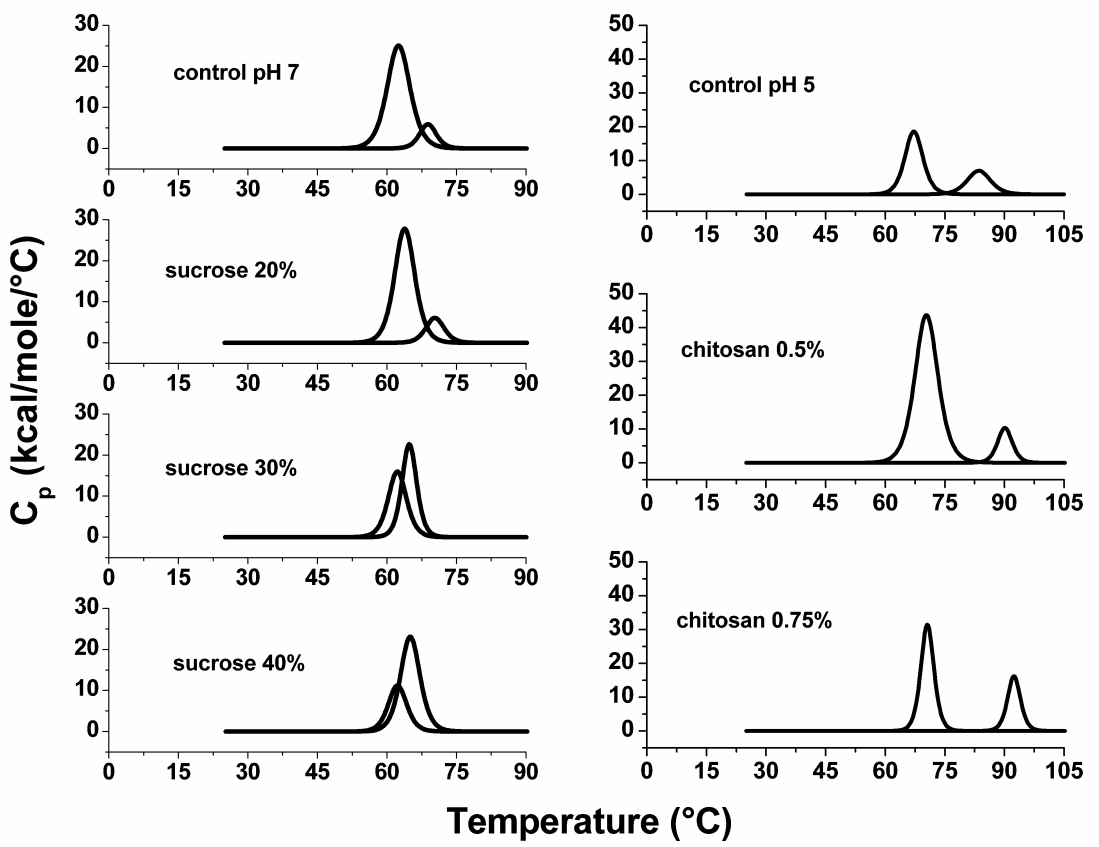

Chapter 3

Stabilization of Measles Virus for Vaccine Formulation

Overview

Measles, an acute respiratory infection caused by a highly contagious paramyxovirus, remains a leading cause of death in children worldwide. On the other hand, given that there is no known animal reservoir for the disease, as well as the effectiveness of vaccination with live attenuated virus, measles is considered to be eradicable. In fact, the World Health Organization (WHO) reported a 60% decrease in measles mortality between 1999 and 2005, attributing the decline to improved vaccination efforts.[1]

Cost is a significant factor when considering improvement to vaccination programs in developing countries. One way to reduce vaccine costs is to generate vaccines with improved stability characteristics; vaccines that do not require a cold chain, for example, should be cheaper to deliver and store. Furthermore, a loss in activity of the vaccine under suboptimal storage conditions is thought to contribute significantly to less effective vaccination programs.[2] The existing commercially available measles vaccines (*e.g.,* Attenuvax®, by Merck, Inc.) are lyophilized formulations of attenuated live virus in the presence of multiple stabilizers. Although WHO requires that these vaccines maintain a minimum titer of 1000 $TCID_{50}$ for 1 week when stored at 37 °C, these vaccines can exceed the requirement by maintaining the minimum titer for up to 4 weeks. Once

reconstituted, however, the vaccine loses 50% of its potency when stored for 1 h at room temperature.[3]

Excipients in the Attenuvax® formulation include sorbitol, sodium phosphate, sucrose, sodium chloride, hydrolyzed gelatin, human albumin, and components of fetal calf serum,[4] each one having been separately identified as a viral stabilizer through the use of a plaque assay. While this empirical approach has led to vaccines with adequate stability for use in the developed world, we propose the use of a more systematic method that has already been employed to stabilize a variety of macromolecular systems,[5, 6] including virally based vaccines.[7] This approach is based upon a method that allows global visualization of changes in physical structure. First, a comprehensive characterization of the molecule or molecular system is conducted under various stress conditions (*e.g.,* temperature, pH, ionic strength, etc.) through the use of a variety of biophysical techniques. The data obtained from these measurements are then used to generate a colored empirical phase diagram (EPD) showing regions of differential physical stability as a function of two different stress factors. From a formulation perspective, an EPD can be used in at least two ways. First, it can give an indication of solution conditions that might be used in stable formulations. Second, those conditions which correspond to apparent phase boundaries (*i.e.,* transitions between regions of differing stability) can be used to develop screening assays to identify stabilizers. One advantage of this approach is that it allows the formulator to view multiple data sets in a single image, as well as conditions of "meta-stability".

Physical measurements (spectroscopy, calorimetry, etc.) of macromolecules or macromolecular assemblies can often be used to derive medium-resolution molecular

descriptions of protein conformation, size, and shape.[8] In the case of a viral system, such detailed interpretations are generally not possible due to the variety of contributions to each piece of experimental data. The pleomorphic measles virion is composed of multiple copies of six different structural proteins (designated N, M, F, H, P, and L), a single copy of negative-sense single stranded RNA, and a host cell-derived lipid bilayer. The experimental data from such a composite system, while unable to directly discriminate structural detail, can still be used to identify conditions under which structural alterations occur (even if the precise nature of the these changes is unclear). The question then arises as to whether these experimentally measured changes are sufficient to serve as a basis for the long term stabilization of something as complex as an enveloped virus. Here we present the results of a comprehensive biophysical characterization of the measles virus (MV), as well as EPD-informed screening of potential stabilizers. Subsequent biological experiments show that excipients identified by this process are able to preserve viral infectivity.

Materials

MV stocks were obtained from the Mayo Clinic (Rochester, MN). This is not wild-type virus; rather, it is a recombinant virus (based on the Edmonston B vaccine strain) encoding the human thyroidal iodide symporter (NIS).[9]

Unless otherwise noted, all potential excipients (see Table 3.1) were obtained from Sigma-Aldrich (St. Louis, MO). Type A porcine gelatin was from Dynagel (Calumet City, IL) or Gelita USA (Chicago, IL). D-trehalose and D-sucrose were from Ferro-Pfanstiehl Laboratories, Inc. (Waukegan, IL). D-mannitol, calcium chloride,

sodium citrate, citric acid, and sodium phosphate dibasic anhydrous were from Fisher Chemical (Fair Lawn, NJ). Concentrated excipient solutions were prepared by dissolution into 20 mM citrate/phosphate (CP) buffer pH 5.5 (final concentrations are reported as weight-by-volume percent, except for glycerol, for which the concentration is reported as volume percent). The pH was adjusted after dissolution using HCl or NaOH. Final solutions were filtered using a 0.22 μm Durapore® (PVDF) membrane (Millipore, Billerica, MA).

6-dodecanoyl-2-dimethylaminonaphthalene (laurdan) and 8-anilino-1-naphthalene sulphonate (ANS) were obtained from Molecular Probes (Eugene, OR); a 1.2 mM stock solution of laurdan and a 10 mM solution of ANS were prepared by dissolution in dimethylsulfoxide (DMSO, Fisher Chemical).

Methods

Virus Purification

Viral stocks received from the Mayo Clinic were further purified by ultracentrifugation to remove residual soluble proteins and cellular debris. A Beckman-Coulter OptimaMax ultracentrifuge fitted with an MLS 50 rotor was used to pellet the virus for 1 h at 62,700 x *g* and 4 °C. The supernatant was discarded and the resulting pellet resuspended in 20 mM pH 7 CP buffer. The process was repeated and the final pellet resuspended to a protein concentration of ~ 1 mg/mL. Prior to the estimation of protein concentration, the suspension was filtered to remove aggregates with a 0.45-μm low protein binding Durapore® (PVDF) membrane (Millipore, Billerica, MA). Protein concentration was estimated by a BCA (bicinchoninic acid) colorimetric technique

(Pierce, Rockford, IL). The purity of viral preparations, based on polyacrylamide gel and Western blot analysis (not shown), is estimated to be > 70%.

Biophysical Characterization

Triplicate samples of 100 μg/mL viral protein in 20 mM CP buffer were prepared over the range of pH 4-8 at one unit intervals by diluting the pH 7 stock solution with buffer at the appropriate pH. Subsequent temperature-dependent biophysical measurements were made over the range of 10-82.5 °C with a temperature ramp rate of 15 °C/h.

Dynamic light scattering (DLS) measurements were obtained with a Brookhaven Instrument Corporation system (Holtzille, NY). Incident light at 532 nm was generated with a 125 mW diode-pumped laser. Except where noted, measurements of the mean effective particle diameter were made as previously described.[10] The mean scattering intensity from triplicate samples at each temperature T was calculated by normalizing each measured value prior to taking the average $\langle \mathbf{a'_T}, \mathbf{b'_T}, \mathbf{c'_T} \rangle$ (where $\mathbf{a_T}$, $\mathbf{b_T}$, and $\mathbf{c_T}$ represent measurements of three independently prepared samples). Normalized values $\mathbf{a'_T}$, $\mathbf{b'_T}$, and $\mathbf{c'_T}$ were calculated as

$$\mathbf{a'_T} = (\mathbf{a_T}/\mathbf{a_{max}}) \times \mathbf{max(a, b, c)} \quad \textbf{(3.1)}$$

$$\mathbf{b'_T} = (\mathbf{b_T}/\mathbf{b_{max}}) \times \mathbf{max(a, b, c)} \quad \textbf{(3.2)}$$

$$\mathbf{c'_T} = (\mathbf{c_T}/\mathbf{c_{max}}) \times \mathbf{max(a, b, c)} \quad \textbf{(3.3)}$$

Circular dichroism spectroscopy (CD) measurements were obtained with a Jasco (Tokyo, Japan) J-810 spectrophotometer. Composite (5 accumulations) spectra of MV were taken at a scan rate of 20 nm/min and a data pitch of 0.5 nm. Variable temperature

experiments monitoring the CD signal at 222 nm were conducted to detect changes in viral protein secondary structure as a function of temperature. Origin® software (OriginLab Corporation, Northampton, MA) was used to calculate midpoint transition temperature (T_m) values by fitting the temperature dependent CD data to sigmoidal functions.

Fluorescence spectra were measured with a step size of 1 nm using a Photon Technology International fluorometer (Birmingham, New Jersey). Slit widths of 4 nm were employed for intrinsic and ANS fluorescence, while those experiments utilizing laurdan were conducted using 3 nm slits. Spectral peak positions were determined by a polynomial fit and derivative analysis using Origin®.

The intrinsic fluorescence emission spectra of the aromatic amino acids tryptophan and tyrosine were collected over the range of 300-400 nm after sample excitation at 280 nm.

The extrinsic fluorescence of the amphiphilic fluorescent probe ANS in the presence of MV particles was also monitored as a function of temperature. ANS is known to have affinity for apolar sites in proteins; it displays weak fluorescence in solution, but, when bound, typically displays enhanced and shifted emission intensities.[11] Samples of MV containing 77 μM ANS were excited at 385 nm and emission spectra were collected from 425 to 550 nm.

Another molecular probe, laurdan, was used to monitor the fluidity of the viral envelope as a function of temperature. The chemical structure of laurdan is such that it readily incorporates into lipid bilayers. During the transition from a gel (less fluid) to a liquid crystalline (more fluid) phase, there is an increase in membrane hydration. This

increase in water content shifts the emission of laurdan excited at 340 nm from approximately 440 nm to around 480-490 nm. A generalized polarization (GP) of laurdan fluorescence has been defined as

$$\mathbf{GP = (I_{440}-I_{480})/ (I_{440}+I_{480})} \qquad \mathbf{(3.4)}$$

where I_x = intensity at wavelength x.[12] Therefore, greater GP values indicate a membrane that is less fluid, and vice versa. MV samples containing 8.5 μM laurdan were incubated at 10 °C in the dark for 30 min prior to excitation at 340 nm. Emission spectra were collected over the range of 400 to 525 nm. Midpoint transition temperatures were calculated as for CD data.

Empirical Phase Diagram

The empirical phase diagram is a visual representation of the entire characterization data set as a single image. Apparent phase transitions (*i.e.,* changes in color) representing changes in the physical state of the virus are displayed as a function of temperature and pH. Because no equilibrium may be present across the colored phases, these are not thermodynamic phase diagrams. Briefly, the EPD is created by constructing a vector representation of the entire data set. First, an *n*-dimensional vector is constructed for every combination of temperature and pH for which a measurement has been taken. The components of the vector are normalized experimental measurements (at the corresponding temperature and pH) from all of the characterization techniques employed (*i.e., n* represents the number of experimental data sets). The projectors of these vectors are then calculated and summed into an *n* x *n* density matrix with *n* eigenvectors and *n* eigenvalues. The three eigenvectors with the greatest eigenvalues are generally sufficient

to represent the bulk (>90%) of the data set, and these are therefore used to transform the original *n*-dimensional vectors to 3 dimensions. The resulting three dimensional vectors are then used to generate a three-color (RGB) "map" of the experimental data. A more complete description of the generation of EPDs has been given elsewhere.[13] The assignment of colors to these vectors is arbitrary, so the individual colors themselves are not meaningful. Rather, only changes in color are used to detect changes in the physical state of the virus.

High-throughput screening of GRAS excipients

Plate-based screening of a potential excipient library[7] was performed with a SpectraMax M5 tunable microplate reader equipped with a temperature-controlled sample chamber (Molecular Devices Corp, Sunnyvale, CA). Measurements of triplicate samples prepared at pH 5.5 in 96-well plates were taken every 1.5 min. The pH value used in these experiments was selected because it lies at an apparent phase boundary in the EPD (see Results).

Aggregation-based excipient screening

Viral aggregation in the presence or absence of potential stabilizers was monitored by measurements of optical density at 360 nm (OD_{360}). Samples were prepared at a viral protein concentration of 160 μg/mL and monitored at 55 °C over the course of 90 min.

Laurdan-based excipient screening

Fluorescence of the molecular probe laurdan at 37 °C was used to monitor the effect of various excipients on the fluidity of the viral membrane. Samples were prepared at a viral protein concentration of 100 μg/mL and a laurdan concentration of 3 μM. The samples were then excited at 340 nm and the emission at 440 and 490 nm was monitored over the course of 2 h. Generalized polarization was calculated according to Equation 3.4.

Infectivity assay

MV stocks for the plaque-based infectivity experiments were obtained from the Serum Institute of India Limited (Pune, India). This is an attenuated vaccine virus strain (Edmonston-Zagreb) produced from human MRC-5 cell culture in roller bottles. The virus was harvested by washing the cells with Minimum Essential Medium (MEM, Eagle, with Hank's salt, L-glutamine, and sodium bicarbonate). The harvest fluids were received from the Serum Institute as frozen liquid aliquots. These were thawed and used without further purification. Stock solutions of each potential stabilizer were prepared as 3x concentrates in 20 mM citrate-phosphate buffer and then adjusted to pH 7 with 1 N HCl or NaOH. Unstabilized vaccine aliquots of 15 mL were thawed in a ~ 20 °C water bath immediately before formulation. Vaccine formulations were prepared by a 1:2 dilution of the excipient concentrates into unstabilized Edmonston-Zagreb virus in MEM. The resulting formulations were aliquoted into duplicate samples and tested immediately and after approximately 24 h at 21 °C in a measles plaque assay. The measles plaque assay was performed with Vero cells in 24-well plates according to the procedure outlined by Schrag *et al*.[14]

Results

Biophysical characterization of MV

The size of the measles virus was examined by a combination of static and dynamic light scattering. Figure 3.1 shows changes in the scattered light intensity and effective hydrodynamic diameter of MV as a function of temperature. At pH 4 and 5, there is a sharp decline in scattered light intensity starting at 25 and 35 °C, respectively (Figure 3.1A). These data reflect extensive aggregation at low pH, as precipitated material was visually observed in these samples. An increase in scattered light intensity starting at around 40 °C is seen for MV at pH 6, while the virus at pH 7 and 8 exhibits an immediate but gradual decline in scattered light until approximately 50 °C. Little to no change in particle size is shown for samples at or above pH 6 (Figure 3.1B/C). In contrast, an acidic environment (pH 4 and 5) appears to induce immediate aggregation, with aggregate size and measurement variability increasing at elevated temperatures. The DLS measurements are only accurate for particle sizes below 1 μm, so the size of particles at pH 4 and 5 should be interpreted on a relative (rather than absolute) basis only.

Far-UV circular dichroism provides information about the secondary structure of macromolecular systems. Both the CD spectra and the unfolding curves reflect additive contributions from the several different viral proteins, although they are presumably dominated by contributions from the most abundant of these proteins (*e.g.,* the N, M, and P proteins).[15] Thus, as expected, the thermal transitions are very broad. The CD spectra of MV show a minimum around 222 nm at each pH, as well as a secondary minimum near 208 nm at pH 6-8 (Figure 3.2). MV at pH 4 and 5 shows substantially lower CD signal

than samples prepared at more neutral pH values. This could be due to pH-dependant loss of helical character, but increased light scattering due to particle aggregation may be enhancing the observed differences. The H protein has recently been shown to be mainly composed of β-sheet secondary structural elements.[16] For this reason, the H protein is presumed not to be the major contributor to the CD spectra of MV. Thermally induced changes in viral protein secondary structure were detected by monitoring the CD at 222 nm as a function of temperature (Figure 3.3). These measurements were normalized between 0 and -1 for ease of visualization. Comparison of the melting curves corresponding to samples prepared over the pH range 4-8 indicates a dependence of structural stability on pH. At pH 4 and 5, the midpoint transition temperatures (T_m) fall between 23 and 30 °C, while for the higher pH samples, the T_m increases to 56-57 °C. This apparent increase in secondary structural stability at higher pH is consistent with visual observations of particle aggregation at pH 4 and 5.

Intrinsic fluorescence measurements were employed to detect changes in the tertiary structure of viral proteins. Discontinuous shifts in the position of the protein intrinsic emission peak or in emission intensity at a particular wavelength can often be used to detect temperature-induced structural changes. In the case of MV, samples across the pH range 4-7 show a gradual temperature-dependent blue shift in peak position that starts at 10 °C (Figure 3.4). The samples at pH 8 also show a blue shift with increasing temperature, but the shift is more gradual up to 53 °C. Above 53 °C, the peak position at pH 8 shifts more drastically to shorter wavelengths. Comparison of the peak positions at 10 °C in Figure 3.4 suggests a dependence on pH; as the acidity of the sample is increased, the peak position shifts to shorter wavelengths. Peak position values could not

be determined across the entire temperature range for all samples because light scattering due to particle aggregation obscured the fluorescence emission. The fluorescence intensity at 322 nm (Figure 3.4), which is due primarily to tryptophan residues, declines with increasing temperature for all samples (note that these values have been normalized between 0 and 1 for ease of visualization). The expected thermal quenching of MV fluorescence is illustrated by samples at pH 7 and 8, which exhibit a smooth curvilinear decline in fluorescence intensity as the temperature is increased. At pH 6, a curvilinear profile similar to that displayed by the more alkaline samples is juxtaposed with a slight increase in fluorescence at about 45 °C. In contrast, the samples at pH 4 and 5 show a sharp and nearly immediate decrease in fluorescence intensity as the temperature is raised above 10 °C. This effect is more pronounced at pH 4 than 5, but both cases are reflective of particle aggregation.

Fluorescence measurements of ANS in the presence of MV were also obtained as another way to detect temperature-induced structural changes. At 10 °C, the peak emission wavelength is seen to be moderately dependent on sample pH, shifting from around 468 nm at pH 4 to almost 470 nm at pH 8 (Figure 3.5). An emission maximum between 468 and 470 nm generally indicates that the probe is extensively bound. The peak position at pH 4 shows an increase in measurement variability as the temperature is increased, but remains relatively stable up to approximately 60 °C, above which an abrupt shift to shorter wavelengths can be seen. At pH 5 and low temperature, ANS peak emission occurs at around 469 nm and stays constant up to 45 °C, after which a shift to longer wavelengths is observed. This red shift in ANS emission suggests a reduction in probe binding and continues across the temperature range. The behavior at pH 5 of ANS

in the presence of MV is unique in this regard; the temperature-induced shifts in peak position for samples prepared at either pH 4 or from pH 6 to 8 are to shorter wavelengths. At pH 6, the peak position remains constant at about 469 nm up to 35 °C, above which it declines smoothly to almost 465 nm at the upper extreme of the temperature range. The peak position at pH 7 also begins around 469 nm, and shows a slight (< 1 nm) decline between 10 and 50 °C, after which the rate of decline increases significantly. The emission peak at pH 8 occurs near 470 nm at low temperature. As the temperature is increased, the peak position remains more or less constant up to about 50 °C, above which it falls to approximately 463 nm at 83 °C. The intensity of ANS fluorescence (normalized between 0 and 1 for ease of visualization) at 469 nm is also depicted as a function of temperature (Figure 3.5). At pH 4, ANS emission intensity declines sharply as the temperature is increased above 12.5 °C. A similar decrease is exhibited by the plot corresponding to pH 5, where a slightly shallower decline in emission intensity begins around 20 °C. The plots for samples from pH 6 to 8 are also very similar to one another. Evidence for a structural transition beginning at around 40 °C is seen in each trace as a slight increase in emission intensity superimposed over the (expected) curvilinear decline due to intrinsic thermal quenching.

Fluorescence of the molecular probe laurdan was used to characterize the fluidity of the viral envelope as a function of temperature. Figure 3.6A illustrates representative fluorescence spectra of laurdan in the presence of MV. In Figure 3.6B, the generalized polarization (GP) is plotted versus temperature. At each pH, a transition from the gel to the liquid crystalline state is observed as the temperature is increased. The midpoints of these transitions (T_m) vary according to pH; samples at pH 6 and 7 have their T_m near 50

°C, while samples at pH 5 or 8 show a slightly lower T_m around 47 °C. Although the T_m values at pH 5 and 8 are very similar, it should be noted that the more acidic sample achieves a much higher degree of membrane hydration at elevated temperatures. The GP trace for samples at pH 4 emphasizes the sensitivity of membrane hydration to acidic conditions in several ways: first the initial GP value is quite low, indicating significant hydration even at low temperature. In addition, the T_m occurs close to 30 °C, indicating a significant reduction in membrane stability.

Empirical phase diagram

As described above, the results from the various techniques were synthesized into a multi-dimensional vector space, from which an EPD that permits ensemble visualization of the entire data set was generated (Figure 3.7). The EPD of MV shows similar behavior (color) between pH 4 and 5, and from pH 6 to 8. Closer inspection, however, reveals at least half a dozen regions of differing stability for MV (although the colors themselves are relative, the different phases are defined according to color continuity). One phase can clearly be seen in green for pH 4 and 5 at low temperatures. There is a step-shaped transition region above this phase that reflects the fact that major structural transitions were detected for low pH samples by all of the techniques between 20 and 35 °C. The blue and purple phases above this transition region may reflect particle aggregation, a phenomenon that was visually observed at elevated temperature in samples prepared at low pH (the colors in these regions may differ due to the divergence in ANS peak position a high temperatures). Also, increased membrane fluidity at elevated temperatures was observed for all samples, and probably contributes to similarities in

color at elevated temperature across the pH range. Again, the data across all techniques indicate that MV particles behave similarly when exposed to pH 6 or 8. This is particularly true of the GP data, in which the temperature dependent traces (Figure 3.6) at each pH between 6 and 8 exhibit only minor differences. This fact is reflected by similarities in the phase diagram at these pH values, especially at lower temperatures; differences in the diagram between pH 6 and 8 above the transition region (~ 45 °C) may be due to differences in behavior at high temperature as detected by DLS. At pH 7, the phases are less well-defined and transitions occur over a wider range of temperatures. This is attributed to the fact that transitions detected at pH 7 by the various techniques are often broader than those measured at pH 6 or 8. Finally, there is a greenish phase at low temperature (< 25 °C) that appears at pH 7 but not for pH 6 or 8. This phase appears to be due to increased low-temperature stability at pH 7 of the CD signal at 222 nm, and is presumed to reflect a "native-like" state of the virus.

Excipient screening

A library of generally recognized as safe (GRAS) excipients[7] was screened for compounds exhibiting the ability to physically stabilize MV particles in solution. Based on the EPD, two high-throughput (HTP) screening assays were developed. The first is selective of those excipients that inhibit aggregation of the virus under challenge conditions of temperature and pH, while the second utilizes fluorescence of the molecular probe laurdan to determine which excipients are able to stabilize the viral envelope (also under stress conditions of temperature and pH).

Based on analysis of the empirical phase diagram, a screening assay based on turbidity changes at 360 nm (OD_{360}) was developed to measure the aggregation of MV at pH 5.5 and 55 °C. This particular degradation pathway may be the result of a variety of structural or conformational changes in the virus. A number of excipients, including certain mono- and disaccharides, amino acids, and sugar alcohols were observed to inhibit the aggregation of MV (Table 3.1). To further refine this list, a second screening assay was developed to search for potential stabilizers on the basis of their ability to stabilize the viral envelope using laurdan fluorescence. To judge the stability of the viral membrane from data generated by this assay, the GP of laurdan in the presence of MV was examined as a function of time. The GP calculated at t = 0 reflects the initial hydration state of the membrane, while the difference between the maximum and minimum GP values is related to the extent of change in the hydration state and fluidity of the membrane. A smaller difference between these values presumably reflects a greater stabilizing effect. Finally, the time at which the minimum value is reached reflects the kinetics of membrane hydration; a longer time to reach a minimum value is assumed to reflect superior stabilization characteristics. Using these criteria, the excipients ascorbic acid, diethanolamine, malic acid, sodium citrate, proline, lysine, pluronic F-68, lactose, dextrose, trehalose, sorbitol, sucrose, and mannitol all appear to confer stability to the viral membrane (data not shown). This is obviously a significant portion of the total set of excipients tested; the list may be further refined by choosing those excipients that also inhibit aggregation. A final list of potential stabilizers can then be created by choosing only one representative excipient from each molecular class (*e.g.,* polyols, sugars, amino acids, etc.). On this basis, gelatin, lactose, proline, malic acid, myo-

inositol, and mannitol were selected for further evaluation (gelatin was not particularly effective in protecting the viral envelope, but was included because of its dramatic effect on the inhibition of aggregation). Myo-inositol was included in this final list of potential stabilizers because in research conducted at the University of Colorado, myo-inositol has been identified as a good stabilizing excipient in dry powder measles vaccine formulations prepared by CO_2-Assisted Nebulization with a Bubble Dryer®.[17] Citrate, another good stabilizer, was included in all samples as a buffer component.

To determine the optimum concentration of the six excipients chosen for further study, each was re-examined using the aggregation-based screening assay, this time at multiple concentrations. Each of the excipients demonstrated a strong dependence of aggregation inhibition on concentration (data not shown). A change was made in the study at this point; gelatin from fish skin was replaced as a potential stabilizer by the more pharmaceutically acceptable gelatin derived from porcine skin. According to the aggregation-based screening assay, the porcine gelatin did not display the same ability to inhibit aggregation as the fish-derived alternative (inhibition of aggregation was < 25% for all concentrations tested). Despite its poor performance in the optimization experiment, porcine gelatin was selected for further study at a concentration of 2.5 % w/v due to the success of the initial material. The other excipients were chosen for further study at the following concentrations: myo-inositol – 0.15 M, malic acid – 0.15 M, lactose – 15 % w/v, proline – 0.15 M, mannitol – 10 % w/v.

Structural studies of MV in the presence of excipients

To obtain more detailed information regarding the specific effect of each selected stabilizer on the physical stability of MV, the virus was studied in the presence of these compounds (at the optimum concentrations given above) by CD, laurdan fluorescence, and right-angle static light scattering. The goal of using these methods was to determine the effect of each stabilizer on viral protein secondary structure, viral membrane integrity, and particle aggregation, respectively. To make these final experiments more relevant to a potential final vaccine formulation, each sample was prepared at pH 7 (in addition to being near physiological pH, the phase diagram indicates superior physical stability at pH 7). Each formulation was analyzed as a function of increasing temperature from 10 to 85 °C.

The normalized CD at 222 nm of MV in the presence of selected excipients was measured as a function of temperature (not shown). Due to interference from the excipients, analysis of CD data for MV in the presence of gelatin or proline was not performed. Fitting the data to a sigmoidal function allows determination of an apparent T_m that can be used to compare the stability of MV protein secondary structure in the presence of each potential stabilizer. Based on these T_m values, none of the excipients tested appeared to significantly stabilize MV protein secondary structure.

The fluorescence of laurdan in the presence of MV and stabilizer allows determination of the effect of these compounds on the GP of the viral membrane. The T_m of the membrane transition was determined for each sample (Table 3.2). Based on a comparison of these T_m values, mannitol, malic acid, and myo-inositol all increased the stability of the viral membrane. While each of the other three excipients did not improve

the T_m of MV, proline strongly reduced (relative to the control) the overall change in GP across the experimental temperature range (data not shown). In this sense it appears to perform better than myo-inositol, which induces a very wide dispersion in GP as the temperature is varied.

Light scattering by MV in the presence of each excipient was also measured during the laurdan experiments (Figure 3.8) by monitoring the fluorescence excitation peak. Changes in the intensity of light scattered by MV particles in solution as a function of temperature can reflect aggregation as well other large-scale structural events (*e.g.,* swelling of viral particles). In the presence of gelatin, there is a very shallow decline in the light scattering of MV from 10 to 50 °C, and additional evidence of structural changes is seen as subsequent small increases in light scattering - one starting at 50 °C, and another at 70 °C. Light scattering by MV in the presence of lactose is fairly constant from 10 to 40 °C, but above 40 °C there is a decrease in light scattering up to 73 °C and another small decrease starting at 80 °C. When formulated with proline, mannitol or myo-inositol, MV exhibits a curvilinear decrease in light scattering between 10 and 60 °C. Above 60 °C, a small increase in light scattering is observable for all three formulations. While the magnitude of the decrease between 10 and 60 °C is similar when the virus is formulated with either myo-inositol or mannitol, an even greater decrease in light scattering is seen in this temperature range when MV is formulated with proline. When MV is in the presence of malic acid, a small decrease in light scattering is observable between 10 and 48 °C, after which the light scattering remains fairly constant.

Infectivity assays

So far, we have described a number of techniques that were used to infer various aspects of the physical stability of MV. To determine whether increased physical stability (as measured by these techniques) can be correlated to the preservation of biological activity, a cell culture-based infectivity assay was performed employing vaccine quality MV in the presence of each of the selected stabilizers. After formulation with excipient, MV was stored for 24 h at 21 °C. Following thermal challenge, Vero cells were infected with each of the formulations and analyzed for infection. Due to significant variability in the count of plaque-forming units (pfu) for the unstabilized measles vaccine, results are reported as percent retained infectivity after 24 h of room temperature incubation. The results of this standard plaque-based assay (Figure 3.9) indicate that formulations containing porcine gelatin (2.5% w/v), mannitol (10% w/v), malic acid (0.15 M), proline (0.15 M), or myo-inositol (0.15 M) were able (on average) to retain their infectivity as compared to formulations with either lactose (15% w/v) or with only 20 mM pH 7 citrate-phosphate buffer. It should be noted that the error in measurements made for formulations containing mannitol or malic acid is large enough to prevent the conclusion that these formulations are statistically superior to the formulation containing only citrate-phosphate buffer.

Discussion

A comprehensive biophysical characterization of MV has been conducted through the use of several spectroscopic and light-scattering techniques, permitting a description of the physical stability of the virus as a function of temperature and pH, two

pharmaceutically relevant stress factors. While we have attempted to utilize a large number of analytical techniques in the characterization experiments to obtain as much information as possible, several other techniques (*e.g.,* calorimetry, Raman and/or FTIR spectroscopy) could have been utilized had experimental resources been unlimited. CD measurements of viral particles at each experimental pH reveal a loss of secondary structure as a function of temperature. This effect manifests at higher temperatures as sample pH is increased, indicating that MV physical stability is highly compromised in an acidic environment. The position of the MV intrinsic fluorescence maximum below 330 nm suggests that the viral amino acid indole chromophores on average reside in a relatively apolar environment. This could at least partially reflect the presence of these side chains in the interior of MV proteins, or it could be that significant numbers of aromatic residues are present in the membrane spanning regions of the viral envelope proteins (*i.e.,* F and H) and are thus normally exposed to the highly apolar regions of the lipid bilayer. At low pH, there is also probably some contribution from the burial of chromophores by aggregation, given that light scattering and CD data show clear evidence of viral aggregation at low temperature and precipitation under acidic conditions (*i.e.,* at pH 4-5). Thermally-induced protein unfolding would manifest as a peak shift to >330 nm; the absence of such a shift should be especially noted and contrasts with the CD results. This suggests that scattering may prevent the structural transitions from being detected. Measurements of ANS fluorescence were also made as an alternative way of probing viral structure. While changes in the fluorescence of ANS in the presence of protein can indicate that apolar protein regions are becoming more accessible to the probe, a complicating factor is the presence of the MV viral envelope,

which itself contains significant apolar character. Given that the probe appears in all samples to be highly bound at low temperature, the probability that the probe is interacting with the bilayer seems high. Another complicating factor is the possibility of charge-charge interactions between the ionized probe and charged or polar protein residues. Nevertheless, shifts in ANS fluorescence spectra are presumably reflective of structural changes in the virus, whatever their nature. This reasonable assumption underlines the utility of the phase diagram approach in the analysis of spectral data pertaining to the physical stability of viral samples. At pH 4 and 5, the strong reduction in ANS fluorescence intensity and large shifts in peak position, both as a function of temperature, agree well with the aforementioned evidence of particle aggregation. The ANS peak position at pH 6, 7, and 8 shifts to shorter wavelengths as temperature is increased, suggesting that temperature-induced structural changes result in increased solvent exposure of apolar regions of the virus. The extent of change in peak position is least at pH 7, suggesting greater physical stability at neutral pH. Additional extrinsic fluorescence measurements of the dye laurdan, used to measure the stability of the viral envelope, exhibit evidence of structural disruption (membrane hydration) starting at 20 °C or lower. For samples at pH 6 and above, this is much lower than the onset temperatures of structural events measured by the other techniques, suggesting that the viral envelope may be a weak point in the overall physical stability of MV above pH 5.

While a detailed molecular model of MV physical stability cannot be derived from these data, their conversion to a vector space of reduced dimensions permits a fairly comprehensive visual representation of stability in the form of an EPD. While the precise mechanisms of physical degradation are not revealed by the EPD, such diagrams can be

used as the first step in a rational process to identify physical stabilizers.[5-7] Based on the EPD's apparent phase boundaries, two assays were designed for the purpose of screening possible stabilizers of MV particles in solution. Compounds from a variety of molecular categories (*e.g.,* sugars, sugar-alcohols, amino acids) were shown to protect the viral membrane and inhibit particle aggregation under stress conditions.

The infectivity of MV is almost certainly heavily dependent on both the conformational stability of the viral proteins and the integrity of the viral membrane. For this reason, CD, laurdan fluorescence, and right-angle light scattering were used in an attempt to determine more specifically the physical effects of the best performing stabilizers identified by the two screening assays. CD measurements indicate that none of the identified compounds stabilize viral protein secondary structure. As a result, we cannot conclude that these agents inhibit aggregation by actually preserving the native state of viral proteins, or that they simply interfere with protein association by direct effects on protein-protein interactions. Additional studies that measure the stabilizing effect of excipients on viral protein tertiary structure are necessary to determine whether the excipients stabilize the native state of the viral proteins. It would not be surprising if such studies showed at least some of the excipients do stabilize protein conformation, given the well-known ability of some of them to stabilize protein native states through a preferential hydration mechanism.[18-20] The laurdan experiments suggest that at least some of the stabilizers also function by inhibiting hydration of the viral envelope. In the case of mannitol and malic acid, the compounds exert their effect by increasing the temperature (T_m) at which the membrane fluidizes. In the case of proline, the magnitude of the overall change in membrane hydration is reduced. Additionally, relative to a neat sample at pH 7

(Figure 3.1), MV formulations containing lactose, gelatin, and malic acid are resistant to temperature-induced changes in viral density (*e.g.,* swelling of viral particles). Given the apparently diverse effects of the six potential excipients on MV physical stability, the ultimate test of the utility of these stabilizers was their evaluation by an accelerated stability study in which viral integrity was measured by a cell culture-based infectivity assay. The infectivity data show that the infectivity of attenuated live virus intended for vaccine purposes is protected by formulations containing mannitol, myo-inositol, proline, malic acid, or gelatin (Figure 3.9). That at least three of these five excipients were found to stabilize the viral envelope emphasizes the critical role played by the membrane in preserving the integrity of the virus. This is not surprising, given that the two viral proteins responsible for virus-host interaction (*i.e.,* H and F proteins) reside at least partially within the bilayer encompassing the viral matrix.[21] A more hydrated bilayer would be more polar due to the presence of water molecules, potentially disrupting its interactions with apolar residues that are typically found at the surface of transmembrane protein regions.[22, 23] The resulting change in free energy as these interactions are altered may be enough to promote conformational changes that interfere with viral attachment and fusion.

The fact that five of the six potential stabilizers identified in our studies were able to preserve the infectivity of MV at least partially validates the EPD/HTP-screening approach to the stabilization of macromolecular systems such as enveloped viruses. Another interesting implication of this success is that the physical changes that are responsible for losses of MV activity must occur in the majority of viral particles even though most of them are presumably inactive. The current work could be improved by

further studies that elucidate the mechanism(s) by which the stabilizers inhibit aggregation of viral particles. In addition, we have not addressed the issue of chemical degradation (*e.g.,* oxidation, deamidation, etc.), which usually plays an equally important role in the stability of macromolecular systems.[24-27] Most importantly, however, the identification of these MV stabilizers can be used to aid the construction of more robust formulations of this important vaccine.

References

1. Wolfson, L. J.; Strebel, P. M.; Gacic-Dobo, M.; Hoekstra, E. J.; McFarland, J. W.; Hersh, B. S., Has the 2005 measles mortality reduction goal been achieved? A natural history modelling study. *Lancet* **2007,** 369, (9557), 191-200.
2. Brandau, D. T.; Jones, L. S.; Wiethoff, C. M.; Rexroad, J.; Middaugh, C. R., Thermal stability of vaccines. *J Pharm Sci* **2003,** 92, (2), 218-31.
3. Plotkin, S. A.; Orenstein, W. A., *Vaccines*. 4th ed.; Saunders: Philadelphia, 2004; 1662 p.
4. *Physicians' desk reference : PDR 2004*. 58th ed.; Thomson PDR: Montvale, N.J., 2004; 3533 p.
5. Jiang, G.; Joshi, S. B.; Peek, L. J.; Brandau, D. T.; Huang, J.; Ferriter, M. S.; Woodley, W. D.; Ford, B. M.; Mar, K. D.; Mikszta, J. A.; Hwang, C. R.; Ulrich, R.; Harvey, N. G.; Middaugh, C. R.; Sullivan, V. J., Anthrax vaccine powder formulations for nasal mucosal delivery. *J Pharm Sci* **2006,** 95, (1), 80-96.
6. Peek, L. J.; Brandau, D. T.; Jones, L. S.; Joshi, S. B.; Middaugh, C. R., A systematic approach to stabilizing EBA-175 RII-NG for use as a malaria vaccine. *Vaccine* **2006,** 24, (31-32), 5839-51.
7. Ausar, S. F.; Espina, M.; Brock, J.; Thyagarayapuran, N.; Repetto, R.; Khandke, L.; Middaugh, C. R., High-throughput screening of stabilizers for respiratory syncytial virus: identification of stabilizers and their effects on the conformational thermostability of viral particles. *Hum Vaccin* **2007,** 3, (3), 94-103.
8. Van Holde, K. E.; Johnson, W. C.; Ho, P. S., *Principles of physical biochemistry*. 2nd ed.; Pearson/Prentice Hall: Upper Saddle River, N.J., 2006; 710 p.

9. Dingli, D.; Peng, K. W.; Harvey, M. E.; Greipp, P. R.; O'Connor, M. K.; Cattaneo, R.; Morris, J. C.; Russell, S. J., Image-guided radiovirotherapy for multiple myeloma using a recombinant measles virus expressing the thyroidal sodium iodide symporter. *Blood* **2004,** 103, (5), 1641-6.

10. Ausar, S. F.; Rexroad, J.; Frolov, V. G.; Look, J. L.; Konar, N.; Middaugh, C. R., Analysis of the thermal and pH stability of human respiratory syncytial virus. *Mol Pharm* **2005,** 2, (6), 491-9.

11. Lakowicz, J. R., *Principles of fluorescence spectroscopy*. 2nd ed.; Kluwer Academic/Plenum: New York, 1999; 698 p.

12. Parasassi, T.; De Stasio, G.; Ravagnan, G.; Rusch, R. M.; Gratton, E., Quantitation of lipid phases in phospholipid vesicles by the generalized polarization of Laurdan fluorescence. *Biophys J* **1991,** 60, (1), 179-89.

13. Kueltzo, L. A.; Ersoy, B.; Ralston, J. P.; Middaugh, C. R., Derivative absorbance spectroscopy and protein phase diagrams as tools for comprehensive protein characterization: a bGCSF case study. *J Pharm Sci* **2003,** 92, (9), 1805-20.

14. Schrag, S. J.; Rota, P. A.; Bellini, W. J., Spontaneous mutation rate of measles virus: direct estimation based on mutations conferring monoclonal antibody resistance. *J Virol* **1999,** 73, (1), 51-4.

15. Cattaneo, R.; Rebmann, G.; Baczko, K.; ter Meulen, V.; Billeter, M. A., Altered ratios of measles virus transcripts in diseased human brains. *Virology* **1987,** 160, (2), 523-6.

16. Colf, L. A.; Juo, Z. S.; Garcia, K. C., Structure of the measles virus hemagglutinin. *Nat Struct Mol Biol* **2007,** 14, (12), 1227-8.

17. Burger, J. L.; Cape, S. P.; Braun, C. S.; Mcadams, D. H.; Best, J. A.; Bhagwat, P.; Pathak, P.; Rebits, L. G.; Sievers, R. E., Stabilizing Formulations for Inhalable Powders of Live-Attenuated Measles Virus Vaccine. *J Aerosol Med* **2008,** 21, (1), 25-34.

18. Kendrick, B. S.; Chang, B. S.; Arakawa, T.; Peterson, B.; Randolph, T. W.; Manning, M. C.; Carpenter, J. F., Preferential exclusion of sucrose from recombinant interleukin-1 receptor antagonist: role in restricted conformational mobility and compaction of native state. *Proc Natl Acad Sci U S A* **1997,** 94, (22), 11917-22.

19. Lee, J. C.; Timasheff, S. N., The stabilization of proteins by sucrose. *J Biol Chem* **1981,** 256, (14), 7193-201.

20. Shimizu, S.; Smith, D. J., Preferential hydration and the exclusion of cosolvents from protein surfaces. *J Chem Phys* **2004,** 121, (2), 1148-54.

21. Fields, B. N.; Knipe, D. M.; Howley, P. M.; Griffin, D. E., *Fields' virology*. 4th ed.; Lippincott Williams & Wilkins: Philadelphia, 2001; 3087 p.

22. Lemmon, M. A.; Engelman, D. M., Specificity and promiscuity in membrane helix interactions. *FEBS Lett* **1994,** 346, (1), 17-20.

23. Rees, D. C.; DeAntonio, L.; Eisenberg, D., Hydrophobic organization of membrane proteins. *Science* **1989,** 245, (4917), 510-3.

24. Evans, R. K.; Nawrocki, D. K.; Isopi, L. A.; Williams, D. M.; Casimiro, D. R.; Chin, S.; Chen, M.; Zhu, D. M.; Shiver, J. W.; Volkin, D. B., Development of stable liquid formulations for adenovirus-based vaccines. *J Pharm Sci* **2004,** 93, (10), 2458-75.

25. Schwendeman, S. P.; Costantino, H. R.; Gupta, R. K.; Siber, G. R.; Klibanov, A. M.; Langer, R., Stabilization of tetanus and diphtheria toxoids against moisture-induced aggregation. *Proc Natl Acad Sci U S A* **1995,** 92, (24), 11234-8.

26. Volkin, D. B.; Mach, H.; Middaugh, C. R., Degradative covalent reactions important to protein stability. *Mol Biotechnol* **1997,** 8, (2), 105-22.

27. Wakankar, A. A.; Borchardt, R. T., Formulation considerations for proteins susceptible to asparagine deamidation and aspartate isomerization. *J Pharm Sci* **2006,** 95, (11), 2321-36.

Table 3.1. Inhibition of aggregation of MV in the presence of various compounds (listed in order of their effectiveness in preventing aggregation).

Excipient	Concentration	Inhibition of Aggregation[a] (%)
Gelatin (fish skin)	2.5%	98
Lactose	10%	98
Gelatin (fish skin)	5%	94
Dextrose	20%	89
Mannitol	10%	88
Sodium Citrate	0.2 M	75
Malic Acid	0.15 M	75
Sorbitol	20%	72
Sucrose	20%	71
Trehalose	20%	69
Lactose	20%	69
Aspartic Acid	0.075 M	69
Diethanolamine	0.3 M	67
Sodium Citrate	0.1 M	66
Glycerol	20%	62
Lactic Acid	0.15 M	62
Sorbitol	10%	59
Glutamic Acid	0.15 M	58
Guanidine	0.3 M	52
Dextrose	10%	52
Glycerol	10%	44
Proline	0.3 M	43
Arginine	0.3 M	42
Sucrose	10%	40

[a] Relative to a control sample at t = 90 min. Inhibition of aggregation calculated as (1-$OD_{360\ sample}/OD_{360\ control}$) x 100%. The relative standard deviation in these calculated values was ≤ 10 %.

Table 3.1, continued.

Excipient	Concentration	Inhibition of Aggregation[a] (%)
Lysine	0.3 M	39
Tween 20	0.1%	39
Trehalose	10%	31
Brij 35	0.1%	19
Glycine	0.3 M	16
Tween 20	0.05%	14
Brij 35	0.05%	6
Albumin	1%	6
Tween 20	0.01%	-2
Tween 80	0.05%	-7
Pluronic F-68	0.01%	-7
Pluronic F-68	0.1%	-12
2-OH propyl γ-CD[b]	5%	-15
Tween 80	0.01%	-17
α-Cyclodextrin	2.5%	-19
2-OH propyl β-CD[b]	5%	-19
2-OH propyl β-CD[b]	10%	-20
Brij 35	0.01%	-21
Tween 80	0.1%	-22
Pluronic F-68	0.05%	-23
Histidine	0.3 M	-28
Albumin	2.5%	-30
2-OH propyl γ-CD[b]	10%	-31
Ascorbic acid	0.15 M	-656
Albumin	5%	-1426

[a] Relative to a control sample at t = 90 min. Inhibition of aggregation calculated as (1-$OD_{360\ sample}/OD_{360\ control}$) x 100%. The relative standard deviation in these calculated values was ≤ 10 %.

[b] CD = cyclodextrin.

Table 3.2. Midpoint transition temperature (T_m) of dye-labeled MV in the presence of selected stabilizers, as calculated from the GP of laurdan fluorescence.

Excipient	Concentration	T_m (°C)
none	-	44.2 ± 2.1
porcine gelatin	2.5%	36.9 ± 1.2
myo-inositol	0.15 M	47.4 ± 0.4
malic acid	0.15 M	47.8 ± 1.3
lactose	15%	38.7 ± 1.3
proline	0.15 M	39.7 ± 0.1
mannitol	10%	50.7 ± 1.5

Figure 3.1. (A) MV static light scattering intensity is shown as a function of temperature. Each point represents the mean of three normalized measurements, as described in the Materials and Methods section. (B and C) The effective diameter of MV, as determined by dynamic light scattering, is shown as a function of temperature. Each point represents the mean value calculated from triplicate samples. All measurements were taken at 90° from the 562 nm light source. Each measurement is composed of 5 accumulations. Error bars represent the standard deviation.

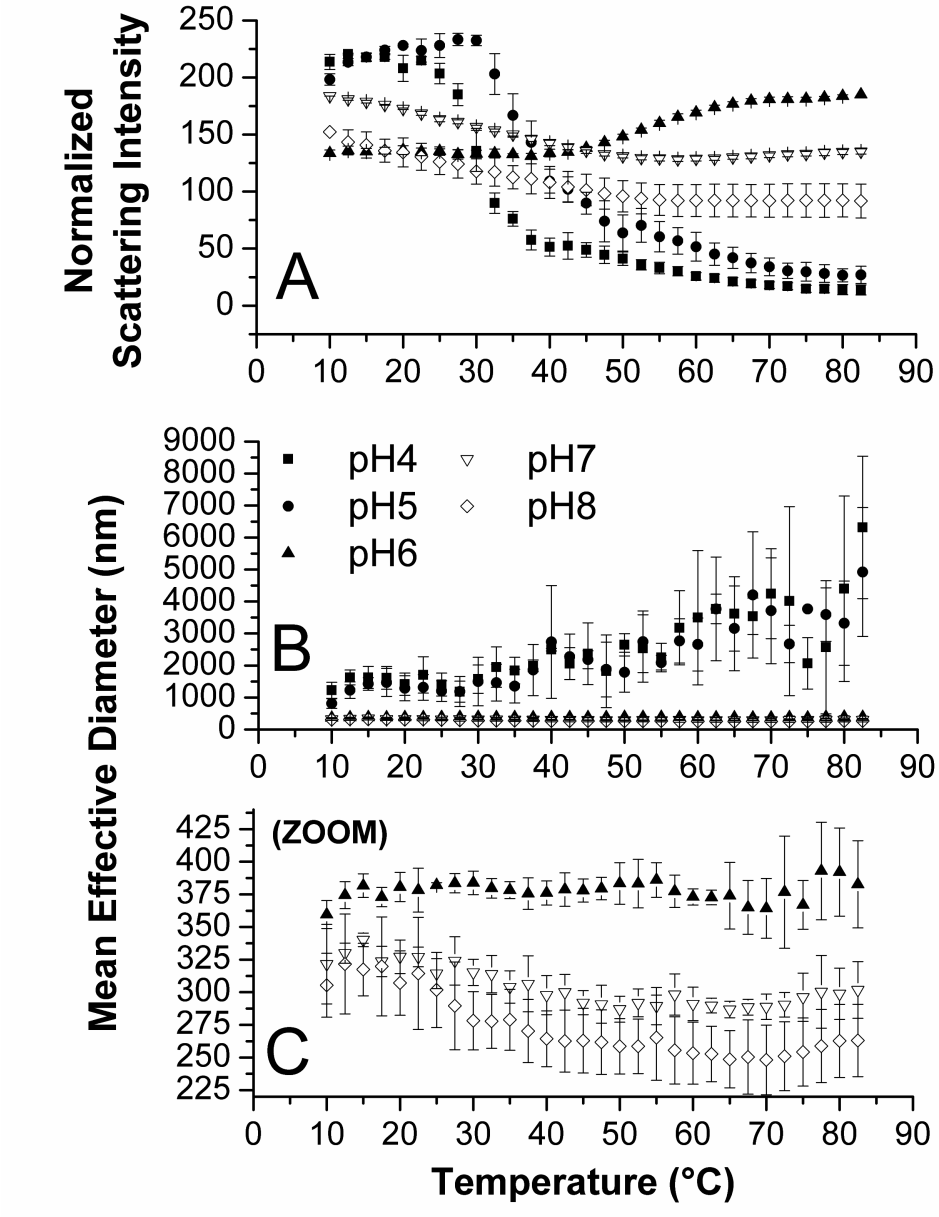

Figure 3.2. Far-UV circular dichroism of MV at 10 °C. A loss of viral protein secondary structure is exhibited at low pH.

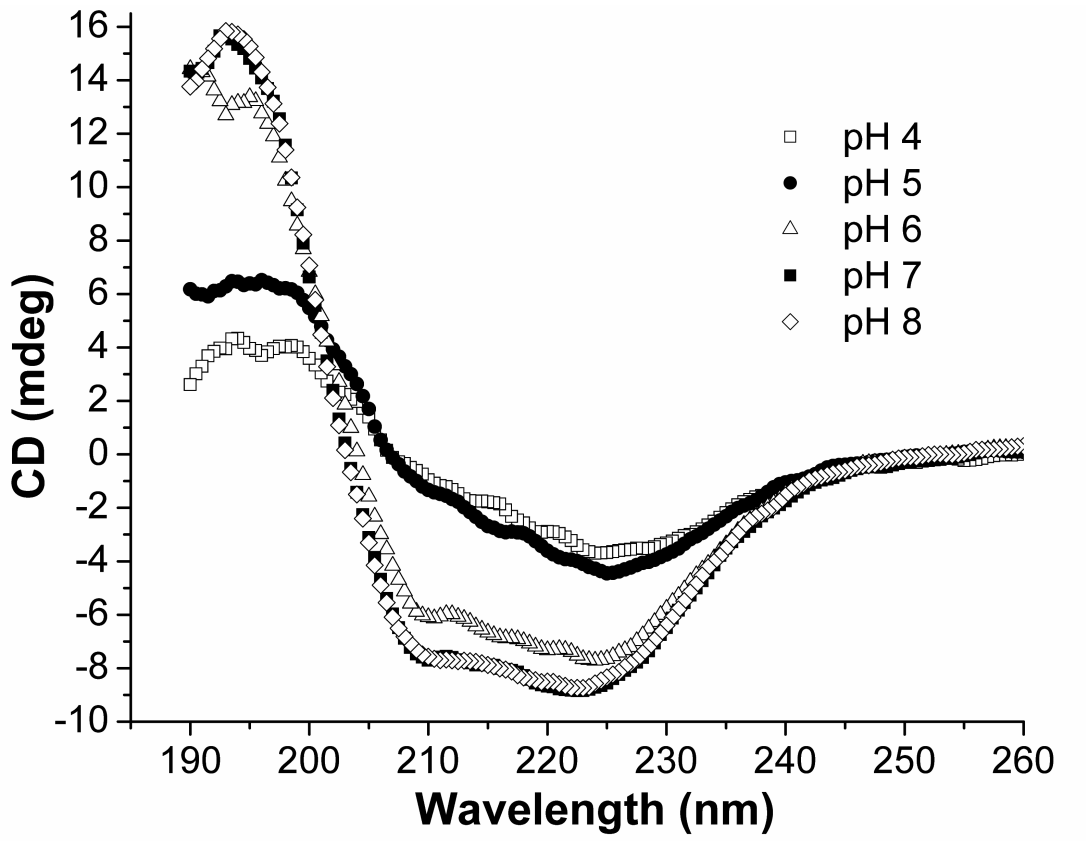

Figure 3.3. CD of MV at 222 nm is shown as a function of temperature. Each point represents the mean of normalized measurements from three independently prepared samples (measurements were normalized between 0 and -1 for ease of visualization). The error bars represent the standard deviation.

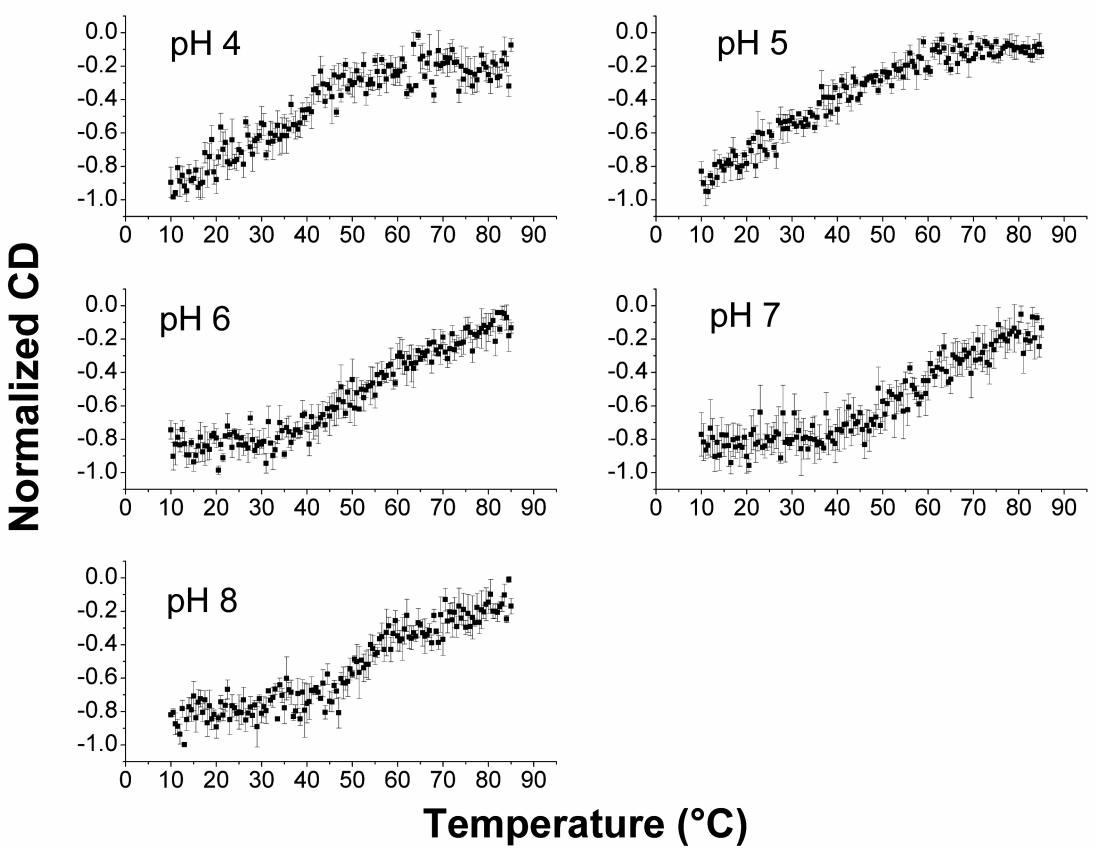

Figure 3.4. Intrinsic fluorescence of MV. The average peak position (n = 3) is shown as a function of temperature. The lower right panel shows the fluorescence intensity at 322 nm, also as a function of temperature (the mean of three normalized measurements is reported). Error bars represent the standard deviation.

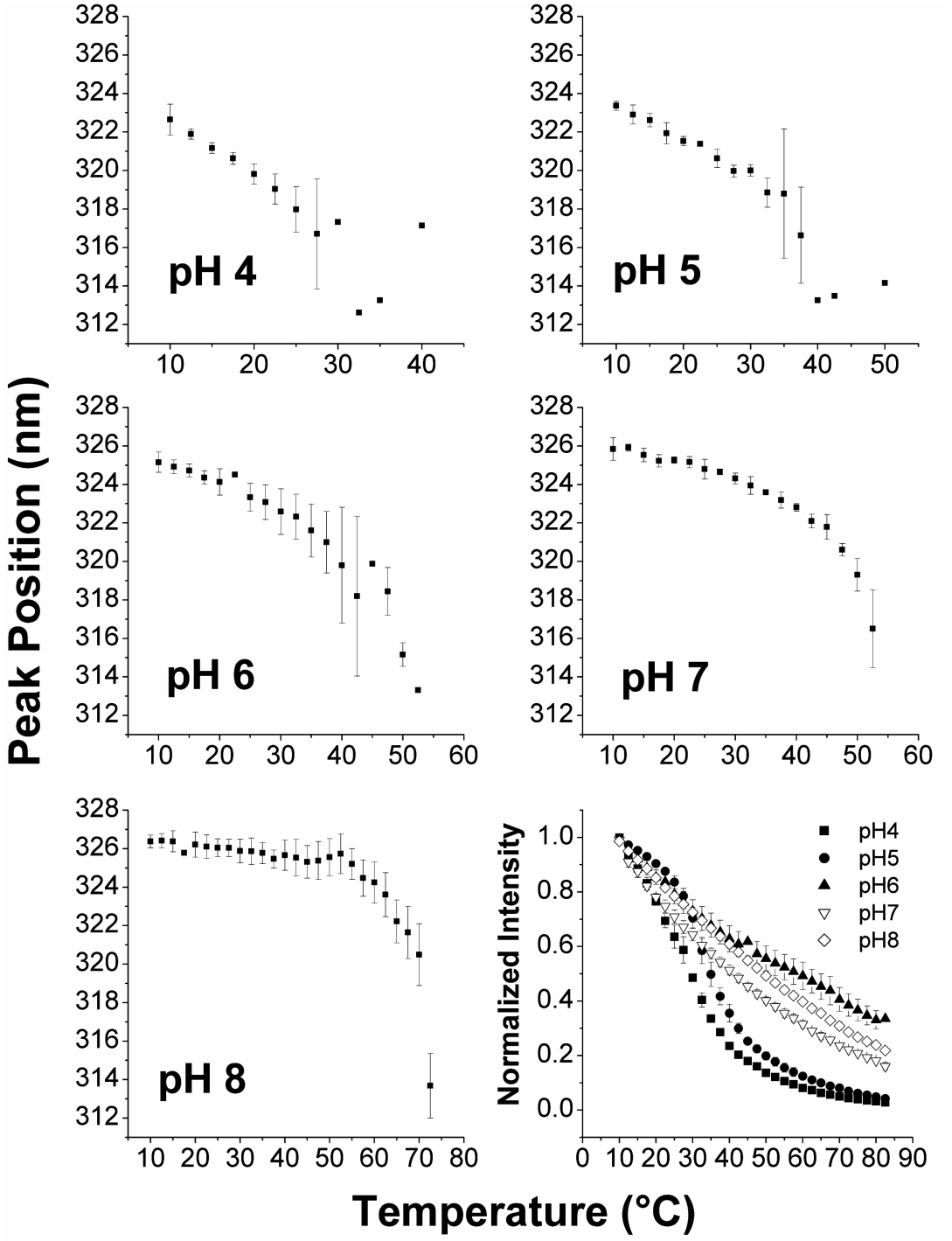

Figure 3.5. Fluorescence of ANS in the presence of MV. The average peak position (n = 3) is shown as a function of temperature. The lower right panel shows the fluorescence intensity at 469 nm, also as a function of temperature (the mean of three normalized measurements is reported). The error bars represent the standard deviation.

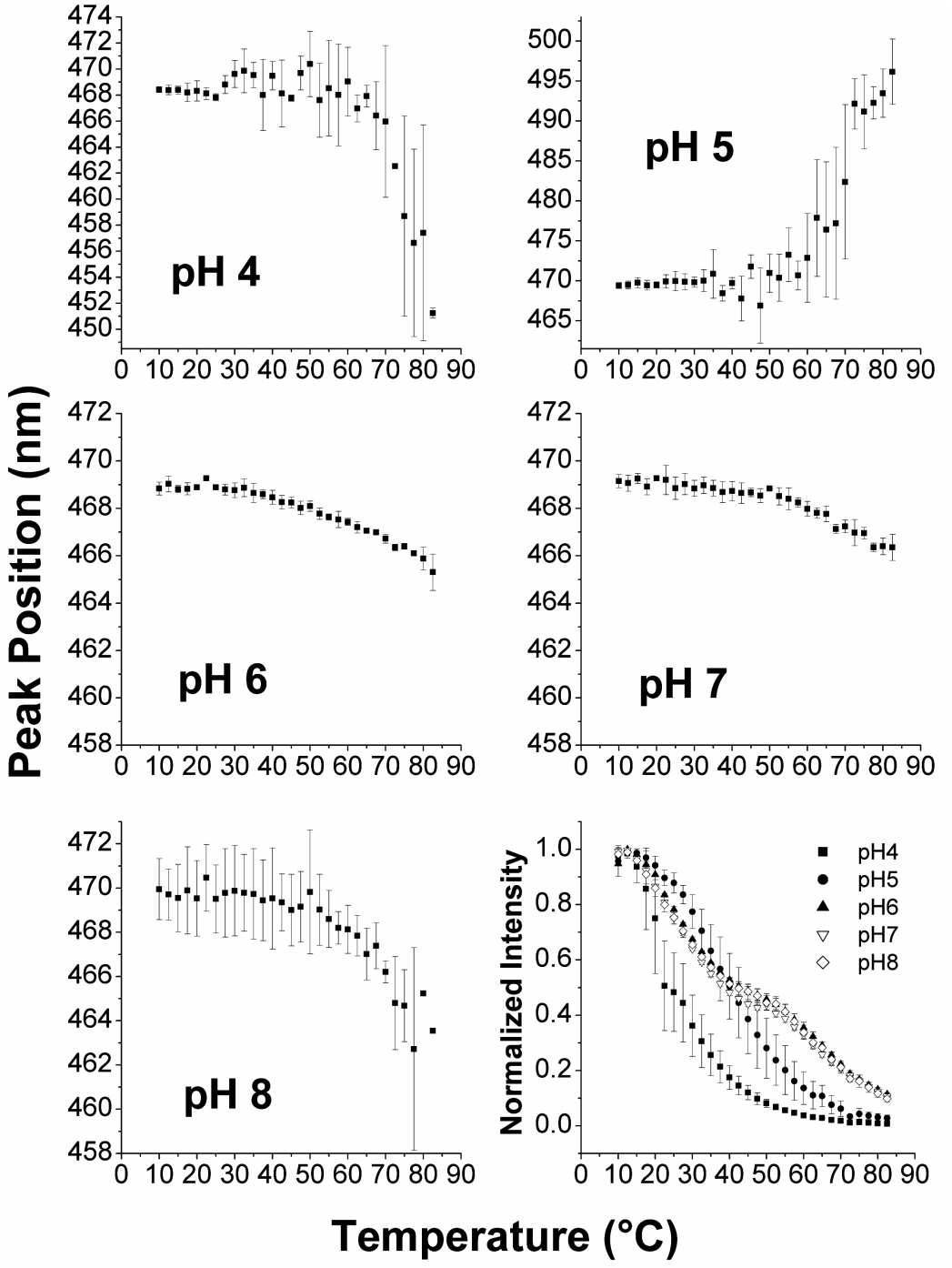

Figure 3.6. Fluorescence of laurdan in the presence of MV. Representative example spectra obtained at pH 7 and various temperatures are shown in (A). Spectra were corrected by subtracting the spectrum at each temperature of a buffer sample containing an equal concentration of dye. Generalized polarization (GP) of laurdan fluorescence in the presence of MV is shown in (B) as a function of temperature. Each point represents the mean GP of triplicate samples. Error bars represent the standard deviation.

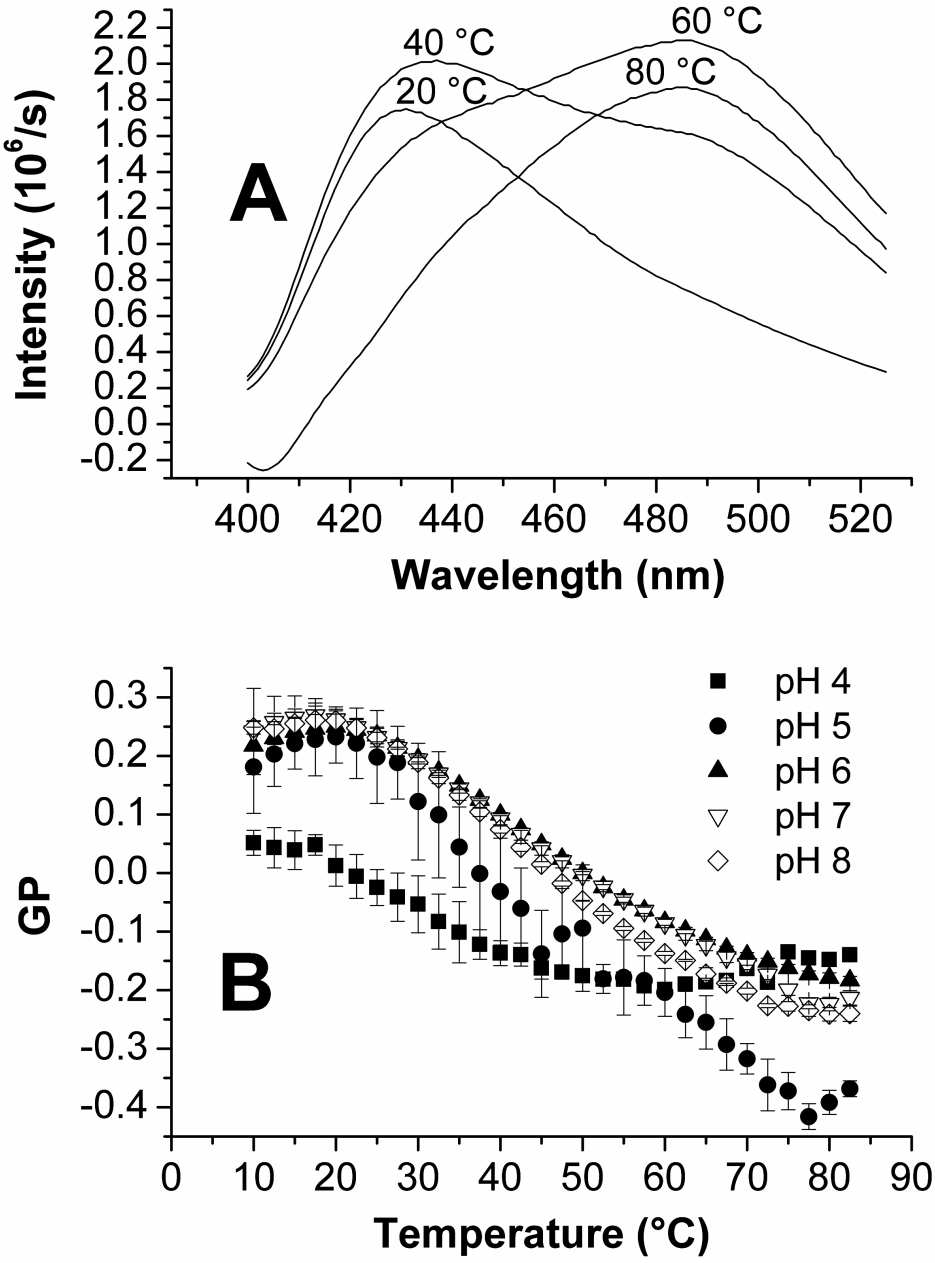

Figure 3.7. Empirical phase diagram (EPD) of MV. Data used to generate the EPD were measurements of mean effective diameter, intensity of (562 nm) light scattered at 90°, CD at 222 nm, intrinsic fluorescence intensity at 322 nm, ANS peak position, ANS fluorescence intensity at 469 nm, and GP of laurdan fluorescence.

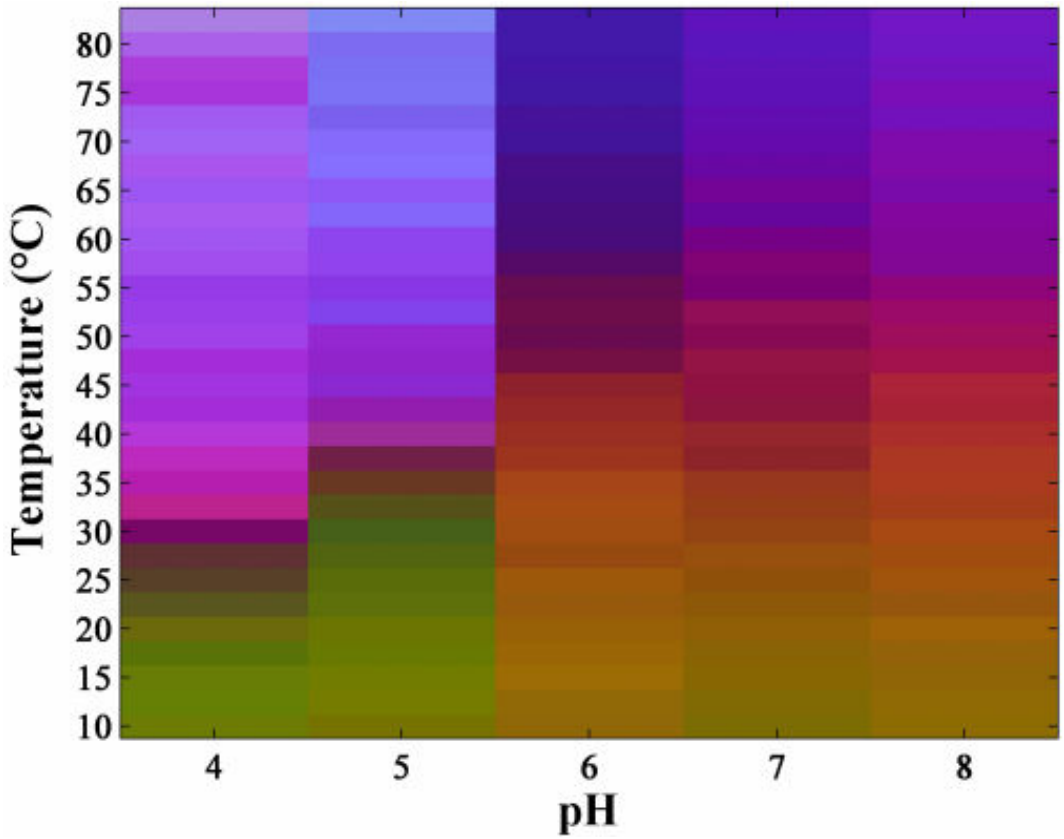

Figure 3.8. Intensity of light scattered by MV in the presence of various stabilizers is presented as a function of temperature. (A) shows the raw values, and (B) shows the intensity normalized between 0 and 1. In each panel, the points represent mean values (n = 3). Error bars represent the standard deviation.

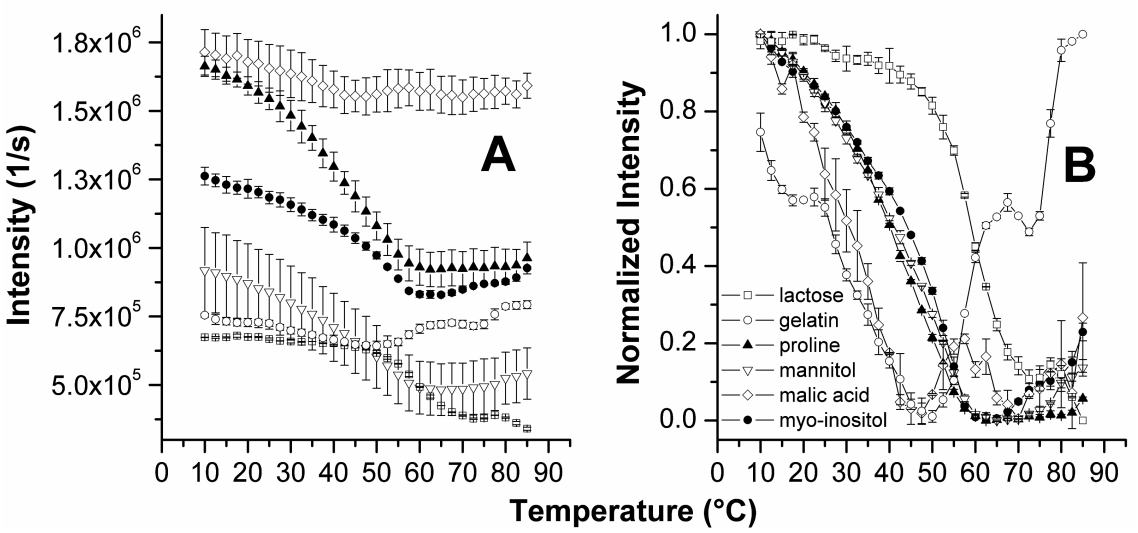

Figure 3.9. Results of plaque-based infectivity assays. Formulations of live, attenuated virus with the indicated stabilizers were incubated for 24 h at 21 °C. The percent infectivity relative to a sample measured prior to incubation is reported. Error bars represent the standard deviation.

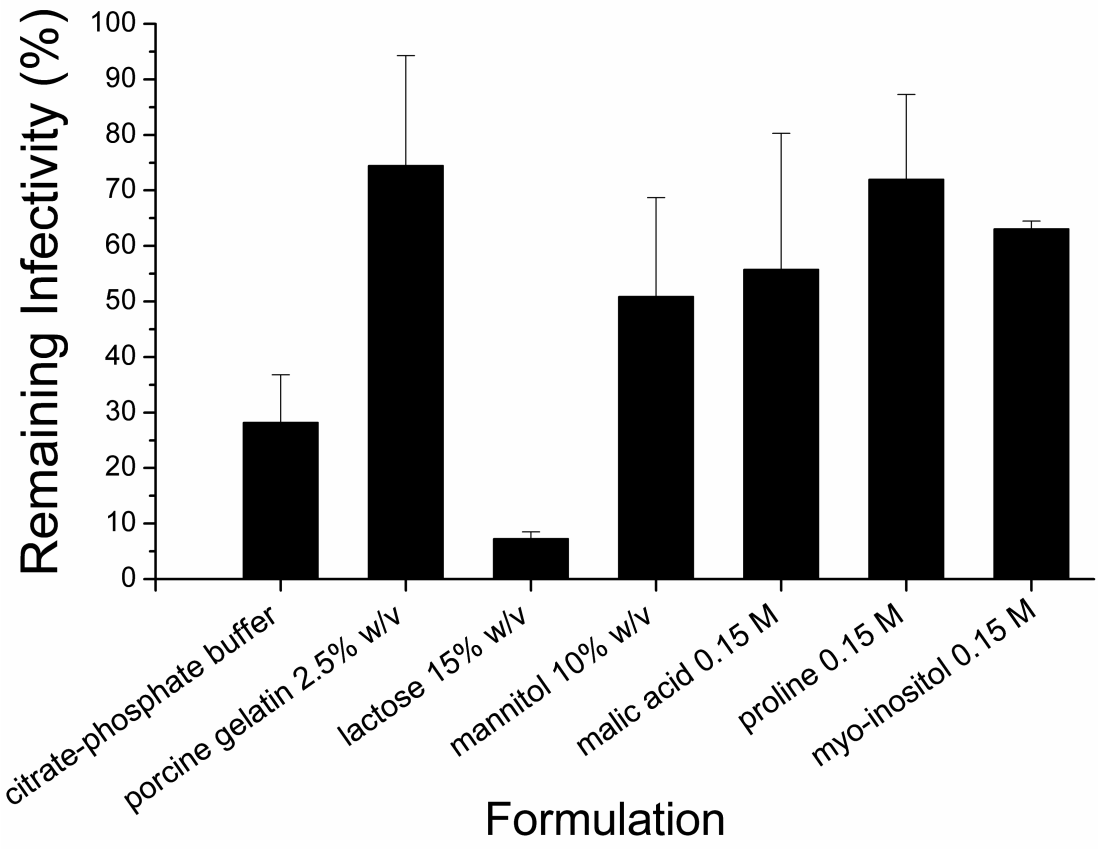

Chapter 4

Influenza Virus-Like Particles: Physical Degradation Pathways and Identification of Stabilizers

Overview

Respiratory infection by the influenza virus is a significant cause of mortality and morbidity worldwide.[1] Vaccination is the most effective measure for preventing infection and reducing the impact of epidemics caused by this highly contagious respiratory pathogen.[2] Nearly all of the commercially available influenza vaccines use the two main viral surface proteins hemagglutinin (HA) and neuraminidase (NA) as their primary antigens, but frequent mutation or reassortment of the segmented viral genome necessitates seasonal reformulation of the vaccine with antigens derived from currently circulating strains. Although humans are susceptible to infection by three genetically distinct types of influenza viruses (A, B, and C), the A strain is by far the most dangerous due to its greater rate of mutation. Small changes in the amino acid sequence of the HA and NA proteins (antigenic drift) are the cause of annual epidemics, while large changes (antigenic shift) result in less frequent but more destructive pandemics.[3]

As of 2005, the World Health Organization (WHO) considered the (type A) avian H1N5 influenza subtype to be the most likely cause of the next pandemic. Simultaneously, WHO acknowledged that current global manufacturing capacity is insufficient to meet global vaccine needs in the event of such a catastrophe.[2] Subtypes of influenza A that are currently circulating among humans include the H1N1, H1N2, and

H3N2 viruses. The typical inactivated influenza vaccine is derived from virus grown in the allantoic cavity of embryonated chicken eggs,[1] making the production process both costly and time-consuming. To provide a cheaper and more easily scalable alternative, a recombinant virus-like particle (VLP) that contains H1N1 influenza HA (as the uncleaved precursor HA0) and NA proteins has been produced in an insect cell/baculoviral expression system, using the murine leukemia virus (MLV) gag protein as the budding engine for particle formation.[4] VLP-based influenza vaccines have been shown in small scale studies to be safe and immunogenic and sometimes even to provide protection from infection by multiple viral subtypes.[5-8]

As an early developmental step towards the creation of a commercially viable vaccine, we have conducted studies to identify physical stabilizers of influenza VLPs. Utilizing a method developed in our laboratory that has already been successfully applied to the stabilization of vaccine-related proteins,[9, 10, 10] virus-like particles,[11, 12] and enveloped viruses,[13, 14] we have conducted a comprehensive physical characterization of influenza VLPs to direct the selection of physical stabilizers from a library of potential excipients. Multiple biophysical techniques, each sensitive to a different level of physical structure, have been used to measure changes in the physical state of VLPs in solution as a function of temperature and pH. The data from all techniques were synthesized into an empirical phase diagram (EPD) that allows visual identification of major physical changes induced by temperature and pH stress. The EPD was then used to determine the optimal formulation pH, and to develop a screening assay for the identification of stabilizers. We present here the results of the biophysical characterization as well as EPD-based screening for physical stabilizers of influenza VLPs.

Materials

Unless otherwise noted, all potential stabilizers (see Results) were obtained from Sigma-Aldrich (St. Louis, MO). Guanidine HCl, calcium chloride dihydrate, dextrose, D-mannitol, citric acid, and sodium phosphate dibasic were from Fisher Chemical (Fair Lawn, NJ). Type A porcine gelatin was purchased from Dynagel (Calumet City, IL) and D-sucrose and D-trehalose from Ferro-Pfanstiehl Laboratories, Inc. (Waukegan, IL). Ectoin (ultra pure) was provided by Bitop AG (Witten, Germany), and NV10 was obtained from Expedeon (formerly Novexin, Cambridge, UK). Concentrated excipient solutions were prepared by dissolution into 20 mM citrate/phosphate (CP) buffer of the appropriate pH. The pH was then adjusted (if necessary) to the target pH using concentrated NaOH or HCl. Final stock solutions were filtered with a 0.22-µm Durapore® (PVDF) membrane syringe filter (Millipore, Billerica, MA). Concentrations are reported in molarity or as percent weight-by-volume.

6-dodecanoyl-2-dimethylaminonaphthalene (laurdan) and 8-anilino-1-naphthalene sulphonate (ANS) were purchased from Molecular Probes (Eugene, OR). A 1.2 mM stock solution of laurdan and a 10 mM solution of ANS were prepared by dissolution in dimethylsulfoxide (DMSO, Fisher Chemical).

Methods

Preparation of VLPs for characterization

VLPs were produced in cultured Sf9 cells infected with a "triple gene" recombinant baculovirus.[4] VLPs were prepared for characterization by dialysis into CP buffer at each unit pH from 4 to 8. Buffer ionic strength was maintained at 0.1 using

NaCl. Material recovered from the dialysis cassettes (10,000 MWCO, Pierce, Rockford, IL) was concentrated at 4 °C with an Amicon® Ultra ultracentrifugation device (10,000 MWCO, Millipore, Billerica, MA) at 3,150 x *g*. The protein concentration of the retentate was estimated by a BCA (bicinchoninic acid) colorimetric technique (Pierce, Rockford, IL). Unless otherwise noted, triplicate samples were prepared at a final protein concentration of 90 μg/mL by diluting the retentate with 20 mM CP buffer of the appropriate pH.

Trypsin treatment of surface hemagglutinin

Trypsin (Sigma, final concentration 5 μg/mL) was added to VLP stock solutions (0.26 mg/mL viral protein in 30% sucrose/Tris-buffered saline, pH 7.4) and incubated for 5 min in a 2-8 °C cold room. After incubation, a three-fold molar excess of trypsin inhibitor from soybean (Fluka) was added and the resulting solution passed through a 0.45-μm syringe filter (Millipore). Samples were then dialyzed into the appropriate CP buffer and concentrated as described above, but using 100,000 MWCO dialysis tubing (Spectrum Laboratories, Rancho Dominguez, CA). Cleavage of HA, as well as non-cleavage of MLV gag, was confirmed by western blot analysis (not shown).

Dynamic light scattering

Dynamic light scattering (DLS) was used to measure changes in the mean effective diameter of VLPs as a function of increasing temperature. Measurements were taken with a Brookhaven Instrument Corporation system (Holtzille, NY). Incident light at 532 nm was generated by a 125 mW diode-pumped laser. Scattered light was collected at

90° to the incident beam, and a digital autocorrelator (BI-9000AT) was used to create the autocorrelation function. Five measurements were taken every 2.5 °C over the range of 10-85 °C. Cumulant analysis was used to extract particle diffusion coefficients from the correlation function and convert them to particle diameters by means of the Stokes-Einstein equation. It should be noted that the effective diameter calculated by this method is accurate for particles of diameter < 1 μm – the values obtained from measurements of larger particles should be used for qualitative comparison only. In addition to particle size, the second cumulant of the distribution of particle diffusion coefficients was also extracted from the correlation function as a measure of sample polydispersity.

Circular dichroism spectroscopy

Circular dichroism spectroscopy (CD) measurements were made with a Jasco J-810 spectrophotometer, using a sensitivity setting of 100 mdeg, a response time of 2 sec, and a band width of 1 nm. Composite (3-5 accumulations) spectra of VLPs were obtained at a scan rate of 20 nm/sec and a data pitch of 0.5 nm/sec. Variable temperature experiments monitoring the CD signal at 227 nm were conducted to detect changes in total VLP protein secondary structure as a function of temperature. Measurements were taken every 0.5 °C over the range of 10-90 °C, with a temperature ramp rate of 15 °C/h and a delay time of 2 sec. Midpoint transition temperature (T_m) values were determined by mathematically fitting the temperature dependent data to a sigmoidal function using the Origin® data analysis software. Both the spectra and the heating traces reflect additive contributions from the three different proteins, although they are presumably dominated by contributions from the most abundant of these proteins. The MLV gag protein has

been shown to be 3-4 times more abundant than the HA protein in these VLPs, while the abundance of HA is perhaps an order of magnitude greater than that of NA.[4]

Fluorescence spectroscopy

Unless otherwise noted, fluorescence emission spectra were collected every 2.5 °C over the range 10-85 °C using a Photon Technology International fluorometer (Birmingham, NJ). The temperature was increased at a rate of 15 °C/h, with a step size of 1 nm and an integration time of 1 sec used for all measurements. Static light scattering was also monitored during fluorescence experiments through the use of a second detector (oriented 180° from the fluorescence detector). Using the Origin® software package, emission peak positions were determined by derivative analysis and T_m values were determined by mathematically fitting the temperature dependent data to a sigmoidal function.

The intrinsic fluorescence of the aromatic amino acids tryptophan and tyrosine was employed to identify changes in VLP protein tertiary structure as a function of temperature. Upon excitation at 280 nm, fluorescence emission spectra were collected from 300 to 380 nm. Excitation and emission slit widths were set to 3 and 4 nm, respectively.

The fluorescence emission of 8-anilino-1-naphthalene sulphonate (ANS) in the presence of VLPs was utilized as an alternative method to monitor the stability of viral protein tertiary structure. ANS, a small molecule that is known to have affinity for the apolar regions of proteins, displays weak fluorescence in solution, but, when bound, exhibits enhanced and (usually blue) shifted emission intensities.[15] The fluorescence

emission spectra of VLP samples prepared with 70 μM ANS were collected from 425 to 550 nm after excitation at 385 nm. While measuring ANS fluorescence, the excitation and emission slit widths were both set to 4 nm.

Another molecular probe, 6-dodecanoyl-2-dimethylaminonaphthalene (laurdan), was used to directly monitor thermally-induced changes in the fluidity of the VLP membrane. The chemical structure of laurdan contains a long acyl chain attached to derivatized naphthalene, thus allowing it to readily incorporate into lipid bilayers. An increase in membrane hydration can drive a transition in bilayer fluidity from a gel (less fluid) to a liquid crystalline (more fluid) phase. When excited at 340 nm, an increase in membrane water content shifts the emission of laurdan from approximately 440 nm to around 490 nm. A useful parameter is the generalized polarization (GP), defined[16] as

$$\mathbf{GP = (I_{440}-I_{480})/ (I_{440}+I_{480})} \qquad \mathbf{(4.1)}$$

where I_x = intensity at wavelength x. Therefore decreasing GP values indicate an increase in membrane fluidity, and vice versa. Slit widths for laurdan experiments were set to 2 nm (excitation) and 5 nm (emission).

Empirical phase diagram

Please refer to Chapter 3 for a description of the algorithm for generating empirical phase diagrams.

Excipient screening

The aggregation of VLPs at pH 6 and 60 °C was monitored by measurements of turbidity (optical density at 350 nm, OD_{350}) as a function of time. Duplicate samples of

VLPs in the presence or absence of various GRAS agents were prepared at a protein concentration of 55 μg/mL by diluting the concentrated retentate (see above) with 20 mM CP buffer and/or a concentrated excipient solution of the appropriate pH. Measurements were taken every 30 sec over a period of two h using a temperature-controlled Agilent 8453 spectrophotometer (Palo Alto, CA).

Results

Dynamic light scattering

DLS measurements of VLP suspensions show evidence of both pH- and temperature-induced changes in particle size (Figure 4.1A). At low temperatures, the particle size at pH 4 or 5 is 2-3 times greater than at pH 6-8, indicating that significant aggregation and/or swelling is induced by acidic pH. Samples at pH 4 do not show a temperature-induced change in particle size until about 75 °C, after which a gradual increase in effective diameter is observed. On the other hand, a sharp increase in particle size at pH 5 is seen at about 50 °C, with another possible increase at about 75-80 °C. Samples at each pH from 6-8 are stable to increasing temperature up until about 58 °C, above which samples at pH 6 and 7 show a marked increase in particle size. Samples at pH 8 also show evidence of an increase in size at about 60 °C. The size increase in the latter case is relatively small and may be due to swelling of VLPs rather than aggregation. In general, the polydispersity of the VLPs (Figure 4.1C) was seen to increase with increasing acidity. The polydispersity of samples at pH 4 and 5 remained nearly constant across the temperature range, while samples at pH 6 and above show an increase in polydispersity near 60 °C, consistent with the changes seen in the size data.

The intensity of scattered light was also recorded during the DLS measurements (Figure 4.1B). Normalized values are reported because instrument settings are optimized for each sample, precluding meaningful direct sample-to-sample comparisons. In general, an increase in particle size or particle refractive index (relative to the solvent) will result in an increase in scattered light intensity. It should be noted, however, that a reduction in refractive index as a result of decreased particle density (*e.g.,* due to swelling) would manifest itself as a lower scattering intensity. This is the best explanation of the data for samples at pH 8, where a smooth and gradual reduction of scattered light intensity is seen over the majority of the temperature ramp. There is a slight disruption of the curvilinear decline around 60 °C that corresponds to the increase in effective diameter seen for these samples in Figure 4.1A. Plots of light scattered by samples at pH 5 also show evidence of structural alterations occurring around 60 °C, manifested by a sharp decrease in scattered light intensity. The plots corresponding to pH 6 and 7 are similar, with the decrease in scattered light occurring at higher temperatures (~ 75 °C). These decreases could be due to settling of precipitated material out of the incident light beam, consistent with the interpretation of the size data given above. The trace for pH 4 shows only a gradual decrease in intensity, with no sharp changes that correlate with measured changes in particle diameter (an exception is the transient reduction in scattering intensity from 30-35 °C, but see the results of laurdan fluorescence experiments below).

Circular dichroism studies

From pH 4 to 8, the CD spectra of influenza VLPs display minima near 210 and 227 nm, suggesting the presence of significant helical character across the pH range of

interest (Figure 4.2A). The loss of signal with increasing temperature (Figure 4.2B) is indicative of a temperature-dependent loss of secondary structure. To further investigate this effect, the signal at 227 nm was monitored as a function of temperature (Figure 4.3). Observed sharp changes in the CD signal are consistent with temperature-dependent protein structural transitions. Samples at pH 6 show the highest T_m at around 55 °C. Samples of increasing acidity have markedly reduced T_m values of 38 (pH 4) and 47 °C (pH 5), while samples at pH 7 or 8 are very similar with T_m values of 53 and 51 °C, respectively. The shapes of the melting curves suggest multiple components, presumably reflecting the heterogeneous nature of the system.

Intrinsic fluorescence studies

The intrinsic fluorescence emission peak position was determined for all samples as a function of temperature (Figure 4.4). In each case, a slight decrease in peak position over the temperature range ~ 10-40 °C is followed by a sharp transition to longer wavelengths. For protein samples, a thermally-induced red shift in peak maximum is observed when fluorescent amino acid side chains are exposed to an environment of increased polarity. This is consistent with an unfolding event in which amino acid fluorophores, normally at least partially buried in the apolar protein core, are exposed to the aqueous solvent. At temperatures between 55-65 °C (depending on pH) the peak maximum returns to shorter wavelengths, consistent with the observed aggregation of VLPs at elevated temperatures. The (normalized) emission intensity at 330 nm was also plotted as a function of temperature (Figure 4.4). In the absence of structural transitions, such plots typically exhibit a smooth curvilinear decline in emission intensity with

increasing temperature due to the intrinsic effect of temperature. Deviations from the curvilinear profile occur for all samples in the range 45-65 °C, confirming that the environments of intrinsic fluorophores are altered upon heating.

ANS fluorescence studies

The peak position (≥ 470 nm) and high intensity of ANS fluorescence emission in the presence of VLPs indicates that ANS is bound to apolar regions of these macromolecular complexes at low temperature. As previously indicated, this is not surprising given the presence of the lipid bilayer. Plots of ANS emission peak position as a function of temperature (Figure 4.5) display a temperature-dependent shift to shorter wavelengths in all samples, followed in some cases (*i.e.,* for pH 5, 6, and 7) by a shift to longer wavelengths. In all samples, the extent of change in peak position (2-3 nm) is much less than that observed by intrinsic fluorescence. The high variability of the peak position and noise at elevated temperature make it difficult to draw substantial conclusions from these data. The relative intensity of ANS at 485 nm (Figure 4.5) manifests more definite evidence of temperature-induced exposure of apolar motifs. This is true in particular for the plots of samples at pH 5-8, in which a slight increase in emission intensity (beginning near 38 °C at pH 5 and 43 °C at pH 6-8) is seen superimposed over the curvilinear decline in emission that corresponds to the expected non-specific thermal quenching of fluorescence.

Laurdan fluorescence studies

Plots of generalized polarization (GP) as a function of temperature (Figure 4.6) indicate a gradual increase in VLP membrane hydration (fluidity) upon heating. Not surprisingly, the pH of VLP suspensions has an effect on the rate and extent of membrane hydration. At low temperatures, the extent of membrane hydration (*i.e.,* GP values) for all samples is very similar. Above 40 °C, samples at pH 4 consistently show the least change in membrane hydration, and, in general, samples prepared at low pH are slower to incorporate water molecules into the bilayer as the temperature is increased (notice that the temperature for which GP = 0 increases for more acidic samples). While the GP values of samples prepared at pH 4, 7, or 8 vary in a sigmoidal fashion with temperature, samples at pH 5 and 6 show a quasi-linear decline in GP over the temperature range examined. The extent of membrane hydration is greatest at high temperature (that is, above 75 °C) for samples at pH 5 and 6.

Static light scattering at 340 nm was also monitored during laurdan fluorescence experiments (data not shown). While these data were essentially similar to the static light scattering measured during the DLS experiments, the transient drop in scattered light intensity observed for samples at pH 4 (Figure 4.1B, 30-35 °C) was not detected during this additional experiment, suggesting that it may have been an artifact.

Empirical phase diagram

An empirical phase diagram (Figure 4.7) was generated from the temperature-dependent data presented in the preceding sections. Approximately 10 different phases can be seen over the experimental space, with the largest phase (pH 6-8, low temperature,

blue) corresponding to the least structurally disrupted state of the VLPs. There is a transition region that appears above this phase between 35 and 55 °C for pH 6-7, and from 35 to 50 °C at pH 8 (purple). The variably colored area above 60 °C for pH 6 and 7 corresponds to particle aggregation. The lack of significant aggregation at pH 8 yields a phase at high temperature (dark red) that is different than that seen at pH 6 or 7. At pH 4 and 5, two different phases are seen at low temperature, both representing significant structural disruption (light blue). Additional temperature-induced conformational changes give rise to multiple phases above 35 °C in the low pH region (green/orange). The apparent phase boundaries between pH 5 and 6 and above 40 °C represent conditions of intermediate stability, providing a starting point for the development of an excipient screening assay.

Excipient screening

A library of GRAS (generally recognized as safe) compounds was screened for potential stabilizers of VLPs in solution. Utilizing the empirical phase diagram that was produced from characterization studies (Figure 4.7), a screening assay was developed to identify excipients that prevent VLP aggregation (the most apparent physical degradation process). Although the choice of initial temperature and pH conditions for the screening assay was guided by the phase diagram (see preceding section), the final conditions were optimized to enhance subtle differences between potential stabilizers. Depending on the behavior of the control samples, percent inhibition of aggregation (Table 4.1) was calculated at either t = 15 or t = 30 minutes - whichever represented the time of maximal aggregation. The most promising aggregation-inhibiting compounds were found in a

variety of molecular classes, including detergents, polyols, amino acids, sugars, and sugar alcohols.

Effect of individual stabilizers

Using the top performing aggregation inhibitors from several molecular classes - namely, trehalose, glycerol, sorbitol, lysine, and diethanolamine (given the propensity of detergents to disrupt lipid bilayers, the apparent success of Tween 20 and Brij 35 as aggregation inhibitors may be artifactual) – CD and fluorescence measurements of VLPs in the presence of potential excipients were conducted. The solution pH was set to 7 for these experiments, to more closely approximate an actual vaccine formulation.

As described in the Methods section, variable-temperature CD measurements were employed to determine if any of the selected compounds stabilize viral protein secondary structure (not illustrated). Of all the compounds tested, only sorbitol appeared to have a possible stabilizing effect on the secondary structure of viral proteins; the T_m of sorbitol-containing samples (55 °C) is slightly elevated relative to the control (54 °C), but formulations containing the other potential excipients show T_m values in the range of 50 °C (trehalose) to 53 °C (lysine).

The intrinsic fluorescence method was employed to measure the effect of potential stabilizers on viral protein tertiary structure. Plots of the emission peak position versus temperature (Figure 4.8) show a transition from approximately 329 nm to 336 nm that begins at or near 40 °C for most of the formulations tested. The exception is the formulation containing lysine, which exhibits its fluorescence peak near 344 nm at low temperature and shows evidence of a possible transition to slightly longer wavelengths

(+1-2 nm) starting at 43 °C (the error in these measurements prevents the conclusion that the shift is statistically significant). The T_m of the control is 51 °C. Diethanolamine is not an effective stabilizer, inducing a T_m of 49 °C, while formulations containing glycerol, trehalose, and sorbitol all show slightly elevated T_m values of 52, 53, and 54 °C, respectively. Static light scattering collected during these experiments (data not shown) indicated similar behavior among all formulations except the one containing lysine. In the presence of lysine, light scattering intensity was reduced greater than tenfold, suggesting structural disruption of the VLPs.

Laurdan fluorescence was used to measure the effect of several compounds on the fluidity of the viral membrane as a function of increasing temperature. In these experiments, those potential excipients which thus far exhibited weak or no positive effect on physical stability (*i.e.,* diethanolamine, glycerol, and lysine) were removed and replaced with glycine, ectoin, and NV10. Glycine was introduced due to a personal communication stating that it may stabilize the influenza HA and/or NA proteins. Ectoin (an organic osmolyte) and NV10 (a 5 kDa linear carbohydrate polymer) were tested as potential novel stabilizers of the viral membrane, based on reports of their general effectiveness in stabilizing macromolecular systems.[17] Upon visual inspection of the temperature-dependent GP data (Figure 4.9), one or two of the compounds tested appear to inhibit the gel-to-liquid crystal transition. Again using sigmoidal fits to approximate the data, T_m values were extracted in order to quantitatively compare the effects of each stabilizer. As compared to a control sample (T_m = 52 °C), formulations containing sorbitol or ectoin have slightly higher T_m values of 54 °C. Given the magnitude of error associated with these measurements, however, the apparent increase in T_m is probably not

significant in both cases. On the other hand, glycine and trehalose do seem to exert a significant stabilizing effect with T_m values of 59 and 60 °C, respectively. NV10 has a negative effect on the stability of the viral envelope, inducing (relative to the control) lower GP values (increased membrane hydration) at temperatures above 20 °C. The T_m calculated for the NV10 formulation is 46 °C.

Discussion

A composite biophysical approach has been used to identify stabilizers of an influenza-based virus-like particle designed as a vaccine antigen. The signals from a variety of spectroscopic and light-scattering techniques were mathematically combined in the form of an EPD to enable visualization of the most important changes in physical structure resulting from exposure to stress conditions (*i.e.,* temperature and pH). Consistent with prior analyses of enveloped viruses,[13, 18] the data suggest a high degree of structural disruption at pH 4 and 5 even at low temperatures, with greater stability and structural similarity from pH 6 to 8 up to ~ 40 °C. Based on the EPD and analysis of data derived from the individual techniques, VLPs prepared at pH 7 are the most resistant to temperature-induced physical disruption. Even though the EPD shows a high degree of similarity between pH 6 and 7, the most conservative approach is to formulate as far as possible from apparent phase boundaries. Such a phase boundary is obvious between pH 5 and 6. Interestingly, many of the fluorescence-based techniques imply very few differences in structure between these conditions; upon inspection, it can be seen that the CD and DLS data are responsible for the major differences seen.

DLS was employed to monitor particle aggregation, one of the most important physical degradation processes detected for influenza VLPs. Although there is a well-known low pH-induced conformational change in influenza HA that leads to fusion of the viral envelope with the host endosomal membrane *in vivo*,[19-21] the uncleaved HA precursor (present in these particles) has been shown not to induce fusion of lipid bilayers.[22] VLPs with trypsin-cleaved HA were observed at pH 5 and 6 by DLS to produce aggregates at 10 °C with an average hydrodynamic diameter greater than 1 μm (Figure 4.10), suggesting that VLPs with uncleaved HA aggregate due to some pH-dependent mechanism other than HA-mediated membrane fusion. Whether this is due to unfolding of HA or other viral protein(s) should be the subject of further study. Regardless of mechanism, the serial decrease in size with increasing pH at 10 °C indicates a significant dependence on proton concentration in the aggregation behavior of influenza VLPs. At pH 8, where the proton concentration is relatively low, the measured size increase upon heating is not nearly as dramatic as pH 3-7 and may be due to particle swelling rather than aggregation.

The presence of double minima near 210 and 227 nm in the CD spectra of influenza VLPs suggests appreciable helical content. Given that the influenza neuraminidase is composed primarily of β-structure,[23] it is probable that the majority of the CD signal derives from the other two viral proteins within the VLPs. Both influenza hemagglutinin[24] and MLV gag[25, 26] have been shown to have substantial amounts of helical character. The shapes of the thermal transitions demonstrate both the heterogeneity of these proteins as well as perhaps the non-two-state nature of the transitions. While the wide range of calculated T_m values (37-55 °C) across samples

prepared at various pH levels indicates that pH has a strong effect on the secondary structural stability of the VLP proteins, it should be noted for low-pH samples that the appearance of aggregates may be artificially lowering the CD signal at elevated temperature. On the other hand, it is clear that low-pH secondary structural alterations begin at temperatures well below those at which thermally-induced aggregation was detected by DLS.

Based on changes in the intrinsic fluorescence of viral aromatic amino acids, the tertiary structures of the VLP proteins respond similarly to increasing temperature over the pH range. For all samples, a thermally-induced red shift in the peak maximum is observed, indicating that fluorescent amino acid side chains become more exposed to an environment of increased polarity. Between 50 and 55 °C at pH 4, 5, and 8, and around 60 °C for pH 6 and 7, the red-shift reverses and an increase in fluorescence intensity is observed. This indicates a return to an environment of decreased polarity, and in the case of samples of pH < 8, can be correlated to particle aggregation.

Fluorescent dyes were useful tools in the identification of subtle responses by VLPs to changes in solution temperature and/or pH. Not unexpectedly, ANS was able to bind extensively to all samples at low temperature, probably due to the presence of the host cell-derived lipid membrane. Analysis of ANS fluorescence intensity as a function of temperature was more effective in detecting differences in samples across the pH range and reflects the relative physical instability of VLPs in acidic media. The use of laurdan to monitor changes in membrane fluidity was also sensitive to physical changes in influenza VLPs. Previous characterization studies of enveloped viruses[13, 14] seem to indicate that the lipid bilayer is no less immune than viral proteins to pharmaceutically

relevant stress conditions such as temperature and pH. This is similarly valid in the context of the VLPs under investigation, which, in addition to the membrane itself, are composed almost entirely of membrane-associated proteins. Thus, no component of these particles is independent of the membrane, and it can readily be appreciated how changes in membrane hydration might influence the overall physical stability of influenza VLPs.

Aggregation was the most dramatic physical degradation pathway observed during the biophysical characterization of influenza VLPs. Although increased temperature is required to cause aggregation between pH 6 and 7, VLPs were seen to aggregate even at low temperature at pH 5 and below (no aggregation was measured above pH 7). This fact is reflected below 40 °C in the EPD as an obvious apparent phase boundary between pH 5 and 6. A central assumption of the EPD-based approach to physical stabilization is that such boundaries provide potential conditions for the screening of physical stabilizers. The rationale behind this concept is that if the macromolecular system is (relatively) unstressed, the relevant degradation pathways will not be (either kinetically or thermodynamically) significant enough to distinguish between a reasonably small subset of possible stabilizers. On the other hand, if the system is exposed to more extreme conditions, chemical stabilizers may be insufficient to prevent stress-induced transitions to (more degraded) low-energy states. In this case, the process of particle aggregation under mildly acidic conditions could be due to the structural perturbation of one or more viral proteins into a non-native aggregation-competent state.[27] A variety of GRAS compounds were found to inhibit particle aggregation through the use of a screening assay operated under conditions of meta-stability identified using the EPD. The most effective of these compounds include

diethanolamine, glycerol, sorbitol, trehalose, and lysine. Based on light scattering and fluorescence data, the apparent stabilization against aggregation by lysine appeared to involve a complete disruption of VLP structure resulting in solvent exposure of normally buried amino acid fluorophores and accompanying particle disintegration. Sorbitol and trehalose, however, were seen to stabilize the tertiary structure of viral proteins, while glycerol and diethanolamine exhibited more or less neutral effects on both tertiary and secondary structure. Given that glycerol and diethanolamine reduce the aggregation of VLPs without preventing changes in protein tertiary structure, it seems likely that these compounds exert their effect by directly interfering with protein-protein interactions. Sorbitol and trehalose, on the other hand, do delay the unfolding of VLP protein tertiary structure in accelerated degradation studies, suggesting that the prevention of aggregation by these two compounds occurs due to the preservation of native-like protein structure(s). This kind of protein stabilization by sugars and polyols has been studied extensively and is thought in most cases to be due to non-specific effects such as preferential hydration.[28-30] There is the potential for specific effects as well. With the exception of lysine, there is some similarity between the chemical structures of the other stabilizers to sialic acid, the natural ligand of the influenza HA protein. Whether the stablizers are able to bind directly to HA spikes on the surface of influenza VLPs is unknown at this time. Finally, trehalose and glycine may possess the ability to stabilize viral envelope-like strucutures by arresting the process of temperature-induced membrane hydration. The ability of trehalose to increase the gel-to-liquid-crystalline phase transition temperature in multilamellar vesicles is well-known,[31-33] and has been proposed to operate by means of direct replacement of water molecules bound to lipid carbonyls[31] or by inducing a closer

lipid packing arrangement as a result of increased interfacial tension.[32] It is possible that glycine in this case is operating through a similar mechanism. Of all the compounds studied, trehalose appears to be the most effective physical stabilizer due to its ability to prevent VLP aggregation, stabilize VLP protein tertiary structure, and prevent temperature-induced hydration of the lipid bilayer.

To summarize, we have employed a biophysical approach to characterize the stability of influenza VLPs as a function of temperature and pH, two pharmaceutically relevant stress factors. While the use of accelerated stability-indicating assays is a common approach, we were able to create and use a visual representation of the entire characterization data set to identify optimal conditions for screening of potential stabilizers. Subsequently, we were able to identify three effective physical stabilizers of influenza VLPs. While additional work is needed to determine the optimal concentration(s) of these stabilizing compounds, their ability to stabilize when used in combination, and their influence on the antigenicity of influenza VLPs, our preliminary identification of potential stabilizers should be useful in the development of stable vaccine formulations.

References

1. Plotkin, S. A.; Orenstein, W. A., *Vaccines*. 4th ed.; Saunders: Philadelphia, 2004; 1662 p.
2. WHO, Influenza vaccines. *Wkly Epidemiol Rec* **2005,** 80, (33), 279-87.
3. Hay, A. J.; Gregory, V.; Douglas, A. R.; Lin, Y. P., The evolution of human influenza viruses. *Philos Trans R Soc Lond B Biol Sci* **2001,** 356, (1416), 1861-70.
4. Haynes, J. R.; Dokken, L.; Wiley, J. A.; Cawthon, A. G.; Bigger, J.; Harmsen, A. G.; Richardson, C., Influenza-pseudotyped Gag virus-like particle vaccines provide broad protection against highly pathogenic avian influenza challenge. *Vaccine* **2009,** 27, (4), 530-41.
5. Bright, R. A.; Carter, D. M.; Crevar, C. J.; Toapanta, F. R.; Steckbeck, J. D.; Cole, K. S.; Kumar, N. M.; Pushko, P.; Smith, G.; Tumpey, T. M.; Ross, T. M., Cross-clade protective immune responses to influenza viruses with H5N1 HA and NA elicited by an influenza virus-like particle. *PLoS ONE* **2008,** 3, (1), e1501.
6. Matassov, D.; Cupo, A.; Galarza, J. M., A novel intranasal virus-like particle (VLP) vaccine designed to protect against the pandemic 1918 influenza A virus (H1N1). *Viral Immunol* **2007,** 20, (3), 441-52.
7. Pushko, P.; Tumpey, T. M.; Van Hoeven, N.; Belser, J. A.; Robinson, R.; Nathan, M.; Smith, G.; Wright, D. C.; Bright, R. A., Evaluation of influenza virus-like particles and Novasome adjuvant as candidate vaccine for avian influenza. *Vaccine* **2007,** 25, (21), 4283-90.

8. Quan, F. S.; Huang, C.; Compans, R. W.; Kang, S. M., Virus-like particle vaccine induces protective immunity against homologous and heterologous strains of influenza virus. *J Virol* **2007,** 81, (7), 3514-24.

9. Peek, L. J.; Brey, R. N.; Middaugh, C. R., A rapid, three-step process for the preformulation of a recombinant ricin toxin A-chain vaccine. *J Pharm Sci* **2007,** 96, (1), 44-60.

10. Jiang, G.; Joshi, S. B.; Peek, L. J.; Brandau, D. T.; Huang, J.; Ferriter, M. S.; Woodley, W. D.; Ford, B. M.; Mar, K. D.; Mikszta, J. A.; Hwang, C. R.; Ulrich, R.; Harvey, N. G.; Middaugh, C. R.; Sullivan, V. J., Anthrax vaccine powder formulations for nasal mucosal delivery. *J Pharm Sci* **2006,** 95, (1), 80-96.

11. Salnikova, M. S.; Joshi, S. B.; Rytting, J. H.; Warny, M.; Middaugh, C. R., Preformulation studies of Clostridium difficile toxoids A and B. *J Pharm Sci* **2008**.

12. Kissmann, J.; Ausar, S. F.; Foubert, T. R.; Brock, J.; Switzer, M. H.; Detzi, E. J.; Vedvick, T. S.; Middaugh, C. R., Physical stabilization of norwalk virus-like particles. *J Pharm Sci* **2008**.

13. Kissmann, J.; Ausar, S. F.; Rudolph, A.; Braun, C.; Cape, S. P.; Sievers, R. E.; Federspiel, M. J.; Joshi, S. B.; Middaugh, C. R., Stabilization of Measles Virus for Vaccine Formulation. *Hum Vaccin* **2008,** 4, (5).

14. Ausar, S. F.; Espina, M.; Brock, J.; Thyagarayapuran, N.; Repetto, R.; Khandke, L.; Middaugh, C. R., High-throughput screening of stabilizers for respiratory syncytial virus: identification of stabilizers and their effects on the conformational thermostability of viral particles. *Hum Vaccin* **2007,** 3, (3), 94-103.

15. Lakowicz, J. R., *Principles of fluorescence spectroscopy*. 2nd ed.; Kluwer Academic/Plenum: New York, 1999; 698 p.

16. Parasassi, T.; De Stasio, G.; Ravagnan, G.; Rusch, R. M.; Gratton, E., Quantitation of lipid phases in phospholipid vesicles by the generalized polarization of Laurdan fluorescence. *Biophys J* **1991,** 60, (1), 179-89.

17. Borges, N.; Ramos, A.; Raven, N. D.; Sharp, R. J.; Santos, H., Comparative study of the thermostabilizing properties of mannosylglycerate and other compatible solutes on model enzymes. *Extremophiles* **2002,** 6, (3), 209-16.

18. Ausar, S. F.; Rexroad, J.; Frolov, V. G.; Look, J. L.; Konar, N.; Middaugh, C. R., Analysis of the thermal and pH stability of human respiratory syncytial virus. *Mol Pharm* **2005,** 2, (6), 491-9.

19. White, J. M., Membrane fusion. *Science* **1992,** 258, (5084), 917-24.

20. White, J. M.; Wilson, I. A., Anti-peptide antibodies detect steps in a protein conformational change: low-pH activation of the influenza virus hemagglutinin. *J Cell Biol* **1987,** 105, (6 Pt 2), 2887-96.

21. Wiley, D. C.; Skehel, J. J., The structure and function of the hemagglutinin membrane glycoprotein of influenza virus. *Annu Rev Biochem* **1987,** 56, 365-94.

22. Kemble, G. W.; Danieli, T.; White, J. M., Lipid-anchored influenza hemagglutinin promotes hemifusion, not complete fusion. *Cell* **1994,** 76, (2), 383-91.

23. Colman, P. M., Influenza virus neuraminidase: structure, antibodies, and inhibitors. *Protein Sci* **1994,** 3, (10), 1687-96.

24. Flanagan, M. T.; Skehel, J. J., The conformation of influenza virus haemagglutinin. *FEBS Lett* **1977,** 80, (1), 57-60.

25. Kelly, B. N.; Howard, B. R.; Wang, H.; Robinson, H.; Sundquist, W. I.; Hill, C. P., Implications for viral capsid assembly from crystal structures of HIV-1 Gag(1-278) and CA(N)(133-278). *Biochemistry* **2006,** 45, (38), 11257-66.

26. Mortuza, G. B.; Dodding, M. P.; Goldstone, D. C.; Haire, L. F.; Stoye, J. P.; Taylor, I. A., Structure of B-MLV capsid amino-terminal domain reveals key features of viral tropism, gag assembly and core formation. *J Mol Biol* **2008,** 376, (5), 1493-508.

27. Chi, E. Y.; Krishnan, S.; Randolph, T. W.; Carpenter, J. F., Physical stability of proteins in aqueous solution: mechanism and driving forces in nonnative protein aggregation. *Pharm Res* **2003,** 20, (9), 1325-36.

28. Lee, J. C.; Timasheff, S. N., The stabilization of proteins by sucrose. *J Biol Chem* **1981,** 256, (14), 7193-201.

29. Shimizu, S.; Smith, D. J., Preferential hydration and the exclusion of cosolvents from protein surfaces. *J Chem Phys* **2004,** 121, (2), 1148-54.

30. Uedaira, H.; Uedaira, H., Role of hydration of polyhydroxy compounds in biological systems. *Cell Mol Biol (Noisy-le-grand)* **2001,** 47, (5), 823-9.

31. Luzardo, M. C.; Amalfa, F.; Nunez, A. M.; Diaz, S.; Biondi De Lopez, A. C.; Disalvo, E. A., Effect of trehalose and sucrose on the hydration and dipole potential of lipid bilayers. *Biophys J* **2000,** 78, (5), 2452-8.

32. Ricker, J. V.; Tsvetkova, N. M.; Wolkers, W. F.; Leidy, C.; Tablin, F.; Longo, M.; Crowe, J. H., Trehalose maintains phase separation in an air-dried binary lipid mixture. *Biophys J* **2003,** 84, (5), 3045-51.

33. Rudolph, A. S.; Crowe, J. H.; Crowe, L. M., Effects of three stabilizing agents--proline, betaine, and trehalose--on membrane phospholipids. *Arch Biochem Biophys* **1986,** 245, (1), 134-43.

Table 4.1. Extent of aggregation of influenza VLPs in the presence of various potential stabilizers (grouped by class).

Excipient	Concentration (molarity or % w/v)	Inhibition[a] (%)
Ascorbic acid	0.15 M	-338.1[b]
Aspartic Acid	0.075 M	-13.5[b]
Lactic Acid	0.15 M	21.8[+]
Malic Acid	0.15 M	16.2
Arginine	0.3 M	70.0
Diethanolamine	0.3 M	67.4
Guanidine HCl	0.3 M	30.1
Histidine	0.3 M	30.2
Lysine	0.3 M	70.1
Proline	0.3 M	21.7
Glycine	0.3 M	12.1
Brij 35	0.01%	67.7
Brij 35	0.05%	36.9
Brij 35	0.10%	60.0
Tween 20	0.01%	60.3[+]
Tween 20	0.05%	98.5[+]
Tween 20	0.10%	91.2[+]
Tween 80	0.01%	57.9
Tween 80	0.05%	45.1
Tween 80	0.10%	52.6
Pluronic F-68	0.01%	3.4[+]
Pluronic F-68	0.05%	65.4[+]
Pluronic F-68	0.10%	43.1[+]
Albumin (human)	1%	-55.2[b]
Albumin (human)	2.5%	-1597.3[b]
Albumin (human)	5%	-1778.7[b]

[a]Relative to the control at t = 15 minutes[+] or t = 30 minutes. Inhibition calculated as $(1-OD_{350\ sample}/OD_{350\ control})(100\%)$. The relative standard deviation in these calculated values was ≤ 10 %.

[b]A negative percent inhibition value indicates that the excipient enhanced aggregation.

Table 4.1, continued.

Excipient	Concentration (molarity or % w/v)	Inhibition[a] (%)
Gelatin (porcine)	2.5%	11.7[+]
Gelatin (porcine)	5%	-54.7[+b]
Lactose	10%	-20.6[+b]
Lactose	15%	60.5
Lactose	20%	75.0[+]
Trehalose	10%	-227.5[+b]
Trehalose	15%	-2.9[b]
Trehalose	20%	84.2[+]
Dextrose	10%	25.9
Dextrose	15%	58.0
Dextrose	20%	66.7
Sucrose	10%	-113.3[+b]
Sucrose	20%	28.4[+]
Mannitol	10%	-19.5[b]
Sorbitol	10%	-66.1[+b]
Sorbitol	15%	45.2
Sorbitol	20%	80.1[+]
Glycerol	5%	23.4
Glycerol	10%	82.3
Glycerol	15%	41.8
Glycerol	20%	69.1
□-Cyclodextrin	2.5%	-91.2[b]
2-OH propyl □-CD[c]	5%	19.2
2-OH propyl □-CD[c]	10%	249.2[d]
2-OH propyl □-CD[c]	5%	27.4
2-OH propyl □-CD[c]	10%	12.1

[a]Relative to the control sample at t = 15 minutes[+] or t = 30 minutes. Inhibition calculated as $(1-OD_{350\ sample}/OD_{350\ control})(100\%)$. The relative standard deviation in these calculated values was ≤ 10 %.

[b]A negative percent inhibition value indicates that the excipient enhanced aggregation.

[c]CD = cyclodextrin.

[d]This percent inhibition value is misleading. The sample precipitated during analysis, apparently lowering the optical density value.

Figure 4.1. Dynamic light scattering by influenza VLPs. Effective diameter (A), static light scatting intensity (B), and sample polydispersity (C) are plotted as a function of temperature. Each point represents the mean of three independent samples, and error bars show the standard deviation.

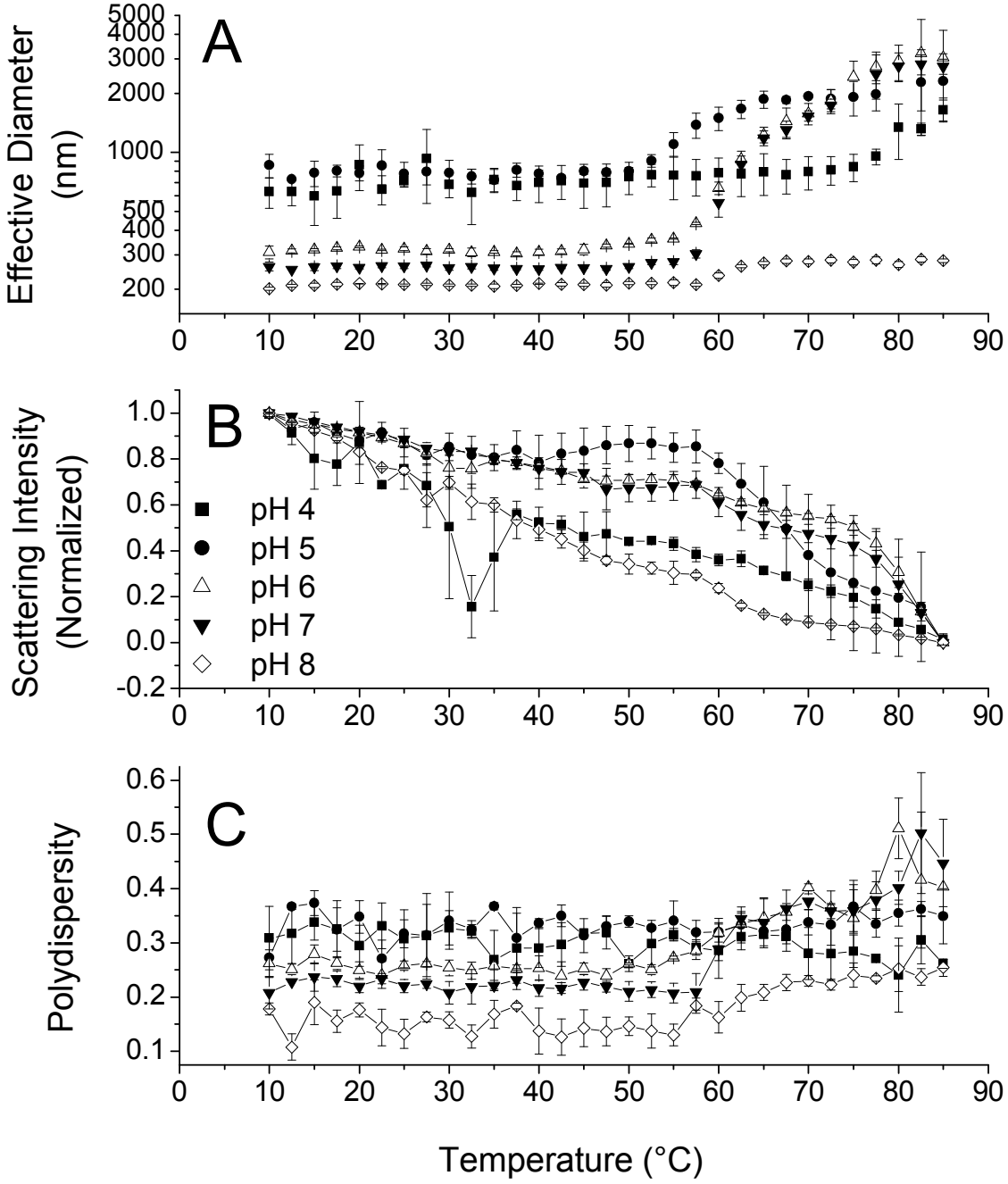

Figure 4.2. Circular dichroism spectra of influenza VLPs. Low temperature (10 °C) spectra at each unit pH from 4 to 8 (A) and pH 7 spectra at a variety of temperatures (B) are presented.

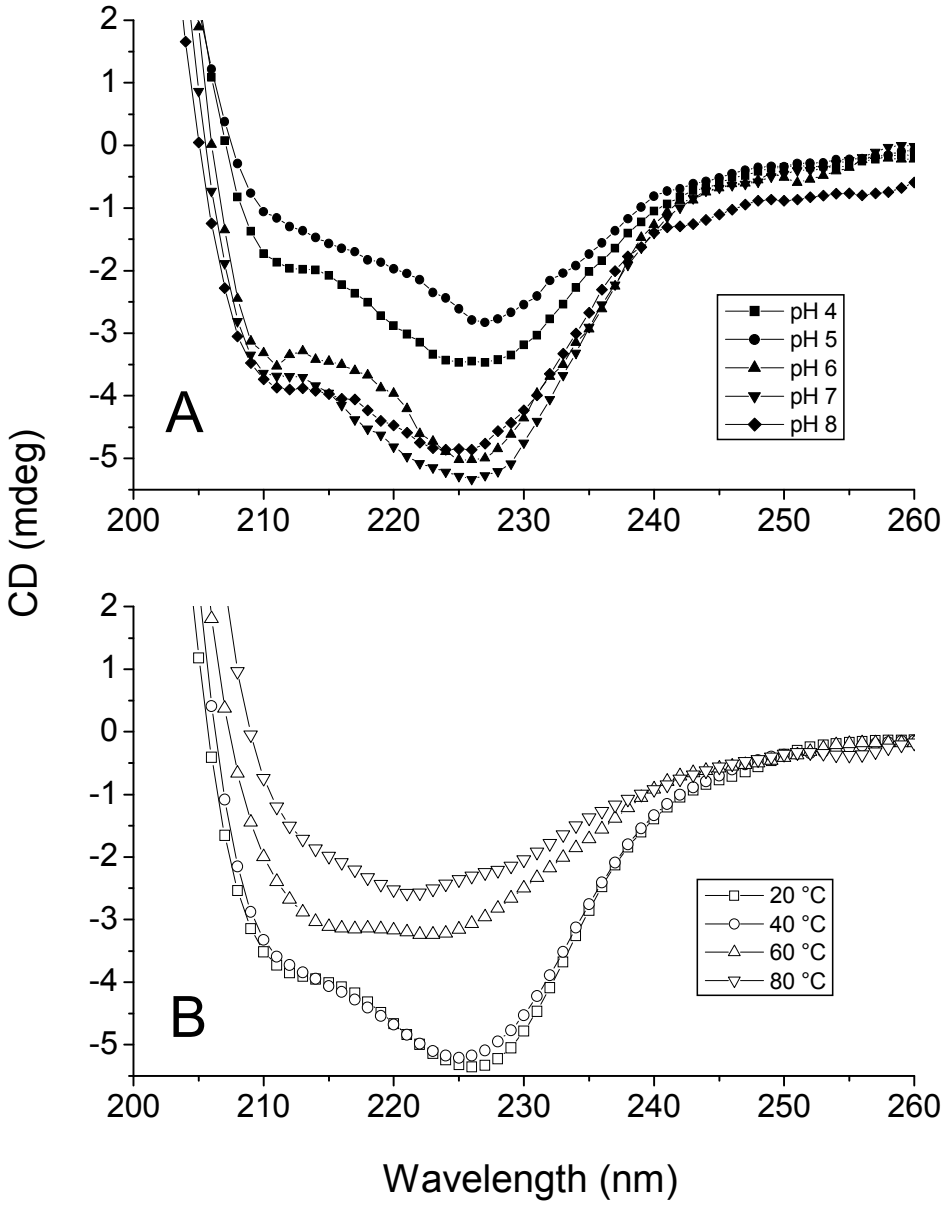

Figure 4.3. The response of influenza VLP protein secondary structure to thermal stress. The normalized (-1 to 0) CD at 227 nm is presented as a function of temperature. Each point represents the mean of three independent samples, and error bars show the standard deviation.

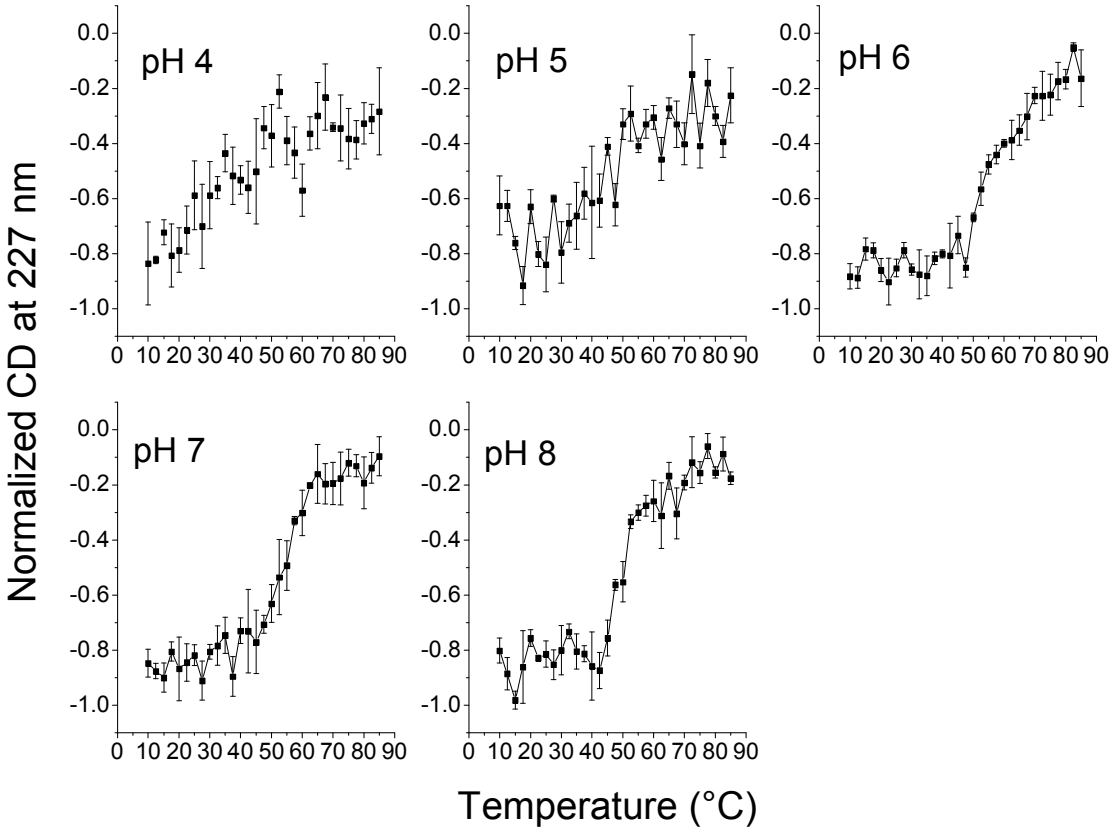

Figure 4.4. Intrinsic fluorescence peak position of influenza VLPs as a function of temperature. Also presented as a function of temperature (lower right) is the normalized (0 to 1) intensity of fluorescence at 330 nm. Each point represents the mean of three independent samples, and error bars show the standard deviation.

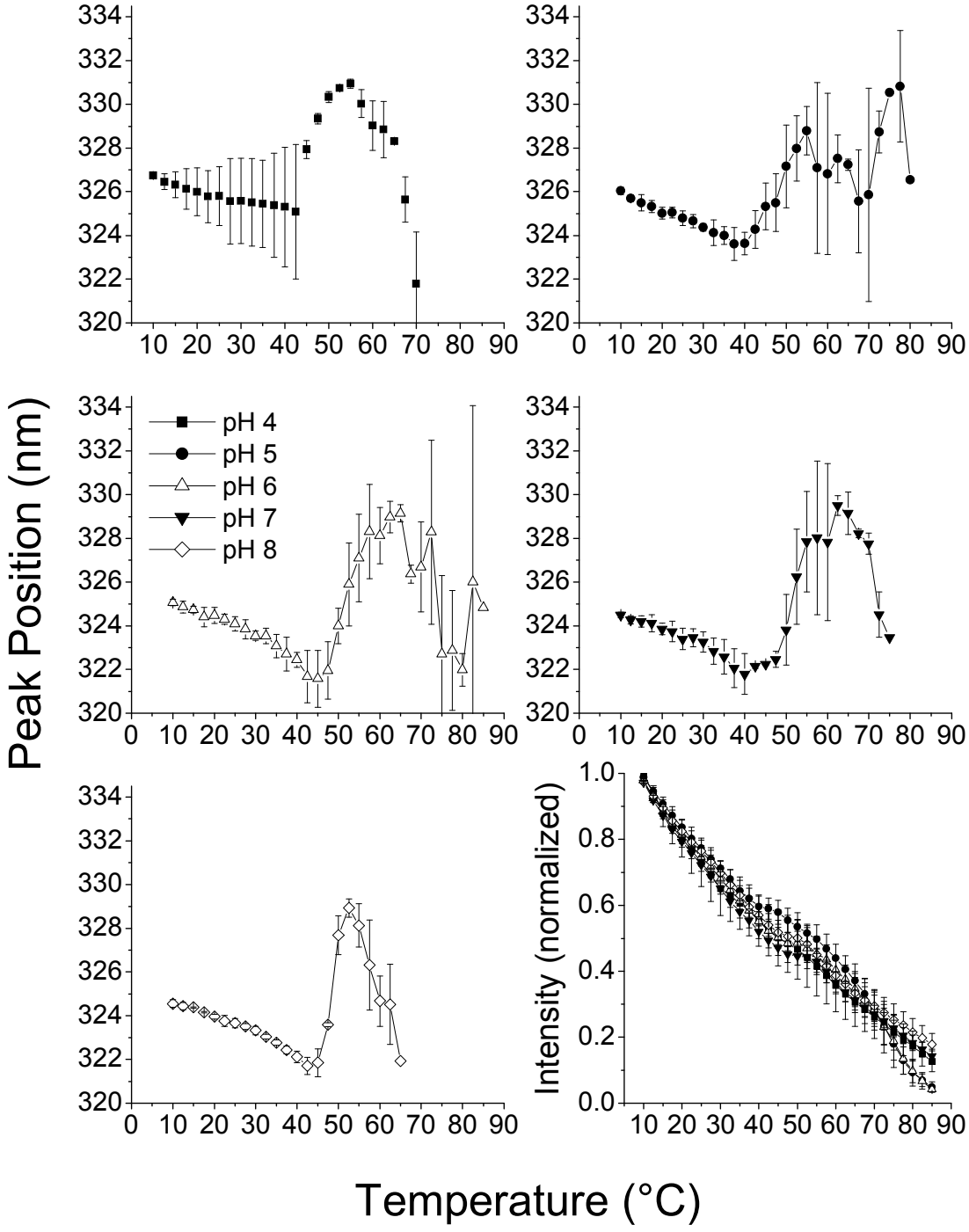

Figure 4.5. Fluorescence of ANS as a probe of influenza VLP physical structure. The wavelength of peak emission is presented as a function of temperature. Also presented as a function of temperature (lower right) is the normalized (0 to 1) intensity of ANS fluorescence at 485 nm. Each point represents the mean of three independent samples, and error bars show the standard deviation.

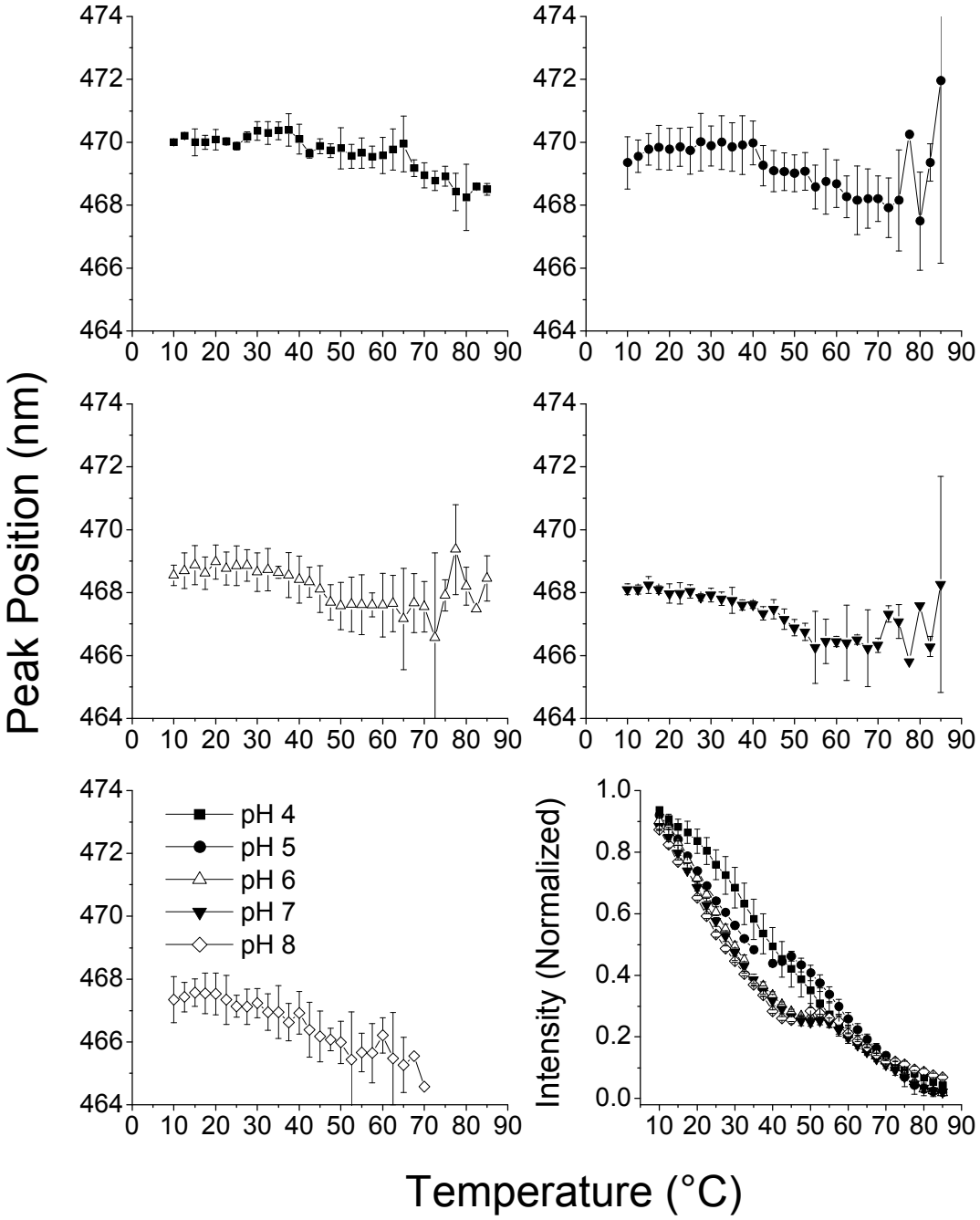

Figure 4.6. Generalized polarization of laurdan fluorescence in the presence of influenza VLPs as a function of temperature. Each point represents the mean of three independent samples, and error bars show the standard deviation.

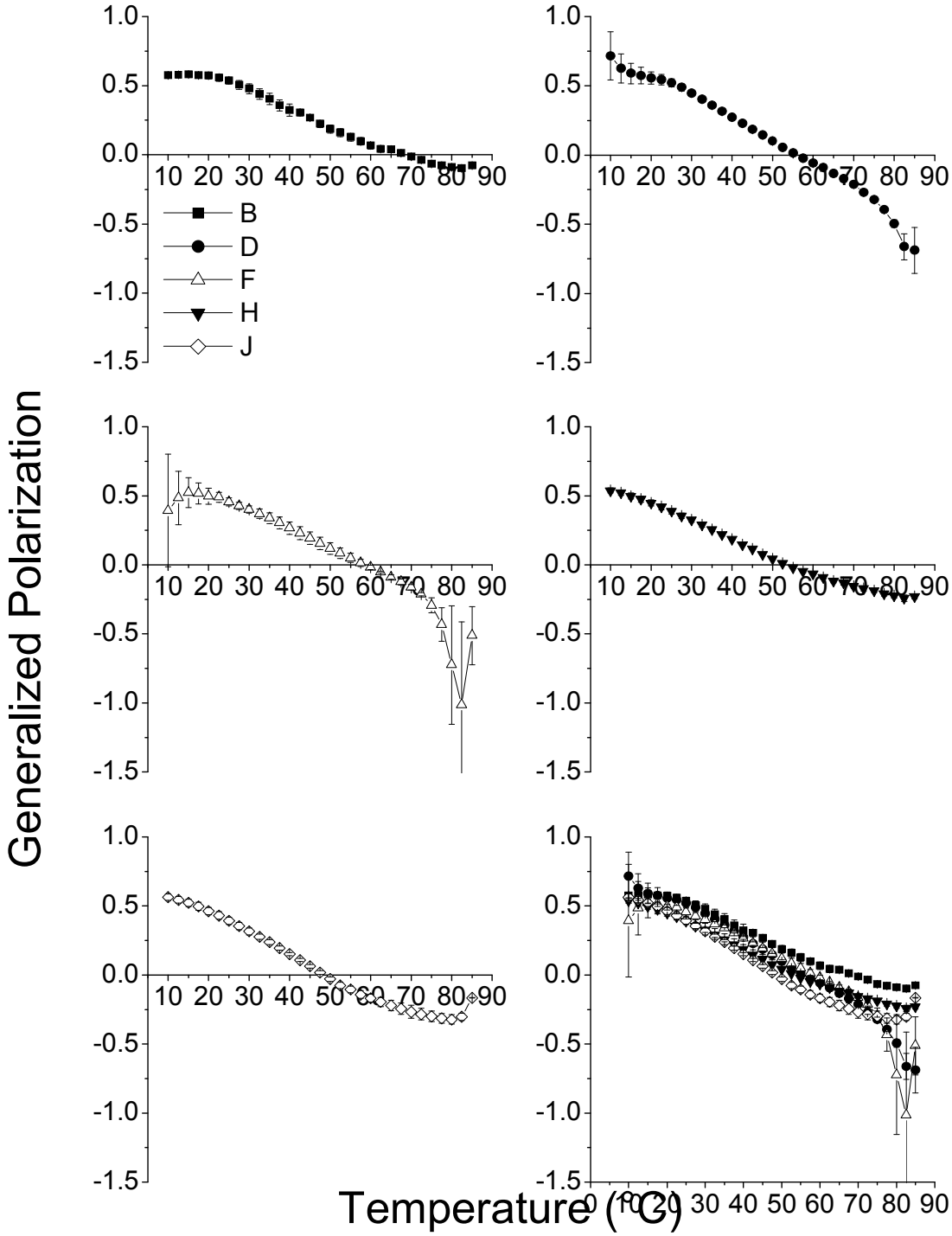

Figure 4.7. Empirical phase diagram derived from biophysical characterization of influenza VLPs. The EPD is prepared from temperature-dependent effective diameter, static light scattering, polydispersity, CD at 227 nm, intrinsic fluorescence (peak position and relative intensity at 330 nm), ANS fluorescence (peak position and relative intensity at 485 nm), and GP of laurdan fluorescence data collected across the pH range from 4 to 8.

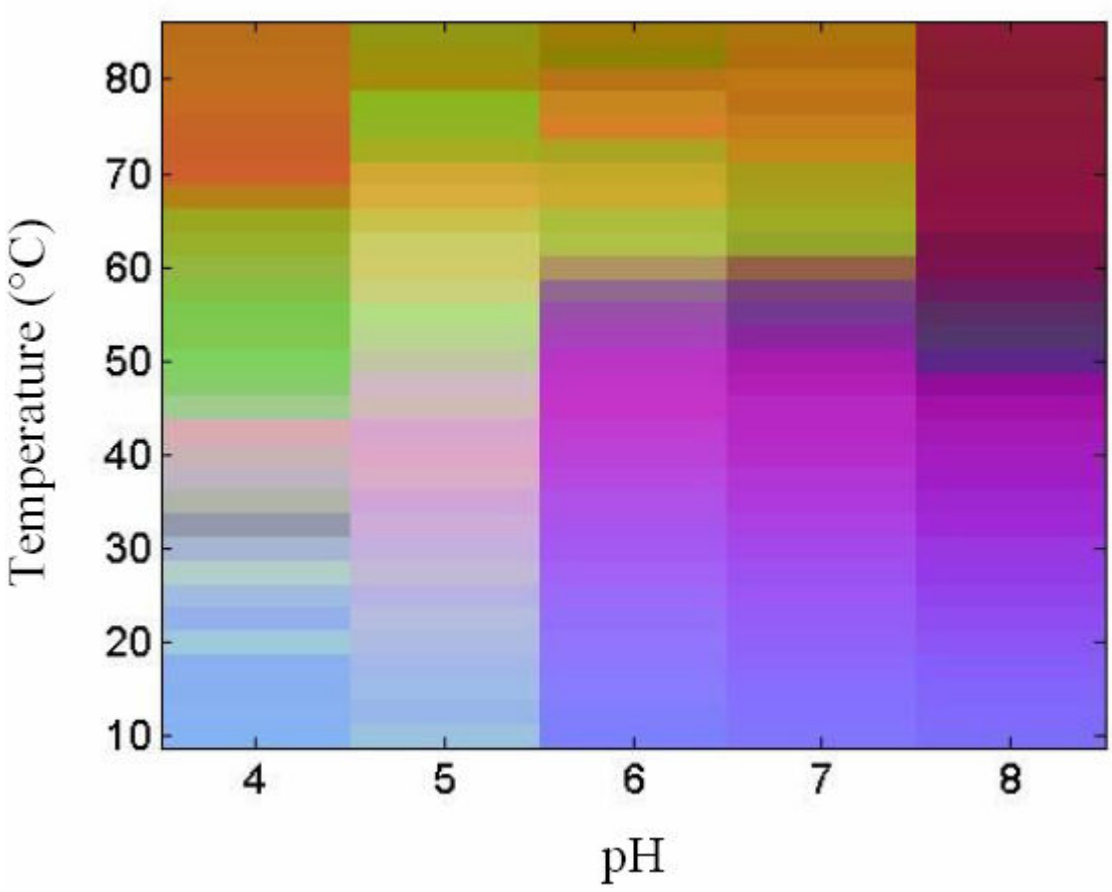

Figure 4.8. The intrinsic fluorescence of influenza VLPS in the presence of selected stabilizers. The position (wavelength) of the peak emission is presented as a function of temperature. Each point represents the mean of two independent samples, and error bars show the standard deviation.

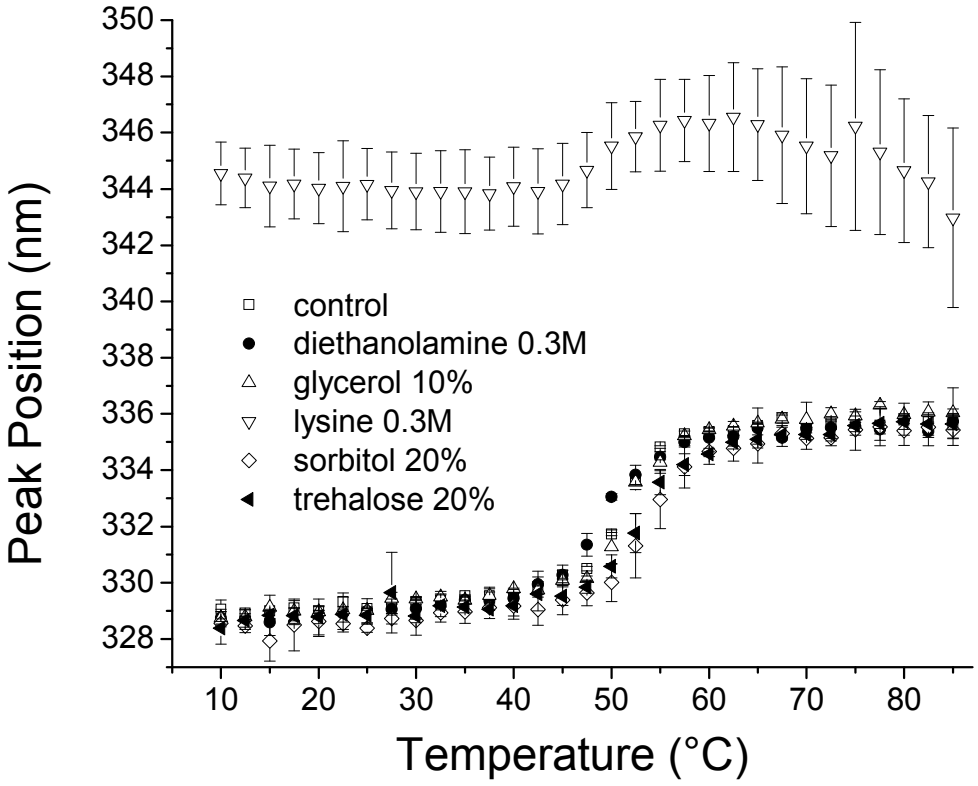

Figure 4.9. Generalized polarization of fluorescence by laurdan in the presence of influenza VLPs formulated with selected stabilizers, presented as a function of temperature. Each point represents the mean of two independent samples, and error bars show the standard deviation.

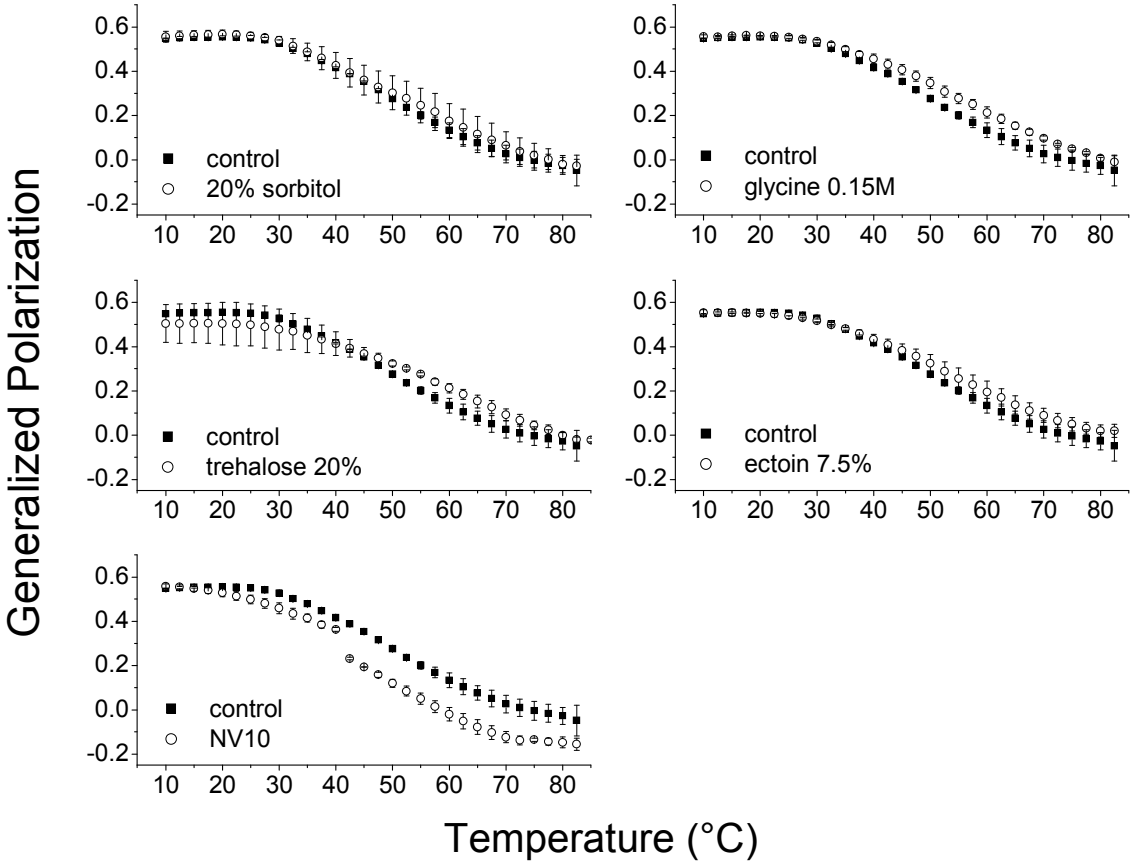

Figure 4.10. Comparison of VLPs with trypsin-cleaved HA to uncleaved VLPs by dynamic light scattering. As a function of temperature, particles with cleaved HA show differences in both scattering intensity (A) and average particle size (B). At low temperature, size differences are observed at pH 5 and 6 (C). Each point represents the mean of three independent samples, and error bars show the standard deviation.

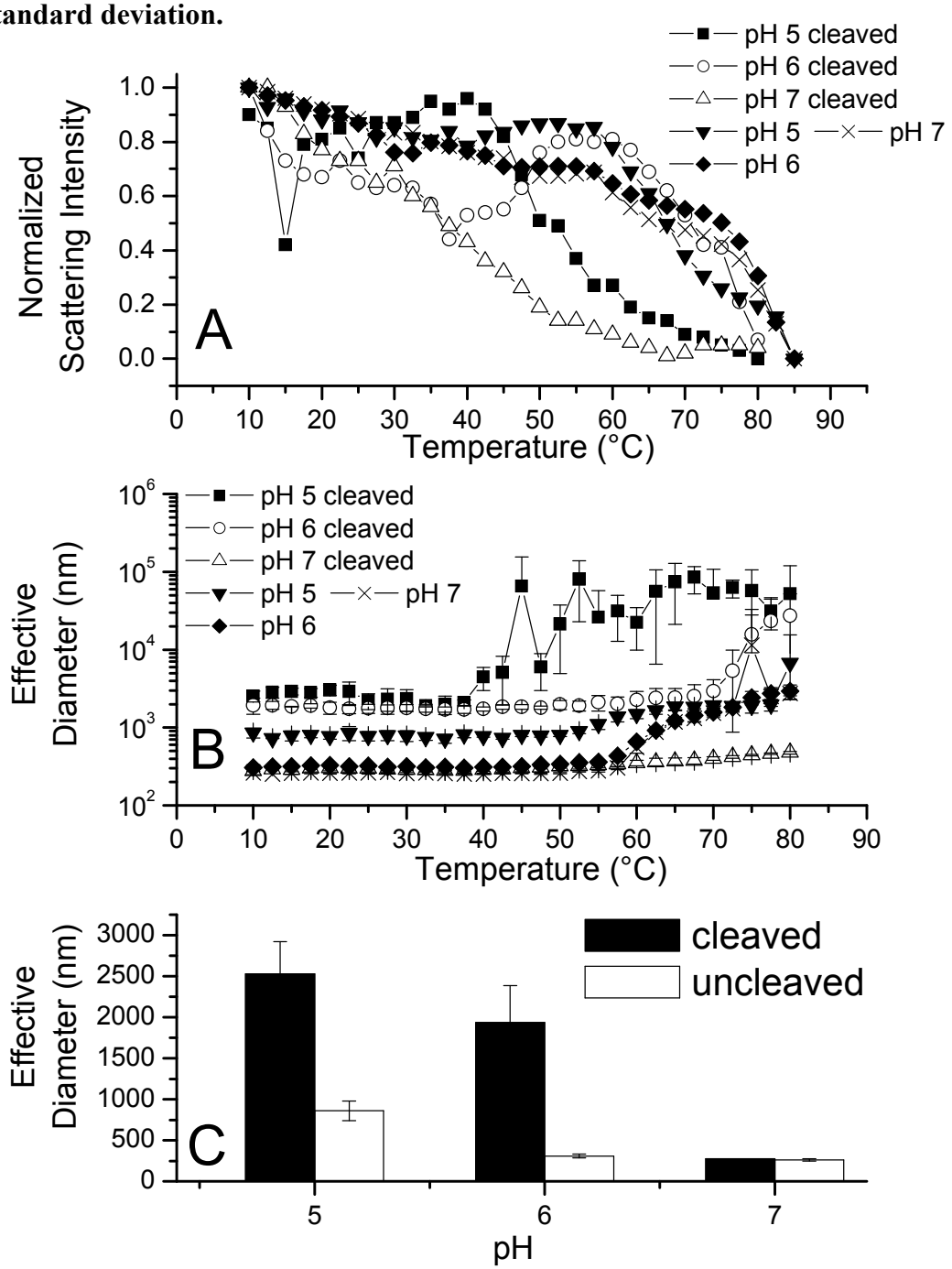

Chapter 5

Conclusions and Future Directions

The formulation of vaccines has traditionally been a challenging task. In particular, the development of thermostable vaccines that can be effectively delivered to cold chain-deficient regions is a slow, difficult, and currently sometimes impossible process. In the case of vaccines against viral diseases, we have hypothesized that this difficulty is due in large part to a requirement that spatially complex neutralizing epitopes be preserved over the course of a vaccine's shelf-life, often (but not always) within a native viral supramolecular structure. Unfortunately for vaccine developers, there are a wide variety of physical degradation processes that can disrupt these epitopes, and some of them can have significant effects on vaccine potency.[1] For this reason, the central focus of this dissertation has been the application of a multi-faceted biophysical, EPD-based approach to the identification of stabilizers that prevent the loss of non-covalent native viral structures. While the EPD method of data analysis has been applied successfully to the characterization and stabilization of a broad spectrum of potentially therapeutic macromolecular systems,[2-17] it has not (with one recent exception[18]) been applied to particles as massive or complex as viruses and virus-like particles. For example, the Norwalk VLP (discussed in Chapter 2), which is the most structurally uncomplicated particle among our four case studies, is composed of 180 self-assembled protein monomers and has a total particulate mass above 10 MDa.[19] The major questions posed by this work are two-fold: first, is the EPD-based approach to stabilization

applicable in the case of these large, structurally complicated particles, and, if so, how can the findings from these case studies be applied to improve the use of this technique in the development of future viral vaccine formulations?

Perhaps the most important application of the EPD-based approach to vaccine stabilization is the determination of optimal stress conditions to be used in the screening of chemical libraries for potential stabilizing excipients. As mentioned in preceding chapters, the use of appropriate stress parameters during screening experiments can be critical to the ability to discriminate between highly effective and marginally effective stabilizers. If the selected stress conditions are too stringent, the formulation scientist risks destruction of the therapeutic entity to an extent such that the stabilizing effects from even the most efficacious of potential excipients are not observable. On the other hand, if the screening conditions are chosen such that significant degradation pathways are either kinetically or thermodynamically inhibited, the differences between highly effective and marginally effective stabilizers may not be apparent. The most significant physical degradation process observed among the four viral vaccine candidates stabilized in this work was particle aggregation, and for all of the candidates studied a number of aggregation-inhibiting compounds were identified by high- or medium-throughput screening assays. Furthermore, in each of the case studies, there was an extremely wide range observed in the degree of aggregation inhibition by various compounds from the chemical library, sometimes even between compounds belonging to the same molecular class (*e.g.,* disaccharides). This suggests that the screening conditions were chosen appropriately in each case, which is in itself is a partial validation of the EPD-based approach. Although there are a variety of potential causes for the observed aggregation of

these potential protein-based therapeutics,[20] it is reasonable to suggest that there are just a few general mechanisms by which these compounds are able to inhibit viral aggregation. The first possibility is that they work by preventing the transition of one or more viral components into a non-native, aggregation-competent conformation. Alternatively, the compounds which inhibit aggregation may have little to no preservative effect on the native conformation of viral components, and simply interfere with the agglomeration of particles whether they are structurally disrupted or not. An additional possibility is that certain compounds may actually disrupt or somehow disintegrate viral particles, thereby abolishing the diagnostic signal presumed to be reflective of particle aggregation (*e.g.,* time-dependent optical density measurements at 360 nm) - this phenomenon was observed for lysine in the presence of influenza VLPs. To discriminate between these three possibilities, additional spectroscopic studies were performed on viral particles in the presence of potential stabilizers to determine whether they exert their stabilizing effects on one or more aspects of viral structure in particular. The measles project was an exception in which the number of desirable post-screening studies was limited by the availability of viral material.

By and large, those compounds that inhibited the aggregation of viral particles exhibited a combination of the different mechanisms described above – certain ones were observed to stabilize one or more aspects of the viral architecture (*i.e.,* viral protein tertiary or secondary structure, or fluidity of the viral envelope), while others did not have a detectable effect on any of the specific aspects of viral structure that were studied. This finding emphasizes the requirement that additional studies be conducted after the initial screening experiments to determine exactly which of the possible mechanisms are

functioning; clearly, the compounds that belong to the former group are the most desirable from a vaccine formulation perspective, since the native state of the virus should be most effective in stimulating a robust and protective immune response. While these experiments demand the availability of additional purified viral stocks, the amount of raw material and other laboratory resources required for preformulation studies conducted in this manner should in many cases still be significantly less than if animal challenge, cell-based, or antibody-based (*e.g.,* ELISA) assays are utilized as primary screening tools. In this sense, it is reasonable to conclude that the EPD-based approach is an appropriate method for the identification of optimal excipient screening conditions, with the caveat that additional studies must be performed in the presence of any stabilizers identified by the screening assay.

The low pH-induced aggregation of viral particles observed in both the influenza and measles vaccine candidates characterized suggests an opportunity to further optimize the EPD-based approach for the stabilization of enveloped viral vaccines. The two EPDs generated by these studies all show strong apparent phase transitions that manifest as a function of pH, usually between pH 5 and 6. Severe particle aggregation was observed even at low temperatures in all three systems when the viral particles were suspended in buffer of pH 5 or lower. In the case of the influenza VLP, the structural sensitivity to pH in this region can at least partially be attributed to well-known conformational changes in the proteins that are responsible for fusion of the viral envelope with the lipid bilayer of host cells. The membrane-bound fusion proteins possessed by all enveloped viruses serve to deliver the viral genome to the cytosol of infected cells either directly from the host cell surface in a pH-independent manner (*e.g.,* measles[21]), or from the interior of a

maturing endosome in response to reduced pH (*e.g.,* rabies and influenza).[22, 23] Indeed, these viruses (or parent viruses in the case of VLPs) have evolved in such a way that enveloped, infection-competent particles are never exposed to acidity greater than that of the endosome during their normal infection cycles, which is in contrast to the Norwalk and other viruses which infect the gastrointestinal tract and thus require insensitivity to low pH.

Based on the results of the studies presented here, the presence of a viral envelope and its associated proteins confers a high sensitivity to pH – but this might have been predicted from the wealth of available virology literature. Furthermore, it is already known that the fusion proteins that are partially responsible for the sensitivity of viral structure to acidic pH are of great importance to vaccine efficacy – that is, they contain critical epitopes that are recognized by the neutralizing immunoglobulins generated by a protective immune response.[24-27] Therefore, the preservation of the native structures of these proteins is an important component of successful vaccine formulation. For this reason, characterization studies for the purpose of formulation were probably not enhanced by measurements conducted at pH 4 or below. The use of a single technique that is sensitive to particle aggregation (such as DLS), rather than the full complement of biophysical techniques, could help rule out the need for additional measurements if low-temperature aggregation is observed to great extent. In retrospect, a better use of the resources spent for those measurements at pH 4 or below would have been analysis of samples at half-unit pH values near the apparent phase boundaries observed at higher pH (*i.e.,* pH 5.5, 6.5, and perhaps even 7.5). Performing these additional measurements (instead of ones at the extremely low pH levels characterized by a high degree of

temperature-independent aggregation) could enhance the sensitivity of the EPD in two ways. First, significantly greater resolution on the pH axis would be obtained, which may be of use in the identification of optimal conditions to be used in excipient screening assays. The molecular switches responsible for viral protein conformation changes are not completely understood for all of the viral species studied here, but in many cases their response to pH may be tightly regulated such that incremental changes in proton concentration may lead to the appearance of unique physical states that could be detected by the EPD. Second, significant particle aggregation at any one pH value has considerable effects on the entire EPD. The algorithm used to generate an EPD was designed to highlight *changes* in the signals measured by a variety of separate techniques - in other words, the composite data signal at any one particular combination of temperature and pH is compared to the entire set of data and tested for difference. If it is significantly different from the data in neighboring parts of the diagram (*i.e.,* similar combination of temperature and pH), a color change will result and the presence of a new physical state will be implied. Whether a difference is significant, however, depends on the range of values present in the data set. If the range of values is small, small differences will appear significant. If the range is wide, small changes will be ignored. Thus, a wide range in particle size imparted by high levels of aggregation will override small, potentially important changes that occur even in other regions of the diagram. In addition, particle aggregation has effects on the signal obtained by other techniques as well – for example, the scattering from aggregated material can result in the artificial loss of signal in any of several spectroscopic techniques. This phenomenon has the potential to influence the entire phase diagram (for the same reason given above), even if it is only

observed at a single pH value. Therefore, excluding from the EPD algorithm extremes of pH that do not assist either the identification of optimal formulation pH or conditions to be used in excipient screening assays may yield more useful diagrams.

Finally, the biophysical data set generated by characterization studies in our laboratory is currently subjected to the EPD-generating algorithm without any preprocessing. The complex structure of viral particles, however, often leads to a high degree of heterogeneity that manifests in the data as noise. This noise can sometimes be detected by the EPD in non-useful ways – in other words, noise in the data can appear as local and transient phase transitions, or mottling, in the EPD. The use of data preprocessing in the form of mathematical noise reduction techniques (such as smoothing) is already being explored by other students in our laboratory, but it is worth mentioning here as another potential avenue for improvement. Overall, however, the EPD represents an extremely versatile technique for the visualization of changes in the physical state of viral vaccines; this fact is reflected by the increasing adoption of this technique by both large and small commercial vaccine developers. It will be exciting to see what new applications and innovations result from its continued development.

References

1. Brandau, D. T.; Jones, L. S.; Wiethoff, C. M.; Rexroad, J.; Middaugh, C. R., Thermal stability of vaccines. *J Pharm Sci* **2003,** 92, (2), 218-31.
2. Ausar, S. F.; Foubert, T. R.; Hudson, M. H.; Vedvick, T. S.; Middaugh, C. R., Conformational stability and disassembly of Norwalk virus-like particles. Effect of pH and temperature. *J Biol Chem* **2006,** 281, (28), 19478-88.
3. Ausar, S. F.; Rexroad, J.; Frolov, V. G.; Look, J. L.; Konar, N.; Middaugh, C. R., Analysis of the thermal and pH stability of human respiratory syncytial virus. *Mol Pharm* **2005,** 2, (6), 491-9.
4. Brandau, D. T.; Joshi, S. B.; Smalter, A. M.; Kim, S.; Steadman, B.; Middaugh, C. R., Stability of the Clostridium botulinum type A neurotoxin complex: an empirical phase diagram based approach. *Mol Pharm* **2007,** 4, (4), 571-82.
5. Cai, S.; He, F.; Samra, H. S.; de la Maza, L. M.; Bottazzi, M. E.; Joshi, S. B.; Middaugh, C. R., Biophysical and Stabilization Studies of the Chlamydia trachomatis Mouse Pneumonitis Major Outer Membrane Protein. *Mol Pharm* **2009**.
6. Fan, H.; Kashi, R. S.; Middaugh, C. R., Conformational lability of two molecular chaperones Hsc70 and gp96: effects of pH and temperature. *Arch Biochem Biophys* **2006,** 447, (1), 34-45.
7. Fan, H.; Li, H.; Zhang, M.; Middaugh, C. R., Effects of solutes on empirical phase diagrams of human fibroblast growth factor 1. *J Pharm Sci* **2007,** 96, (6), 1490-503.

8. Fan, H.; Ralston, J.; Dibiase, M.; Faulkner, E.; Middaugh, C. R., Solution behavior of IFN-beta-1a: an empirical phase diagram based approach. *J Pharm Sci* **2005,** 94, (9), 1893-911.

9. He, F.; Joshi, S. B.; Bosman, F.; Verhaeghe, M.; Middaugh, C. R., Structural stability of hepatitis C virus envelope glycoprotein E1: effect of pH and dissociative detergents. *J Pharm Sci* **2009,** 98, (9), 3340-57.

10. Jiang, G.; Joshi, S. B.; Peek, L. J.; Brandau, D. T.; Huang, J.; Ferriter, M. S.; Woodley, W. D.; Ford, B. M.; Mar, K. D.; Mikszta, J. A.; Hwang, C. R.; Ulrich, R.; Harvey, N. G.; Middaugh, C. R.; Sullivan, V. J., Anthrax vaccine powder formulations for nasal mucosal delivery. *J Pharm Sci* **2006,** 95, (1), 80-96.

11. Kueltzo, L. A.; Ersoy, B.; Ralston, J. P.; Middaugh, C. R., Derivative absorbance spectroscopy and protein phase diagrams as tools for comprehensive protein characterization: a bGCSF case study. *J Pharm Sci* **2003,** 92, (9), 1805-20.

12. Kueltzo, L. A.; Middaugh, C. R., Structural characterization of bovine granulocyte colony stimulating factor: effect of temperature and pH. *J Pharm Sci* **2003,** 92, (9), 1793-804.

13. Nonoyama, A.; Laurence, J. S.; Garriques, L.; Qi, H.; Le, T.; Middaugh, C. R., A biophysical characterization of the peptide drug pramlintide (AC137) using empirical phase diagrams. *J Pharm Sci* **2008,** 97, (7), 2552-67.

14. Peek, L. J.; Brandau, D. T.; Jones, L. S.; Joshi, S. B.; Middaugh, C. R., A systematic approach to stabilizing EBA-175 RII-NG for use as a malaria vaccine. *Vaccine* **2006,** 24, (31-32), 5839-51.

15. Rexroad, J.; Evans, R. K.; Middaugh, C. R., Effect of pH and ionic strength on the physical stability of adenovirus type 5. *J Pharm Sci* **2006,** 95, (2), 237-47.

16. Rexroad, J.; Martin, T. T.; McNeilly, D.; Godwin, S.; Middaugh, C. R., Thermal stability of adenovirus type 2 as a function of pH. *J Pharm Sci* **2006,** 95, (7), 1469-79.

17. Ruponen, M.; Braun, C. S.; Middaugh, C. R., Biophysical characterization of polymeric and liposomal gene delivery systems using empirical phase diagrams. *J Pharm Sci* **2006,** 95, (10), 2101-14.

18. Zeng, Y.; Fan, H.; Chiueh, G.; Pham, B.; Martin, R.; Lechuga-Ballesteros, D.; Truong, V. L.; Joshi, S. B.; Middaugh, C. R., Towards development of stable formulations of a live attenuated bacterial vaccine: A preformulation study facilitated by a biophysical approach. *Hum Vaccin* **2009,** 5, (5).

19. Prasad, B. V.; Hardy, M. E.; Dokland, T.; Bella, J.; Rossmann, M. G.; Estes, M. K., X-ray crystallographic structure of the Norwalk virus capsid. *Science* **1999,** 286, (5438), 287-90.

20. Chi, E. Y.; Krishnan, S.; Randolph, T. W.; Carpenter, J. F., Physical stability of proteins in aqueous solution: mechanism and driving forces in nonnative protein aggregation. *Pharm Res* **2003,** 20, (9), 1325-36.

21. Yanagi, Y.; Takeda, M.; Ohno, S., Measles virus: cellular receptors, tropism and pathogenesis. *J Gen Virol* **2006,** 87, (Pt 10), 2767-79.

22. Gaudin, Y.; Tuffereau, C.; Durrer, P.; Brunner, J.; Flamand, A.; Ruigrok, R., Rabies virus-induced membrane fusion. *Mol Membr Biol* **1999,** 16, (1), 21-31.

23. Huang, Q.; Sivaramakrishna, R. P.; Ludwig, K.; Korte, T.; Bottcher, C.; Herrmann, A., Early steps of the conformational change of influenza virus hemagglutinin to a fusion active state: stability and energetics of the hemagglutinin. *Biochim Biophys Acta* **2003,** 1614, (1), 3-13.

24. Bouche, F. B.; Ertl, O. T.; Muller, C. P., Neutralizing B cell response in measles. *Viral Immunol* **2002,** 15, (3), 451-71.

25. Klasse, P. J.; Sattentau, Q. J., Occupancy and mechanism in antibody-mediated neutralization of animal viruses. *J Gen Virol* **2002,** 83, (Pt 9), 2091-108.

26. Spackman, E., A brief introduction to the avian influenza virus. *Methods Mol Biol* **2008,** 436, 1-6.

27. Wunner, W. H.; Larson, J. K.; Dietzschold, B.; Smith, C. L., The molecular biology of rabies viruses. *Rev Infect Dis* **1988,** 10 Suppl 4, S771-84.